

UNIVERSITY OF OKLAHOMA

GRADUATE COLLEGE

APPLICATION OF MODERN 3D SEISMIC DATA ACQUIRED FOR DEEPER
RESOURCE PLAYS TO SHALLOWER MATURE FIELDS – A RED FORK CASE
STUDY

A THESIS

SUBMITTED TO THE GRADUATE FACULTY

in partial fulfillment of the requirements for the

Degree of

MASTER OF SCIENCE

By

ANDREW PEERY
Norman, Oklahoma
2017

APPLICATION OF MODERN 3D SEISMIC DATA ACQUIRED FOR DEEPER
RESOURCE PLAYS TO SHALLOWER MATURE FIELDS – A RED FORK CASE
STUDY

A THESIS APPROVED FOR THE
CONOCOPHILLIPS SCHOOL OF GEOLOGY AND GEOPHYSICS

BY

Dr. Kurt J. Marfurt, Chair

Dr. Nori Nakata

Dr. Matthew Pranter

Simply thanks for my wife Robyn who put up with me and dealt with being a pseudo single parent at times as I went to school. And for my kids Colton and Kali. Remember you are never too old to learn and now we have more time for Minecraft again.

Acknowledgements

I would like to thank Dr. Marfurt for all the knowledge imparted during my time in graduate school and the guidance throughout this thesis. I also want to thank my other committee members Dr. Nakata and Dr. Pranter. I was lucky enough to be working and had colleagues to lean on for questions but the time you take away from your students and your personal time reading my thesis and attending my defense is appreciated immensely.

I would like to thank White Star Petroleum, Joe Craig, and Dan Bafia for permission to use these data for the thesis. It is exciting to be able to work with something that could ultimately be impactful. Also, thanks to my colleagues that have helped along this process including Mark Aisenberg, Keith Cardon, Sam McManus, Scott Causey, and Matt Newsom.

I also want to recognize OPIC, David Brown, and Jeff Dillon for taking their time pulling and setting up the core to be viewed and used in my thesis.

And a special thanks to Rebecca Fay. I would be lost and never graduate without your help and important reminders!

Table of Contents

Acknowledgements	iv
List of Tables	vi
List of Figures.....	vii
Abstract.....	xvi
CHAPTER I: INTRODUCTION	1
CHAPTER II: GEOLOGIC OVERVIEW	5
CHAPTER III: SEISMIC DATA QUALITY, DATA CONDITIONING, AND WELL CONTROL	21
CHAPTER IV: INVERSION	33
CHAPTER V: INTERPRETATION	47
CHAPTER VI: CONCLUSIONS.....	81
References	82
Appendix A: 5D INTERPOLATION.....	85

List of Tables

Table 1. Acquisition Parameters.....	24
--------------------------------------	----

List of Figures

Figure 1. Vertically exaggerated cartoon showing (a) an original horizontal wellbore design and (b) a re-worked plan to intercept a shallow sand.	4
Figure 2. Stratigraphic chart for the Cherokee Platform, Des Moinesian series. (Modified from Keller, 2008).....	7
Figure 3. Oklahoma geologic provinces. Red star highlights the Cherokee Platform in which the survey resides. (Modified from Northcutt and Campbell, 1988).....	8
Figure 4. Location of Nemaha and Wilzetta Faults in Oklahoma Geologic Survey database of faults. (Wilzetta from Way, 1968). Green box highlights study area.....	9
Figure 5. Principle rock types of early Pennsylvanian (Morrow and Atokan) age in Oklahoma (After Johnson, 2008). Green box highlights study area.	10
Figure 6. Principle rock types of middle Pennsylvanian (Des Moinesian) age in Oklahoma (After Johnson, 2008). Green box highlights study area.	11
Figure 7. Generalized cartoon highlighting the effects of differential compaction between the Bartlesville sandstone and surrounding shale depositions. The preferential lows created by the compacting shales set up accommodation space for the deposition of the Red Fork sandstone. Note the limited stacked sands.	12
Figure 8. Generalized depositional environments of the Red Fork sandstone in Oklahoma, (After Andrews, 1997).....	13
Figure 9. Generalized isochor of the Red Fork interval. Top of Pink Limestone to top of Inola limestone in Oklahoma, (After Andrews, 1997). Green box highlights study area.	14

Figure 10. Isochor from well data in the study area of the Red Fork interval (top of Pink Limestone to top of Inola limestone). Generally averaging 100 ft as shown by Andrews (1997) with some local maximums of 150 ft. Red lines are faults interpreted from the smaller area covered by the 3D seismic survey..... 15

Figure 11. Generalized structure map of the Pink Limestone in Oklahoma, (After Andrews, 1997). Green box highlights study area. 16

Figure 12. Net sand example. Vertical pink line denotes 75API gamma ray. Dashed uranium stripped gamma ray left of 75API indicates net clean sand highlighted by the green shading. Uranium stripped gamma measures potassium and thorium excluding uranium which can be precipitated by ground water circulation..... 17

Figure 13. Wells (a) and (b) allow a calibration between gamma ray response and spontaneous potential (SP) response. This allows net pay to be picked reliably on older SP logs like well (c)..... 18

Figure 14. Generalized log responses from different depositional environments. Study area includes meandering channels and regressive barrier islands, (After AAPG Wiki). 19

Figure 15. Log responses from the study area. (a) Coarsening up barrier or reworked marine bar and (b) a channel cut with a fluvial fining upward sequence..... 20

Figure 16. Representative west to east inline from the 3D survey. The Checkerboard Limestone is middle Pennsylvanian in age and a continuous shallow marker in this survey. The target Red Fork falls between the Pink Lime and the Inola Lime. The data are of excellent quality and free from shot generated noise at this scale. 25

Figure 17. Zoomed view of Figure 16 with cartoon sand bodies drawn in. The Red Fork sand is evident by the larger trough under the Pink Lime and the higher amplitude of the Pink and Inola Limestone horizons. Also evident is a lower Red Fork episode with a shale stringer separating the two in places. 26

Figure 18. $\frac{1}{4}$ wavelet tuning frequency. Statistical wavelet extracted from Checkerboard to Inola Limestone shows usable frequencies to nearly 140 Hz. Using an average velocity in the Red Fork sand interval of 12,500 ft/s and 135 Hz the $\frac{1}{4}$ wavelength limit to resolution is 23 ft. 27

Figure 19. Well log and synthetics for data used in the inversion. Red Fork interval bound by Pink Lime and Inola Lime (red box). Synthetic using extracted wavelet. 28

Figure 20. Wedge model setup to define tuning frequency. The model is defined by the initial well from Figure 19. That same well is copied to a location 1 mile away and the basal portion of the Red Fork interval is removed until near zero to model the effect of thickness on tuning frequency. 29

Figure 21. Wedge model with wavelet extracted from seismic data; tuning thickness about 20 ft. 30

Figure 22. Representative migrated gathers for the survey (a) before, and (b) after mute and trim statics. Red Fork interval bound in red. Data not phase matched to wells at this state. 31

Figure 23. Extracted statistical wavelet from the input gathers used for inversion (a). Note the gathers provided did not include 5-dimensional interpolation nor any high frequency spectral recovery. After a pass of spectral whitening (b) the temporal resolution are more balanced and improved. 32

Figure 24. Petrophysical analysis over the Red Fork interval showing a clean sand with minimal calcite and roughly 20% shale at 75% water saturation..... 37

Figure 25. Initial fluid substitution parameters obtained from petrophysical analysis shown in Figure 24. 38

Figure 26. (a) compressional sonic data and (b) shear sonic data for (blue) 100% brine, (red) 100% gas, and (green) 100% oil. Red Fork interval highlighted in blue. 39

Figure 27. Synthetic modeled with (a) 100% water, (b) 100% oil, and (c) 100% gas in Red Fork interval bound by the Pink and Inola limestones..... 40

Figure 28. Amplitude data for Red Fork interval with fluid substitutions for well x with (a) original fluid content, (b) 100% brine, (c) 100% oil, (d) and 100% gas. Notice increase in amplitude for water, slight decrease for oil, and a large decrease for gas from initial reservoir fluids. Well locations indicated by arrows and blue traces..... 41

Figure 29. Cross plots of (a) $\ln(Z_s)$ vs. $\ln(Z_p)$ and (b) $\ln(\rho)$ vs. $\ln(Z_p)$. Best fit line added in red. Deviations from the line indicate desired fluid anomalies. (Modified from Russell, 2006). 42

Figure 30. Well tie for the inversion with a .92 correlation with minimal stretching and squeezing. Error mainly contained to top and bottom of the window indicated by yellow lines..... 43

Figure 31. Horizon slice along the lowest impedance value in the Red Fork formation from a post-stack P-wave impedance volume. Input data have 5-dimensional interpolation and bandwidth recovery applied. Red boxes highlight sand filled channels that are not well delineated from the floodplain..... 44

Figure 32. Horizon slice along the lowest impedance value in the Red Fork formation from a pre-stack P-wave impedance volume without 5-dimensional interpolation and bandwidth recovery. Note the better detail the pre-stack inversion yields in the northern main channel sand, the more appropriate lower impedance values for thinner east-west channel, and the southern sand bodies highlighted by red boxes. 45

Figure 33. Horizon slice along the lowest impedance value in the Red Fork formation from a pre-stack P-wave impedance volume. Input data have 5-dimensional interpolation and bandwidth recovery applied. Note the improved delineation of low impedance sand bodies. 46

Figure 34. Most negative curvature co-rendered with variance to differentiate faults from channel edges. 54

Figure 35. Horizon slice along lowest impedance value in the Red Fork formation through the pre-stack P-wave impedance volume with Pink Lime structure. Low impedance coupled with structural highs indicate potential targets (10 ft contours, bold contours at 50 ft and labeled at 100 ft). 55

Figure 36. Horizon slice along lowest impedance value in the Red Fork formation through the pre-stack p-wave impedance volume with Red Fork producing wells. Structural and stratigraphic traps from Figure 35 are confirmed with producing wells. 56

Figure 37. Input volumes used as input to self-organizing maps algorithm. SOM will cluster facies depending on their multi-attribute response. 57

Figure 38. A posterior analysis of SOM clusters using well control separating (d, e) shales appearing brown and light tan (a, b, c) from sands appearing as yellow and light blue. SOM appears to resolve (e) a sandier shale from (d) a more conventional shale.

The sands appear to separate based on (a) a tighter sand vs. (b, c) more porous sands but no clear evidence of gas or oil charged pore space is evident. 58

Figure 39. (a) Net sand (API<75) thickness map, computed from well control only, compared to (b) Z_p along the Red Fork formation. The roughly similar look between the two suggests a statistical correlation. 59

Figure 40. Acoustic impedance response cross plotted with net sand from raster logs. A clear trend is evident with a lower Z_p trending towards higher clean net sand (API<75). 60

Figure 41. (a) Z_p and (b) the converted net sand data computed from the previously derived linear regression ($NET\ SAND = (-0.0091) * Z_p + 290$) 61

Figure 42. Net sand from (a) Z_p linear regression compared to (b) the well log data. Note the higher detail in the area of the isolated sand in the northeast (yellow box) where limited well data are available due to pre 1950's wells with no logs. 62

Figure 43. Net sand from (a) interpolated well data and (b) linear regression using the well data and seismic impedance data. The anomalous area in the northwest of the image comes from a large amount of source and receiver gaps due to survey obstacles (Figure 44). 63

Figure 44. South to North crossline highlighting the near surface cultural moves (red polygon) from the existing producing field. Map view with red box outlining impacted area. 5-dimensional interpolation is able to predict the structural nature of the image but without enough real data due to the survey obstacles and the proximity to survey boundary it is unable to accurately predict the amplitudes. 64

Figure 45. (a) Minimum Z_p value along the Red Fork interval with Pink Lime structural contours compared to (b) net sand derived from the linear regression with Pink Lime structure. 65

Figure 46. Acoustic impedance response cross plotted with net sand from raster logs. Confirmation that the 5-dimensional interpolation and spectral enhancement (a) gives a more correct result than without (b). 66

Figure 47. (a) Acoustic impedance response cross plotted with net sand from raster logs compared to (b) net sand calculated by removing and predicting each well from surrounding well data. 6 ft. difference in error between each method lends confidence to net sand from Z_p 67

Figure 48. Map view of Red Fork sand body with drilled wells. Figure 49 shows well to well cross section highlighted in turquoise. Horizontal well highlighted in red arrow is a recompletion candidate. Red lines indicate faults. Red stars indicate Red Fork producers. Green text reports cumulative oil production, red text cumulative gas production. 68

Figure 49. Well to well cross section from map in figure 48. Highlighting the structural trap and the stratigraphic pinch out at A'. Net sand colored in pink. 69

Figure 50. Red Fork interval from the horizontal recompletion candidate. Notice the significant gas show, oil cut, and visible porosity. The better show also appears deeper in the sand body. 70

Figure 51. (a) White box highlights intersection of horizontal wellbore and the Red Fork formation and (b) the special location highlighted by white line. Note that (a) shows an upper and lower Red Fork sand corresponding to (c) an offset well log showing an

upper and lower sand separated by a shale break. The sands appear to be compartmentalized as indicated by the better oil cut and gas show in the lower sand indicated by the mud log (Figure 50). 71

Figure 52. Hixson #1 (3313'-3319') showing basal shale with erosional contact with large rip up clasts. 12" ruler for scale..... 72

Figure 53. Hixson #1 (3303'-3313') showing a general coarsening up trend. Grain sizes are generally consistent, sub rounded, sub angular. Coarsening up log signature appears from fewer clasts in the matrix. 12" ruler for scale. 73

Figure 54. Hixson #1 (3293'-3303') showing coarsening up sequence with an erosional storm deposit at roughly 3295.3' below which corresponds to the cleanest gamma response and highest inferred porosity/permeability. Erosional surface evident at 3295.2' with abundant clasts again. 3294' is a relative thick shale package that could serve as a flow barrier. 12" ruler for scale..... 74

Figure 55. Hixson #1 (3283'-3293') Abundant clasts with a smaller fluvial interval that is low in mud content. Water sprayed on core highlights mud content in the abundant ripple sets from 3284'-3286.5'. 12" ruler for scale. 75

Figure 56. Two appealing targets for new drilling are (a) an isolated sand body similar to the main larger sand body and (b) a completely isolated sand body. Note that the setup is similar to the proven sand with equivalent net sand values, a similar structural position, and a stratigraphic pinch out for body (a). Body (b) is a riskier option but with upside potential for production..... 76

Figure 57. Prospective sand body flanked by dry holes. Deep resistivity values are (1) 2 ohm, (2) 2.5 ohm, and (3) 5 ohm. (a) Map view shows the relative position of the wells.

Assuming 16% porosity from the well used in the inversion workflow and a formation water resistivity of 0.04 ohm the water saturation for well (1) is .72, (2) .64, and (3) .45.

..... 77

Figure 58. Red Fork time horizon with Z_p values in color. Seismic vertically exaggerated 25x. Evidence that the sand body does dip to the south-southwest. 78

Figure 59. (a) White box highlights undrilled sand body similar to offsetting drilled body highlighted by star. (b) Well log from offsetting body shows 40 ft. of net sand with the upper 2/3s showing 15 ohm yielding 0.26 water saturation. No cumulative production is available but the wells initial production was 25 barrels of oil and 250 MCF of gas. 79

Figure 60. (a) White box highlights undrilled up dip portion of productive field. (b) Cross section A-A' (highlighted in light blue on map). Down dip portions of sand body non productive with the last well out of the sand body showing no sand in Red Fork interval (Pink Lime to Inola Lime). Field has produced over 2 million barrels of oil from known production. 80

Figure 61. Horizon slices through a coherence volume in (a) a dataset without 5D interpolation and (b) a dataset with 5D interpolation. Notice the (Red boxes) missing faults in the 5D interpolated volume that is noticeable in the data without 5D interpolation. Also evident are the missing and difficult to see (Green arrows) narrow channels. The 5D dataset does help the (Orange arrows) edge of the data. 86

Abstract

Utilizing a modern 3D survey acquired for a deeper resource play one can also examine potential drilling hazards and behind pipe pay in shallower formations. This study concentrates on the Red Fork sands that have been one of the major Pennsylvanian sandstone targets since the early 1900s. Many historical producers in this study had been found prior to any seismic data, while all of the producers were drilled prior to access to 3D seismic.

Armed with a modern 3D seismic survey, opportunities exist to evaluate overlooked and under drilled sand bodies. Using state of the art 5D interpolation and pre-stack inversion, justified by the deeper resource plays, allows one to image and evaluate the subtler features of more conventional sandstone reservoirs above the resource target formations. Well logs and historical production data aid in evaluating any potential upside potential for hydrocarbons that has remained undrilled.

Pre-stack acoustic impedance inversion highlights previously untapped reserves in the Red Fork formation that can be commercially viable. 5-dimensional trace interpolation regularizes the data and is instrumental in refining the impedance estimation and overall image quality of the seismic data. This allows for a better statistical correlation of Z_p to net sand thickness allowing it to be used as a proxy in identifying potential targets.

CHAPTER I: INTRODUCTION

With the prevalence of resource plays stemming from horizontal drilling and hydraulic fracturing, the Cherokee Platform of Northern Oklahoma has seen a resurgence of activity resulting in an economic “unconventional” Mississippian Lime play in the suppressed oil price environment. Exploration and production operators have been producing oil and gas from Pennsylvanian aged sands on the Cherokee Platform for over 100 years (Mills-Bullard 1928). With the new Woodford and Mississippi Lime resource plays that economically justify the acquisition of modern wide azimuth 3D seismic data, one can now image more subtle components of the previous conventional plays that were tagged by vertical wells and sparse 2D seismic data.

Landing horizontal wells in the deeper resource plays requires careful mapping of potential geohazards in the shallow section, which may encounter gas or result in the loss of expensive drilling mud. At the very least, the operator should modify the drill path to avoid such hazards (Figure 1). However, these “hazards” may hold economic reserves, particularly if the infrastructure and drilling has been previously justified by the deeper resource play. Such shallow targets that could hold reserves that the operator can target with new vertical drilling or catalogue an inventory of horizontal wells that could be recompleted at the shallower objective after the deeper reservoir plays out.

Seismic reflection data are used to image the subsurface indirectly (Zhou 2014), where ideally the reflected waves correspond to geological boundaries of changing lithologies (Russell 2006). Reflections are generated wherever there is a change in P-velocity, v_P , S-velocity, v_S , and density, ρ , between the different geologic layers.

With stacked data, one is only able to estimate P-impedances, $Z_P = \rho v_P$. In contrast, pre-stack migrated seismic data provides measures of amplitude variation with offset (AVO). As Del Moro (2012) showed for a Red Fork play to the west, coupled with well log control and an accurate low frequency model, these AVO effects can be pre-stack inverted to estimate not only Z_P , but also shear wave impedance, $Z_S = \rho v_S$. For high quality data and shallower targets (more specifically surveys that afford larger angles of incidence), one may also estimate the density, ρ . While the elastic parameter pair (Z_P, Z_S) or (Z_P, ν) where ν is Poisson's ratio are commonly used in conventional clastic reservoirs, particularly in more unconsolidated rocks, the pair of $(\lambda\rho, \mu\rho)$ is more commonly used in more lithified rocks like shale resource and limestone plays (Goodway, 2009). The information content in these alternative cross plots is identical, but the breakout of different lithologies slightly different. Foster (2010) shows that these estimations provide greater insight to the mechanical properties of lithified Paleozoic rocks.

5-dimensional trace interpolation allows an interpreter to obtain a better image when surface constraints hamper regular seismic data acquisition (Trad, 2009). Downton (2008) also shows the impact interpolating the data has on overall signal to noise ratio and how regularizing the azimuthal and offset bins while preserving AVO has on improving a pre-stack impedance inversion.

I hypothesize that pre-stack impedance inversion will yield a clear image that contrasts porous sandstone reservoirs in the Red Fork formation. Because impedance data is correlated to porosity, I anticipate a correlation between acoustic impedance and net sandstone thickness. With these correlations, I then hope to further refine my

reservoir image utilizing self-organizing mapping algorithms to differentiate sands from shales, channel sands from marine sands, and producing sands from non-producing sands. These data can then be used in exploration to high-grade prospective locations.

I begin my thesis in Chapter 2 with a review of the geologic setting, focusing on the Red Fork interval. Next, in chapter 3, I summarize the 3D seismic, well control, and production data available for the study. With the key wells tied to the 3D seismic data volume, I then perform pre-stack and post stack seismic inversions in Chapter 4. These data are then used to generate rock property volumes aiding in identifying potential sandstone bodies.

In Chapter 5 I integrate the impedance volumes with conventional time structure maps generated from seismic time horizons depth converted with well control. I also generate geometric attributes to form an integrated interpretation for the Red Fork interval. I use self-organizing maps to better delineate facies of interest. In addition to 3D visualization, I validate my interpretation using historical production data from numerous Red Fork wells.

I conclude with a summary of the workflow and its applicability to the Red Fork play in Oklahoma and shallower targets in general.

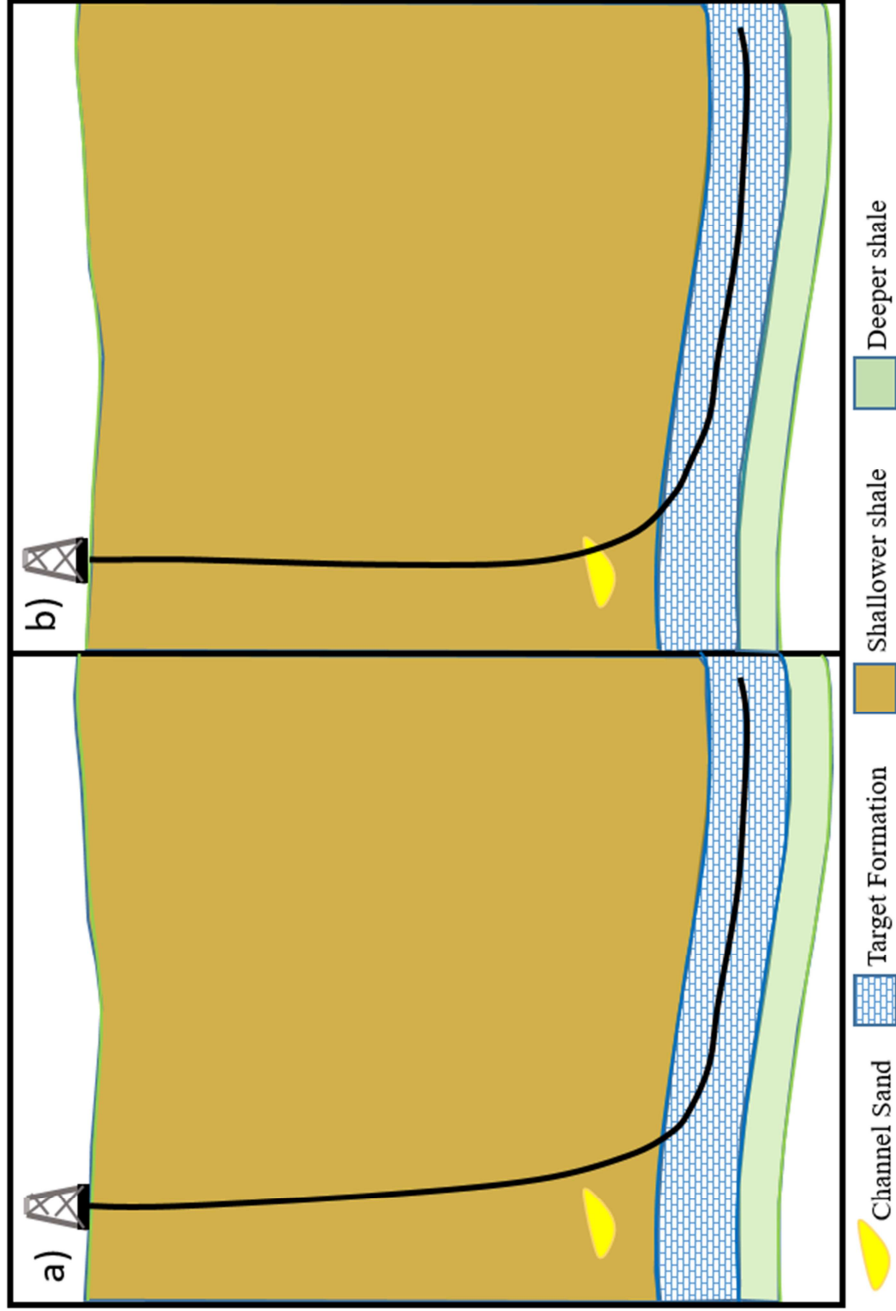


Figure 1. Vertically exaggerated cartoon showing (a) an original horizontal wellbore design and (b) a re-worked plan to intercept a shallow sand.

CHAPTER II: GEOLOGIC OVERVIEW

Figure 2 highlights the early Pennsylvanian period. Specifically, the Red Fork sand stone from the Krebs group will be the focus for this study. The Red Fork deposition interval is underlain by the Inola Limestone and overlain by the Pink Limestone. Figure 3 shows the location of the study area within northeastern Oklahoma, which is roughly bound by the Nemaha Ridge to the west and the Wilzetta Fault to the east (Figure 4). After deposition of the Woodford shale and Mississippi limestone the platform was uplifted. This uplift exposed the Mississippian formation on the platform and created the early Pennsylvanian unconformity at the top of the Mississippi lime (Figure 5). This accounts for the thinner Mississippian section on the Platform and the missing early Pennsylvanian formations. Figure 6 shows the Des Moinesian depositional environment. The study interval focuses on the Krebs group, specifically the Red Fork sandstone with the local depositional environment being influenced by the compacting shales around the deposition of the Bartlesville sandstone (Figure 7). Accommodation space created by the compacting shales from the Bartlesville episode provided a preferential path for the Red Fork sand depositions.

Andrews (1997) describes the Red Fork sandstone as one of the most widespread Cherokee plays in Oklahoma (Figure 8). Regional thickness (Figure 9) for the Red Fork interval is generally 100 feet or less on the Cherokee Platform. Figure 10 shows the local Red Fork interval in the study area. The high stand depositions on the platform are generally limited to one or two episodes unlike in the Anadarko Basin where there are up to four identified Red Fork episodes (Andrews 1997). Post

deposition structural traps can be seen by identifying and mapping the overlying Pink Limestone (Figure 11).

Figure 12 is the modern type log for the study area. Spectral gamma ray logs measure uranium, potassium, and thorium. This allows for the removal of the uranium component that can be influenced by uranium salts migrating into the formation from water giving a false hotter gamma response (Petro Wiki 2012). However, in practice, there is only one spectral gamma ray log in the survey and the difference in net sand thickness between the full spectrum gamma and the uranium stripped gamma is only two feet. This implies negligible effects of uranium salt migration and I can confidently pick net sands on standard gamma ray logs. With this definition, the shaded green in Figure 12 is my ideal definition of clean net sand where the stripped gamma response is lower than 75 API. Clean net sand is my definition for reservoir quality sandstone for the study area. Some older electronic logs include only spontaneous potential (SP) curve. Here, the net sand is picked in a similar manner calibrated from multiple logs that contain both gamma and SP curves (Figure 13).

Figure 14 shows idealized log responses from multiple depositional environments. The environments in the study area include meandering channels and regressive barrier islands or marine bar sands. Figure 15 shows a representative log for each depositional environment.

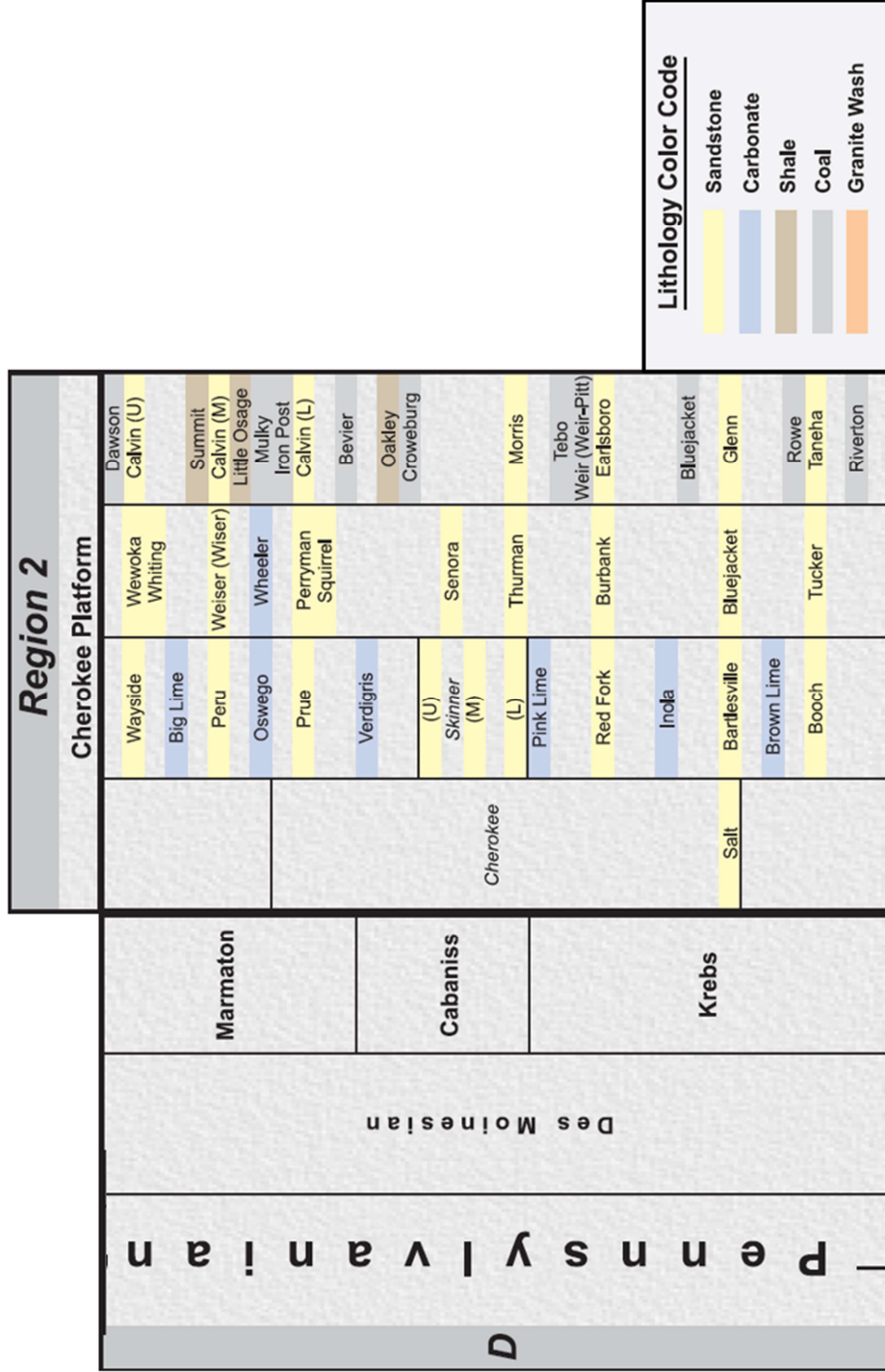


Figure 2. Stratigraphic chart for the Cherokee Platform, Des Moinesian series. (Modified from Keller, 2008).

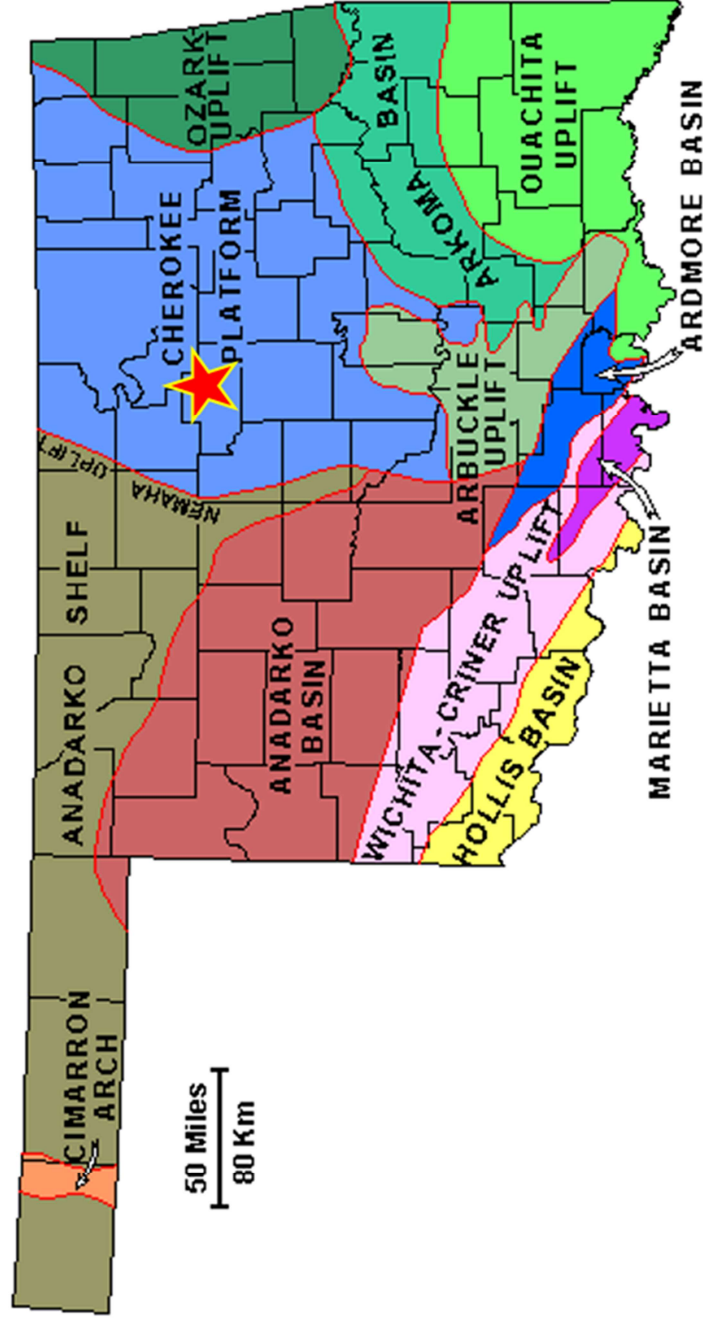


Figure 3. Oklahoma geologic provinces. Red star highlights the Cherokee Platform in which the survey resides. (Modified from Northcutt and Campbell, 1988).

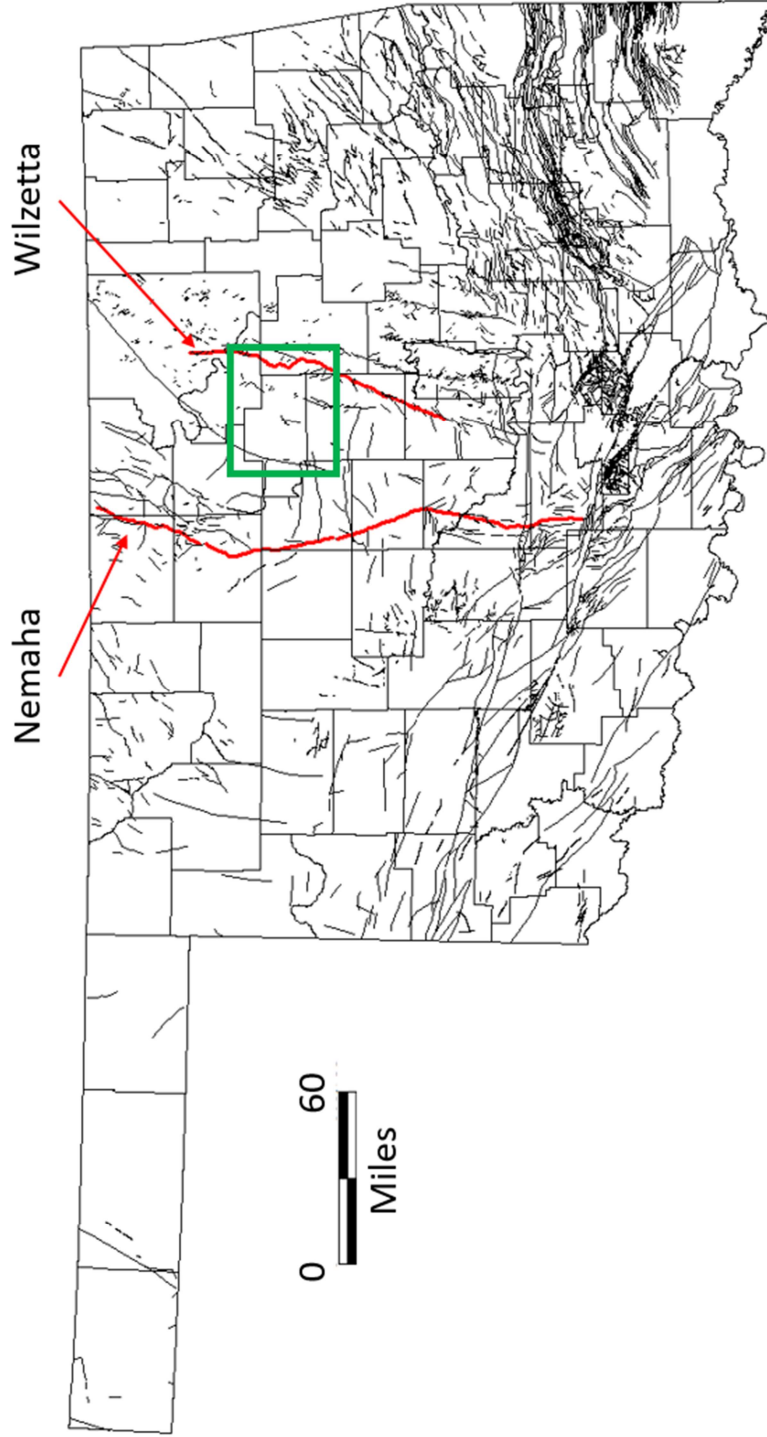


Figure 4. Location of Nemaha and Wilzetta Faults in Oklahoma Geologic Survey database of faults. (Wiltzetta from Way, 1968). Green box highlights study area.

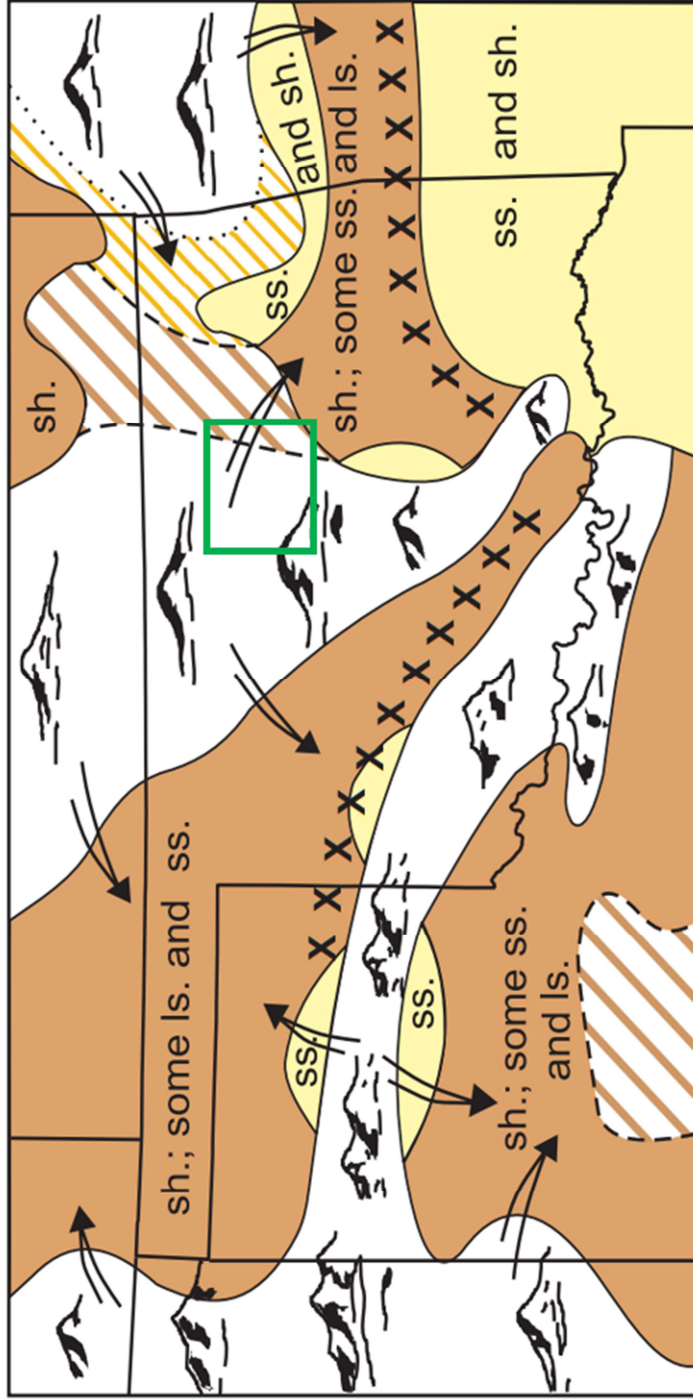


Figure 5. Principle rock types of early Pennsylvanian (Morrow and Atokan) age in Oklahoma (After Johnson, 2008). Green box highlights study area.

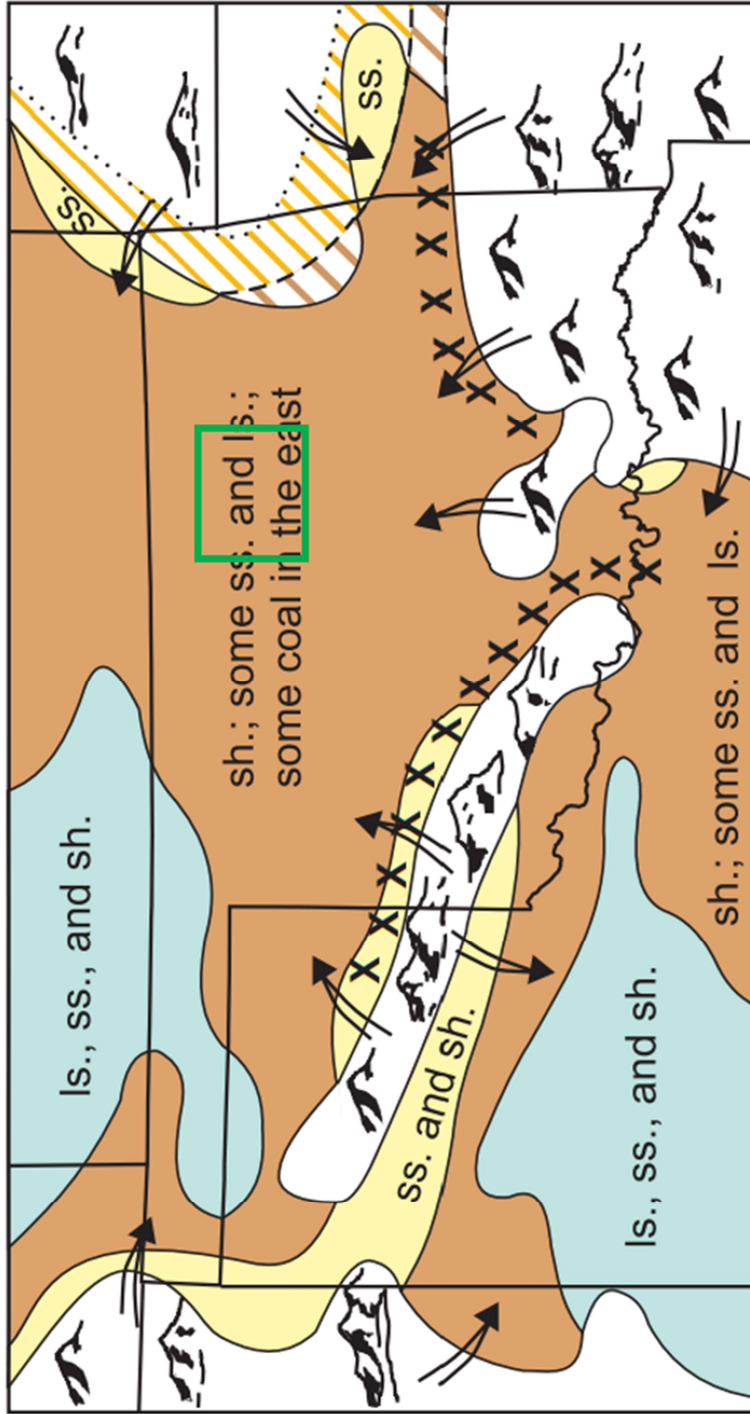


Figure 6. Principle rock types of middle Pennsylvanian (Des Moinesian) age in Oklahoma (After Johnson, 2008). Green box highlights study area.

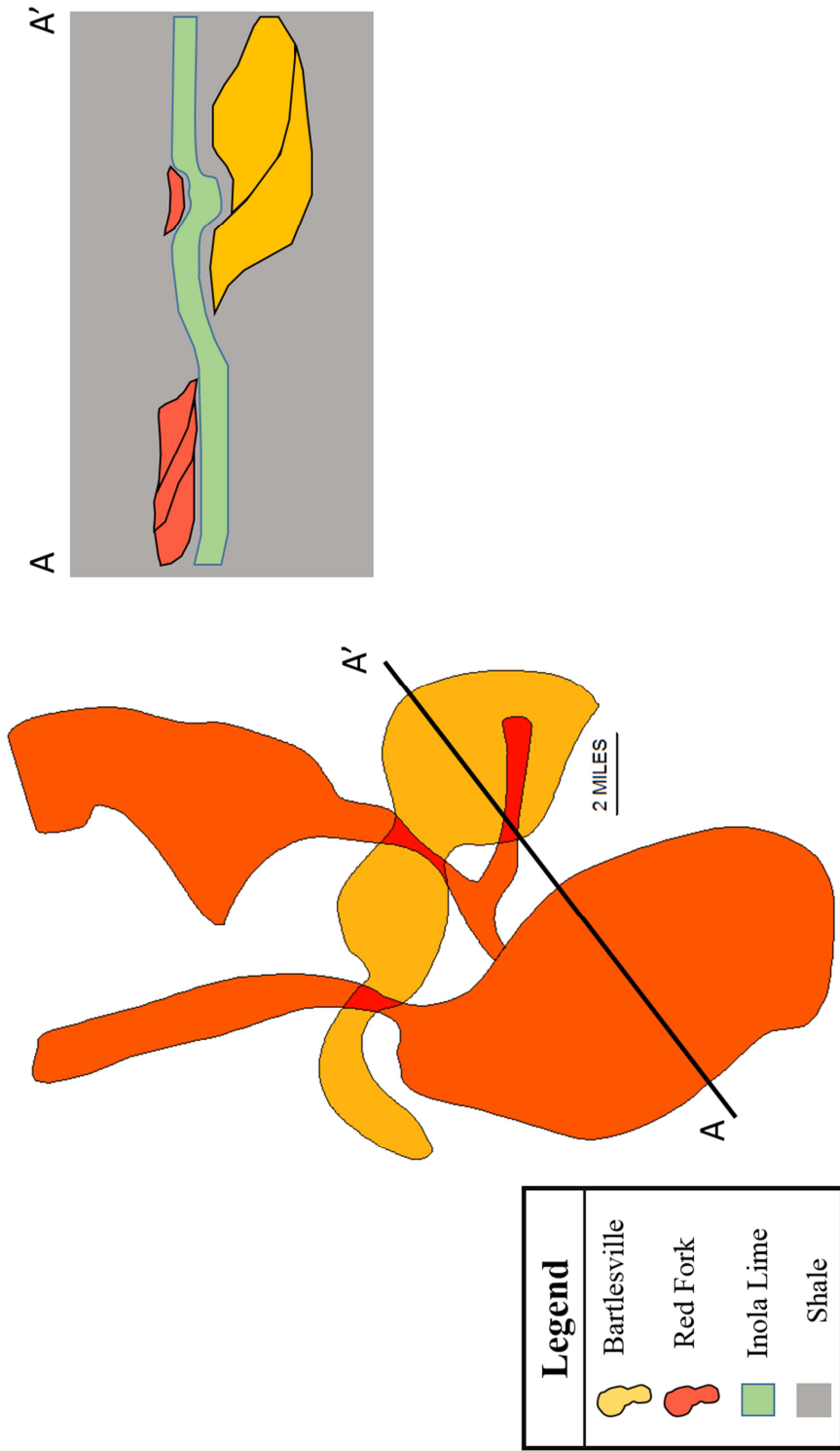


Figure 7. Generalized cartoon highlighting the effects of differential compaction between the Bartlesville sandstone and surrounding shale depositions. The preferential lows created by the compacting shales set up accommodation space for the deposition of the Red Fork sandstone. Note the limited stacked sands.

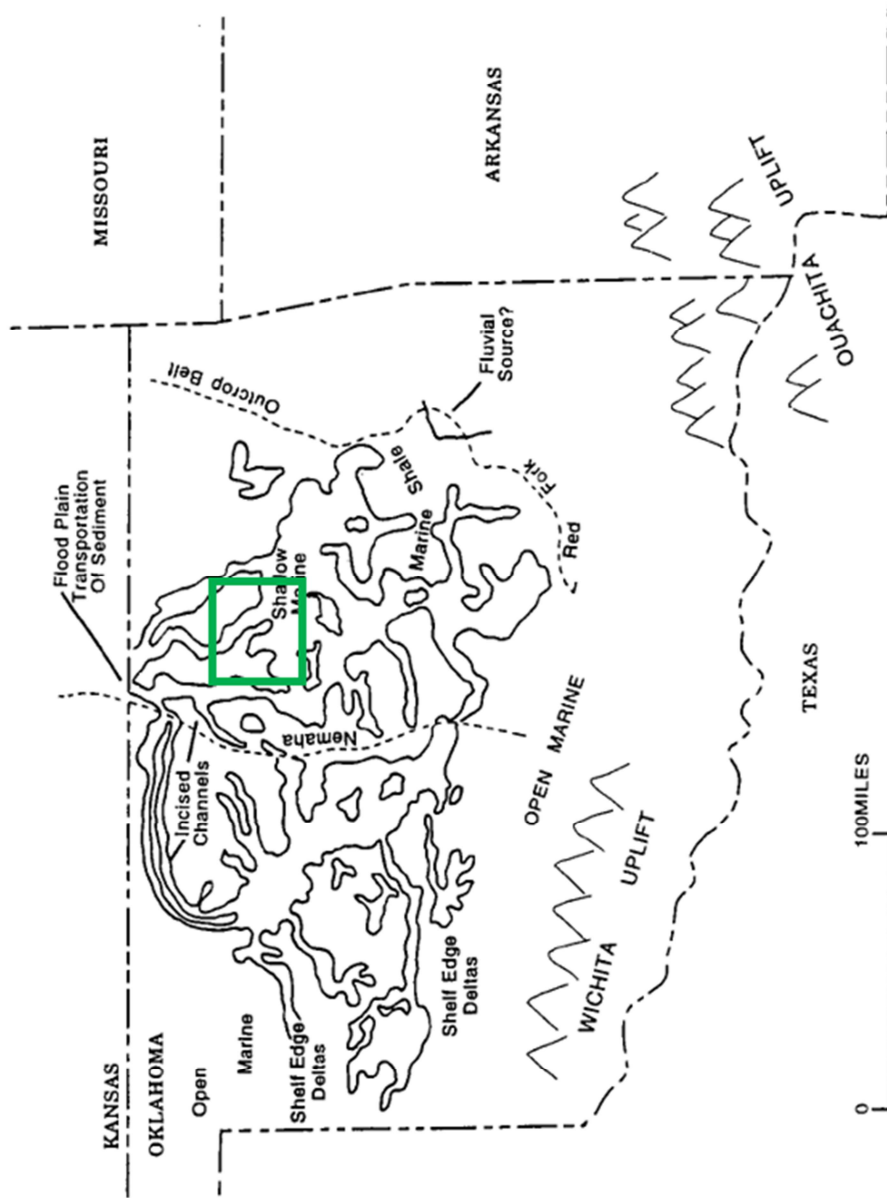


Figure 8. Generalized depositional environments of the Red Fork sandstone in Oklahoma, (After Andrews, 1997).

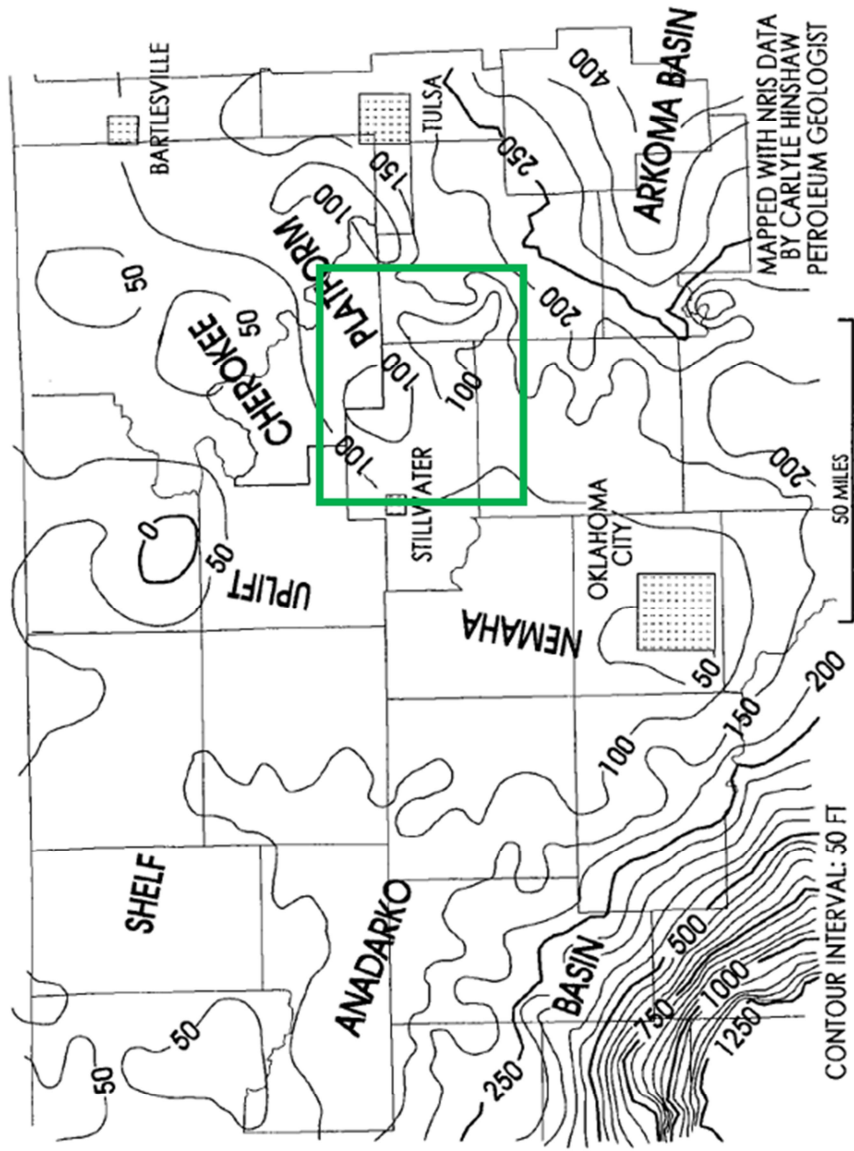


Figure 9. Generalized isochor of the Red Fork interval. Top of Pink Limestone to top of Inola limestone in Oklahoma, (After Andrews, 1997).
Green box highlights study area.

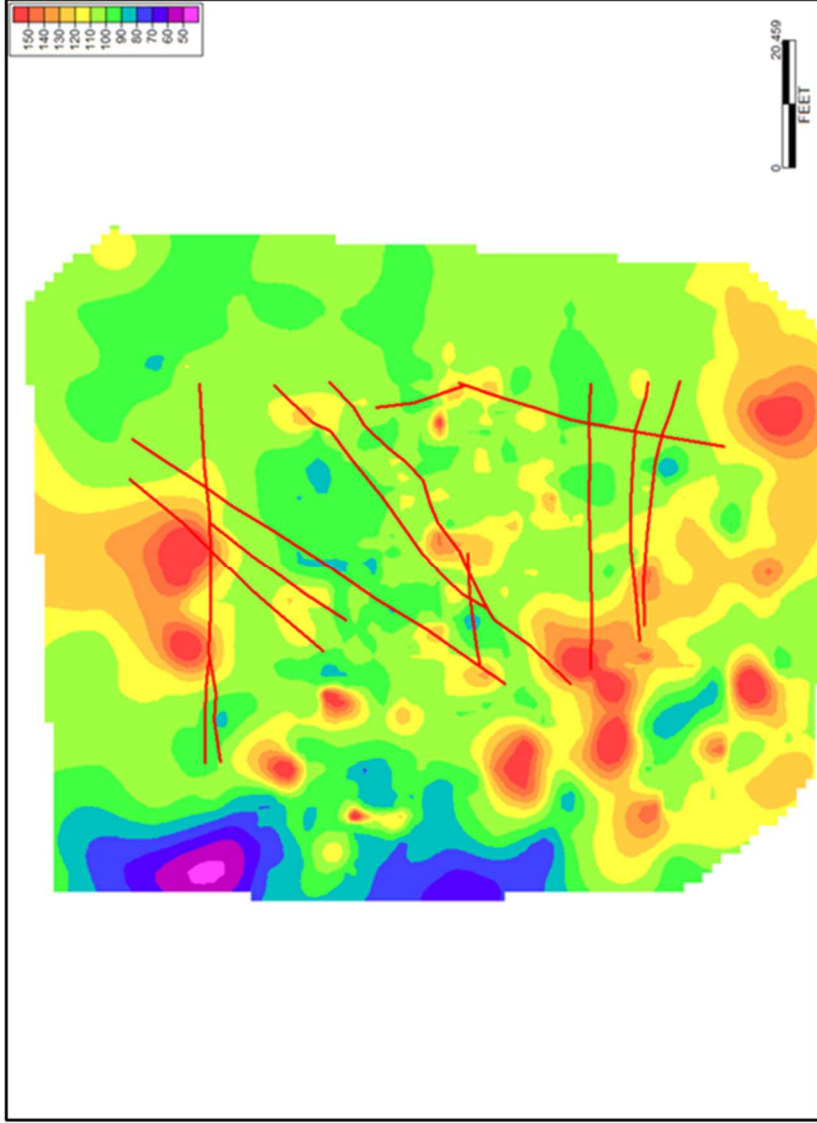


Figure 10. Isochor from well data in the study area of the Red Fork interval (top of Pink Limestone to top of Inola limestone). Generally averaging 100 ft as shown by Andrews (1997) with some local maximums of 150 ft. Red lines are faults interpreted from the smaller area covered by the 3D seismic survey.

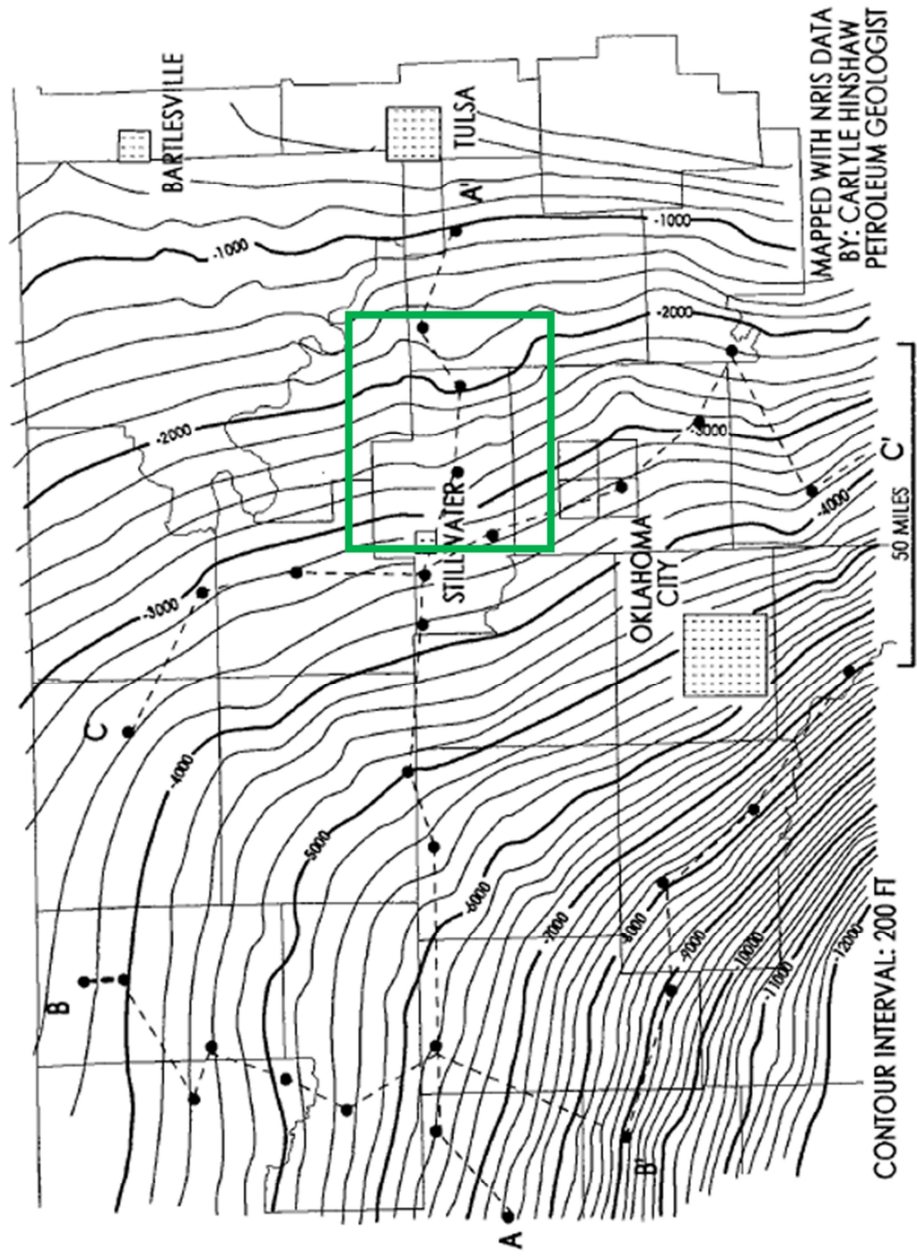


Figure 11. Generalized structure map of the Pink Limestone in Oklahoma, (After Andrews, 1997). Green box highlights study area.

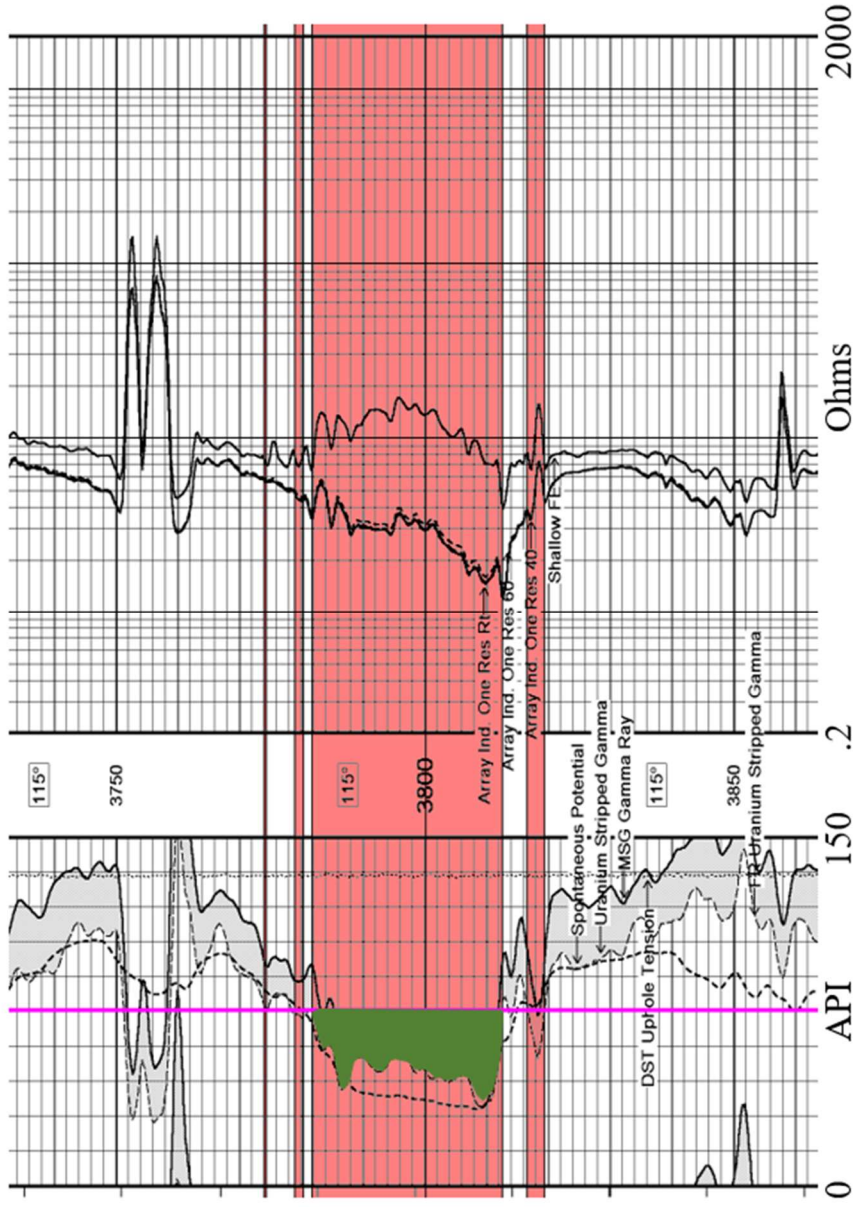


Figure 12. Net sand example. Vertical pink line denotes 75API gamma ray. Dashed uranium stripped gamma ray left of 75API indicates net clean sand highlighted by the green shading. Uranium stripped gamma measures potassium and thorium excluding uranium which can be precipitated by ground water circulation.

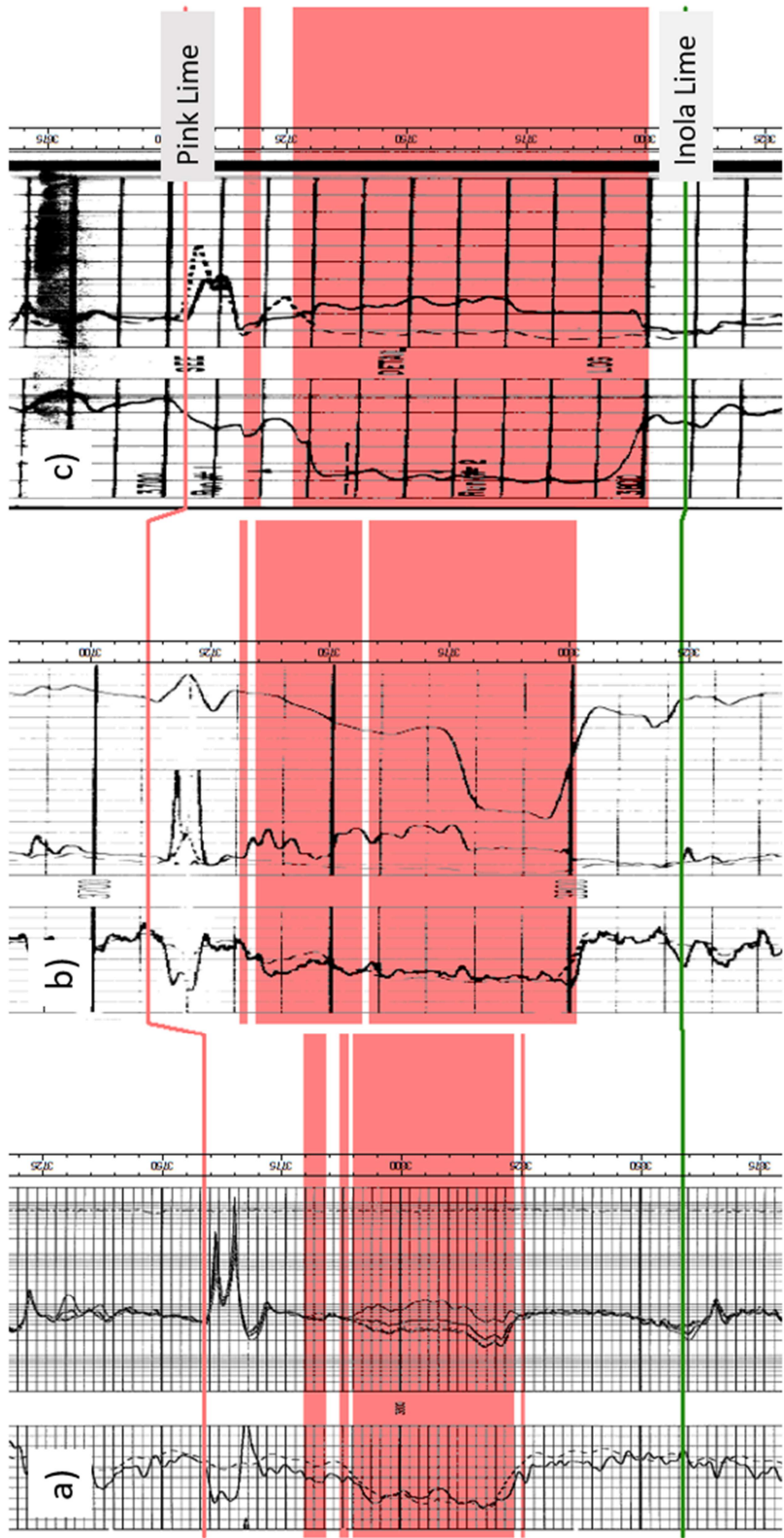


Figure 13. Wells (a) and (b) allow a calibration between gamma ray response and spontaneous potential (SP) response. This allows net pay to be picked reliably on older SP logs like well (c).

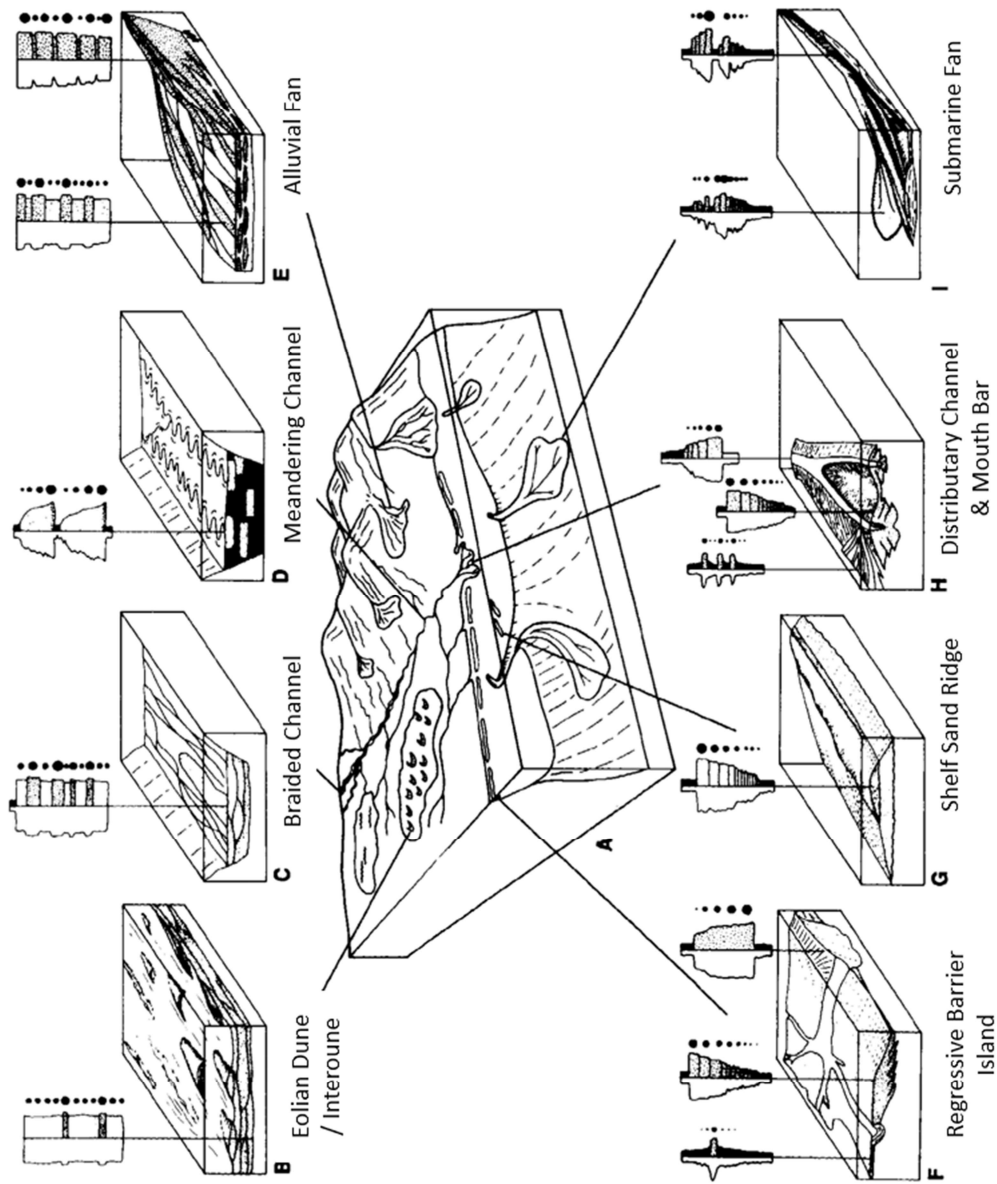


Figure 14. Generalized log responses from different depositional environments. Study area includes meandering channels and regressive barrier islands, (After AAPG Wiki).

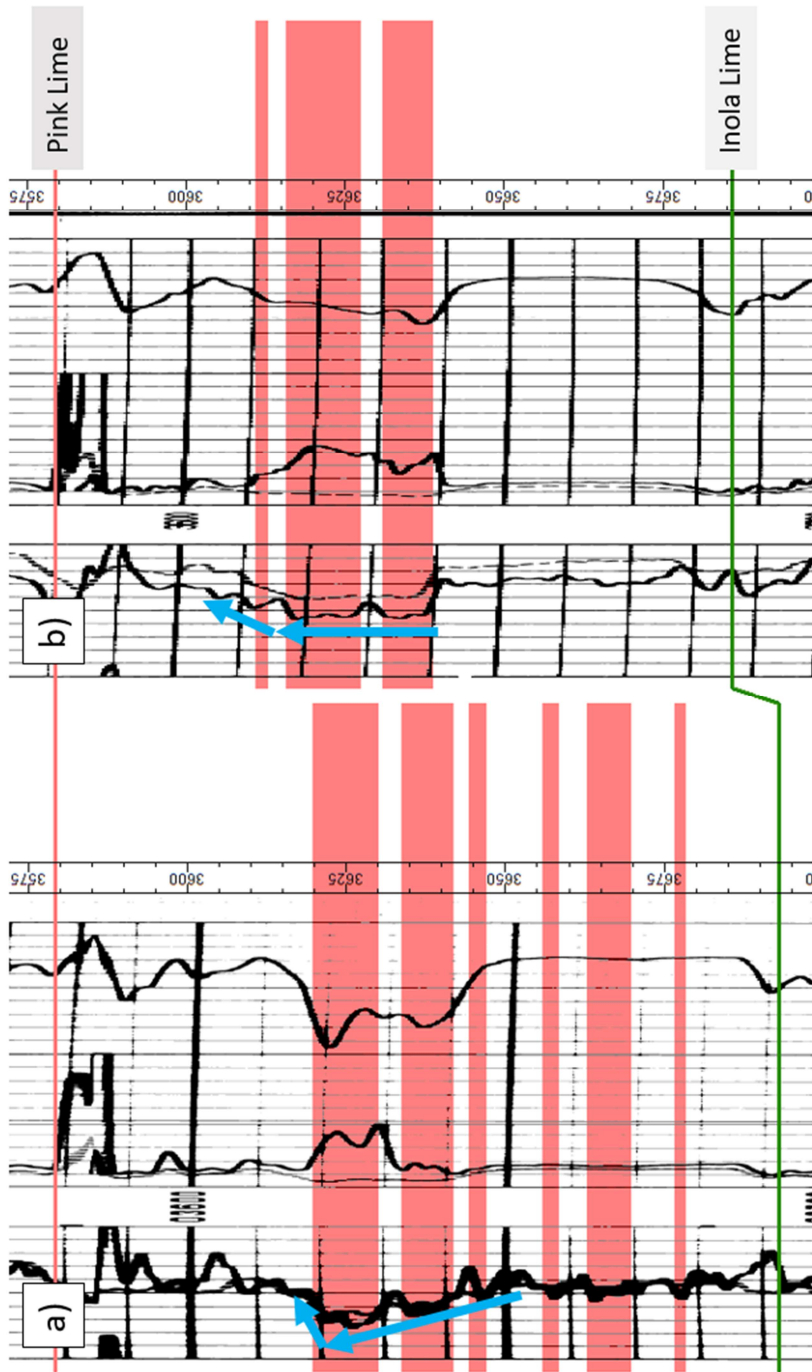


Figure 15. Log responses from the study area. (a) Coarsening up barrier or reworked marine bar and (b) a channel cut with a fluvial fining upward sequence.

CHAPTER III: SEISMIC DATA QUALITY, DATA CONDITIONING, AND WELL CONTROL

The seismic data for the study are of modern vintage acquired in 2014. The data were acquired with a wide azimuthal design and a high frequency effort (Table 1). The company elected to use predominately Vibroseis sources with dynamite infill to minimize acquisition gaps with total project costs in mind. The data were with the goal of preserving amplitude and special attention to phase matching the different sources.

The data for the study was processed with the ultimate goal of pre-stack inversion in mind. Aisenberg (2013) shows the importance that careful processing plays in the confidence of the inverted data. Quality control of the shot gathers were followed by a relative amplitude scaling and surface consistent deconvolution. Tomographic refraction statics preceded velocity analysis and surface consistent residual statics. 5-dimensional trace interpolation was performed on the input to migration velocity analysis and the final pre-stack migrated dataset.

Figure 16 shows a representative line through the 3D survey. The data contain minimal noise and are of exceptional quality. Looking in more detail, Figure 17 highlights the channel visible on the stacked data. In this area, there are two Red Fork episodes visible that appear compartmentalized to the east and west but could be treated as one flow unit in the heart of the channel where there appears to be no shale separation. As evident by viewing the stacked data, picking the sand top, base, and the shale stringers is difficult. Barber (2010) showed picking the Red Fork to be easier and more consistent on inverted data.

The vertical resolution is roughly defined as the $\frac{1}{4}$ wavelength of the data (Zohu 2014). Figure 18 describes the bandwidth and velocity for the Red Fork interval. Averaging the velocity over that interval gives 12,500 ft/s with 135Hz signal yielding a calculated $\frac{1}{4}$ wavelength of 23ft.

I constructed a simple wedge model to quantify the seismic response that can be seen from the sand and what the data driven tuning frequency may be. Figure 19 shows the well used for the wedge model and eventually the inversions. Figure 20 lays out the wedge model. I use the original thickness from the well, then copy that well to a location with roughly a mile in separation. I can then edit the lower portion of the Red Fork until it reaches zero sand in the transposed well. Using a wavelet extracted from the seismic data, the shallow nature of the study area allows for high frequency penetration to the Red Fork yielding a tuning frequency of roughly 20 ft in thickness, matching the calculated $\frac{1}{4}$ wavelength (Figure 21).

The company also provided pre-stack migrated gathers were not 5D interpolated. Figure 22 shows a before and after comparison between the original data and the conditioned gathers to be used as input to pre-stack impedance inversion. The data were muted followed by a light application of trim statics. Spectral balancing was also applied to increase the temporal resolution and balance the spectrum (Figure 23).

The study area is both well data rich and poor. There are 6279 wells within the study area of which 2404 have a variety of raster logs and 154 have digital gamma ray logs. 1945 of these logs cover the Pink Lime to the Inola Limestone which encompass the Red Fork formation (Figure 2). Of these only 12 wells have sonic logs, 2 with compressional logs over the Red Fork formation and only a single shear wave sonic log.

These data, with the seismic data, provide measures of the thickness and structure of the Red Fork formation and constrain the net sand values. There are also 203 wells that have cumulative production data from the Red Fork formation to aid in evaluating potential prospective locations.

Receiver Spacing:	165 ft
Receiver Line Spacing:	660 ft
Source Spacing:	165 ft
Source Line Spacing:	660 ft
Source Type:	Vibrator with dynamite infill
Sweep Frequencies:	4-134Hz Linear Sweep
Trace Length:	3 s
Sample Rate:	2 ms
Bin Size:	82.5 ft X 82.5 ft
Recording Patch:	20 lines x 96 channels per line
Offset Coverage:	82.5 ft – 7,590 ft

Table 1. Acquisition Parameters

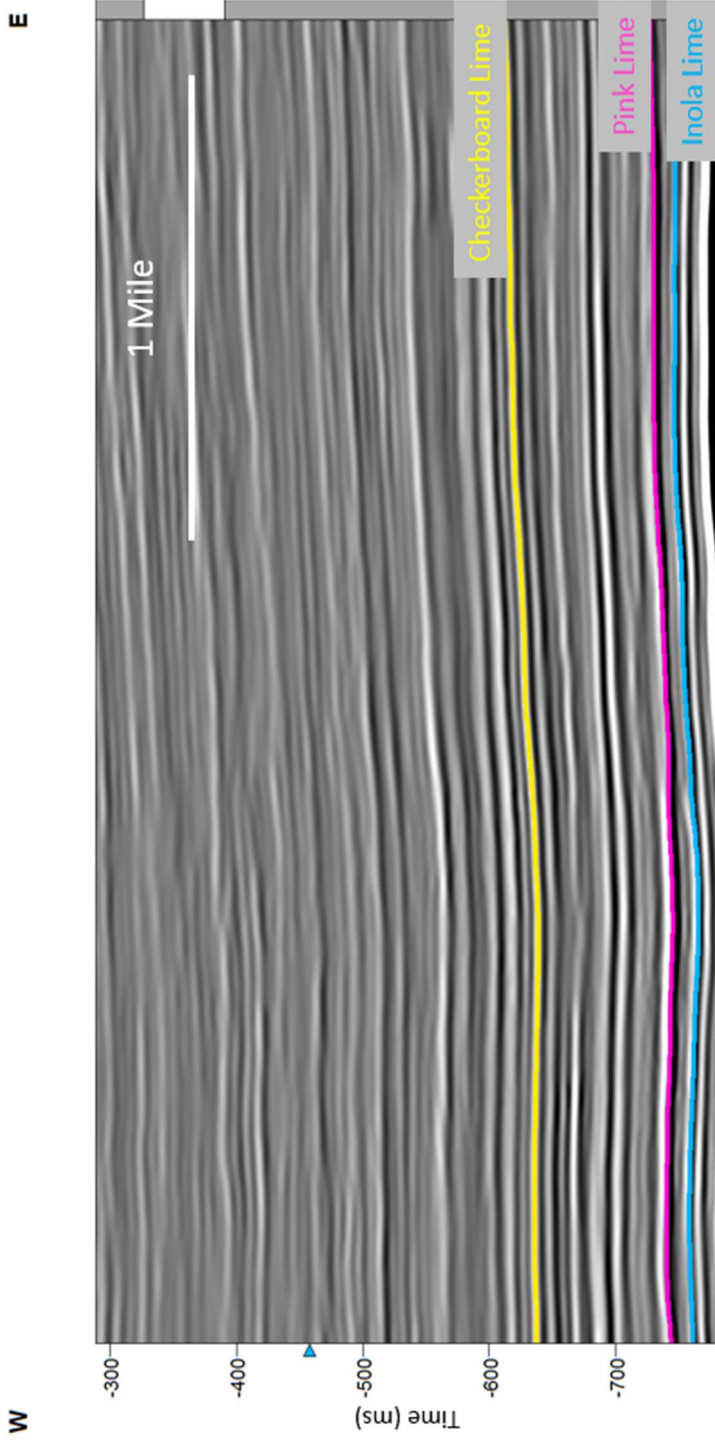


Figure 16. Representative west to east inline from the 3D survey. The Checkerboard Limestone is middle Pennsylvanian in age and a continuous shallow marker in this survey. The target Red Fork falls between the Pink Lime and the Inola Lime. The data are of excellent quality and free from shot generated noise at this scale.

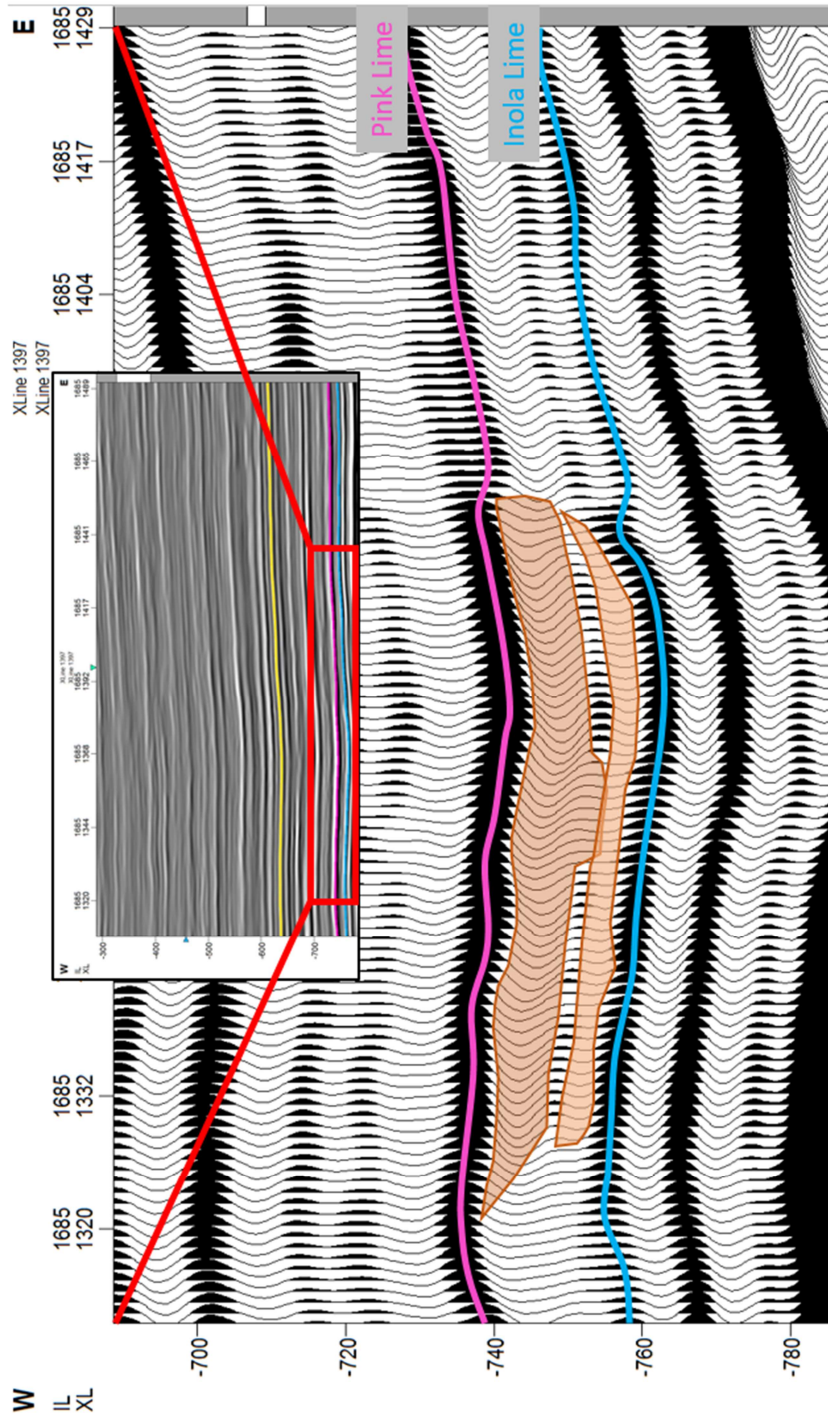
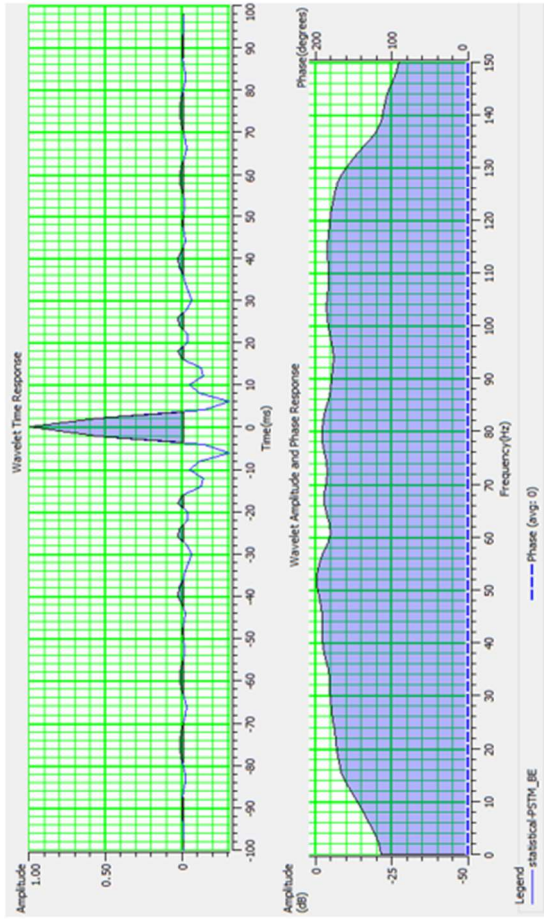


Figure 17. Zoomed view of Figure 16 with cartoon sand bodies drawn in. The Red Fork sand is evident by the larger trough under the Pink Lime and the higher amplitude of the Pink and Inola Limestone horizons. Also evident is a lower Red Fork episode with a shale stringer separating the two in places.



$$\lambda = V/F = \frac{12,500 \text{ ft/s}}{135 \text{ Hz}} = 92.5 \text{ ft}$$

$$\lambda / 4 = 23 \text{ ft}$$

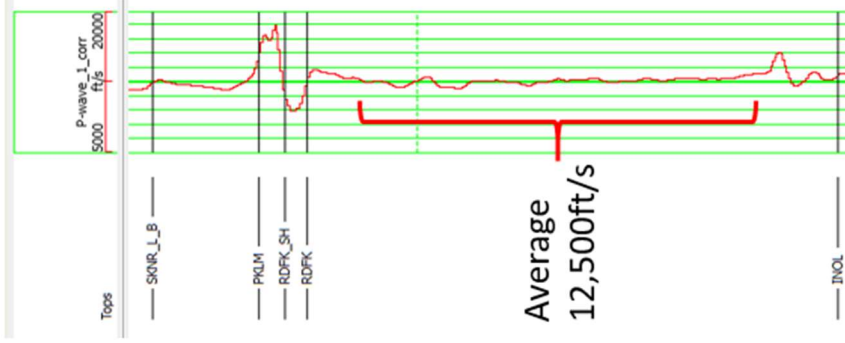


Figure 18. $\frac{1}{4}$ wavelet tuning frequency. Statistical wavelet extracted from Checkerboard to Inola Limestone shows usable frequencies to nearly 140 Hz. Using an average velocity in the Red Fork sand interval of 12,500 ft/s and 135 Hz the $\frac{1}{4}$ wavelength limit to resolution is 23 ft.

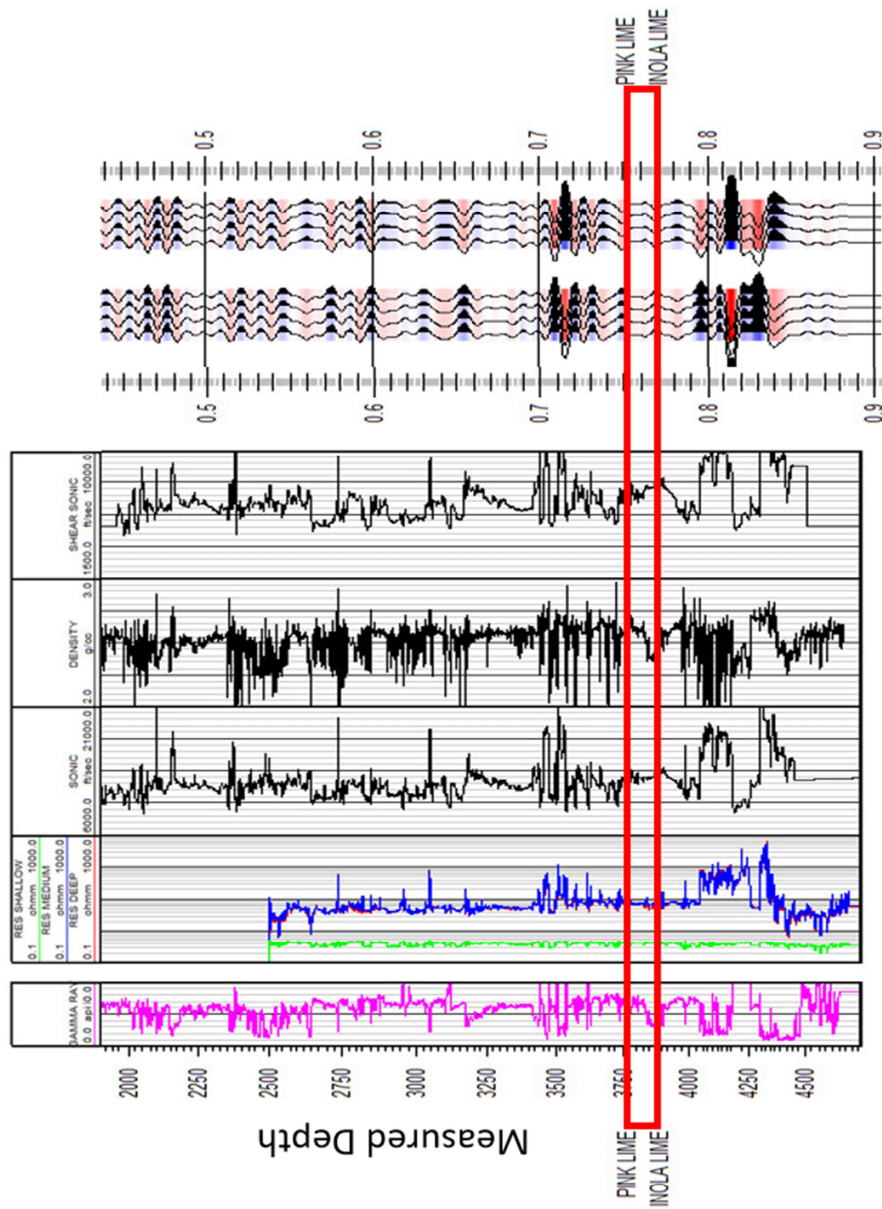


Figure 19. Well log and synthetics for data used in the inversion. Red Fork interval bound by Pink Lime and Inola Lime (red box). Synthetic using extracted wavelet.

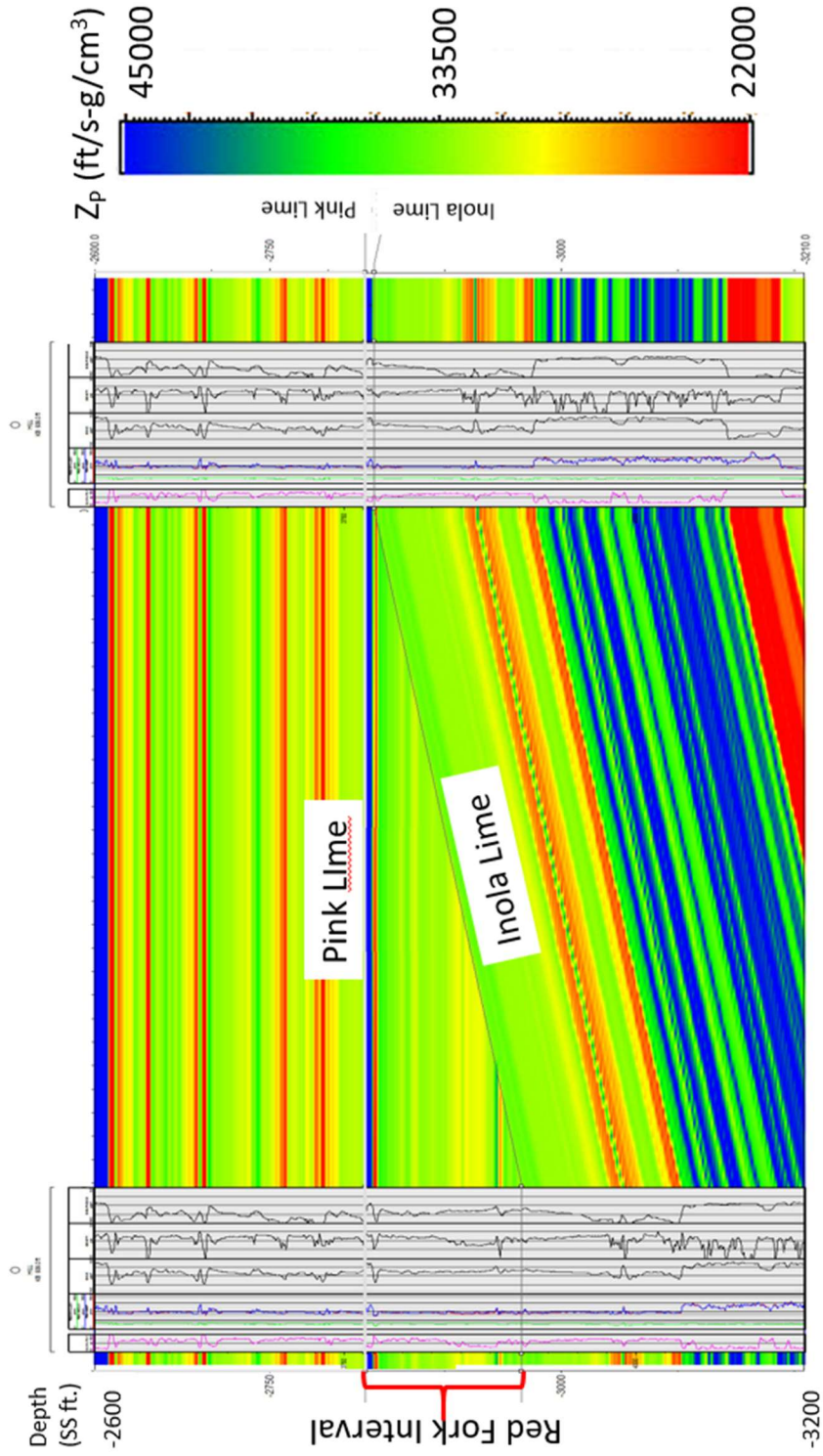


Figure 20. Wedge model setup to define tuning frequency. The model is defined by the initial well from Figure 19. That same well is copied to a location 1 mile away and the basal portion of the Red Fork interval is removed until near zero to model the effect of thickness on tuning frequency.

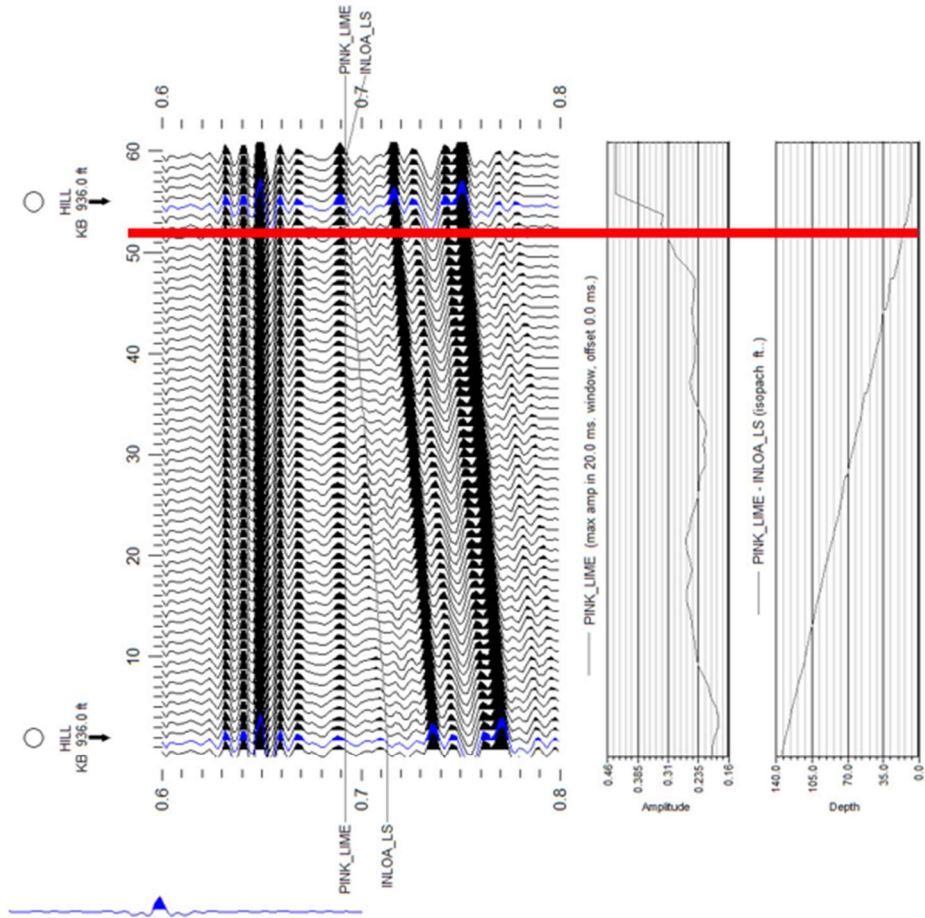


Figure 21. Wedge model with wavelet extracted from seismic data; tuning thickness is about 20 ft.

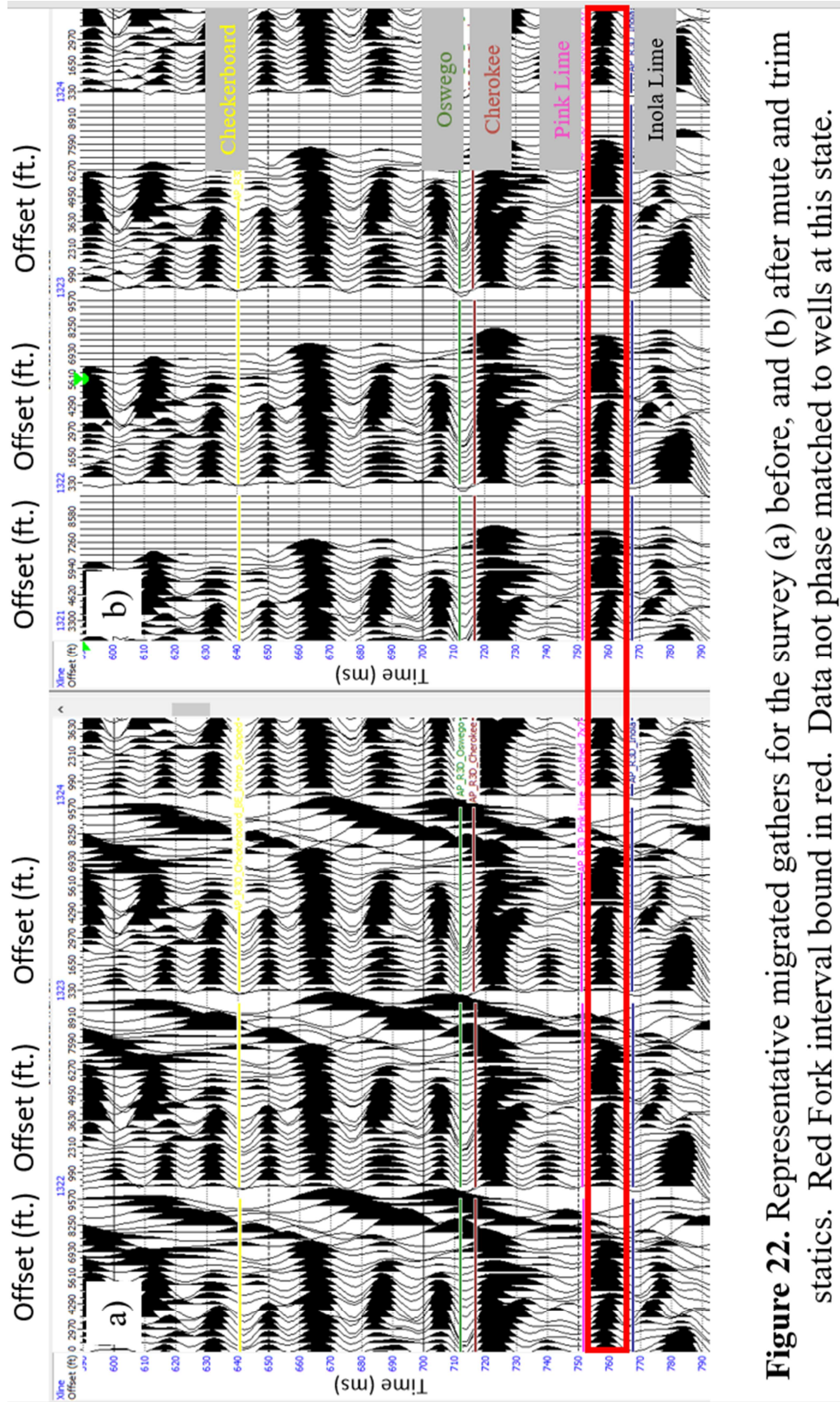


Figure 22. Representative migrated gathers for the survey (a) before, and (b) after mute and trim statics. Red Fork interval bound in red. Data not phase matched to wells at this state.

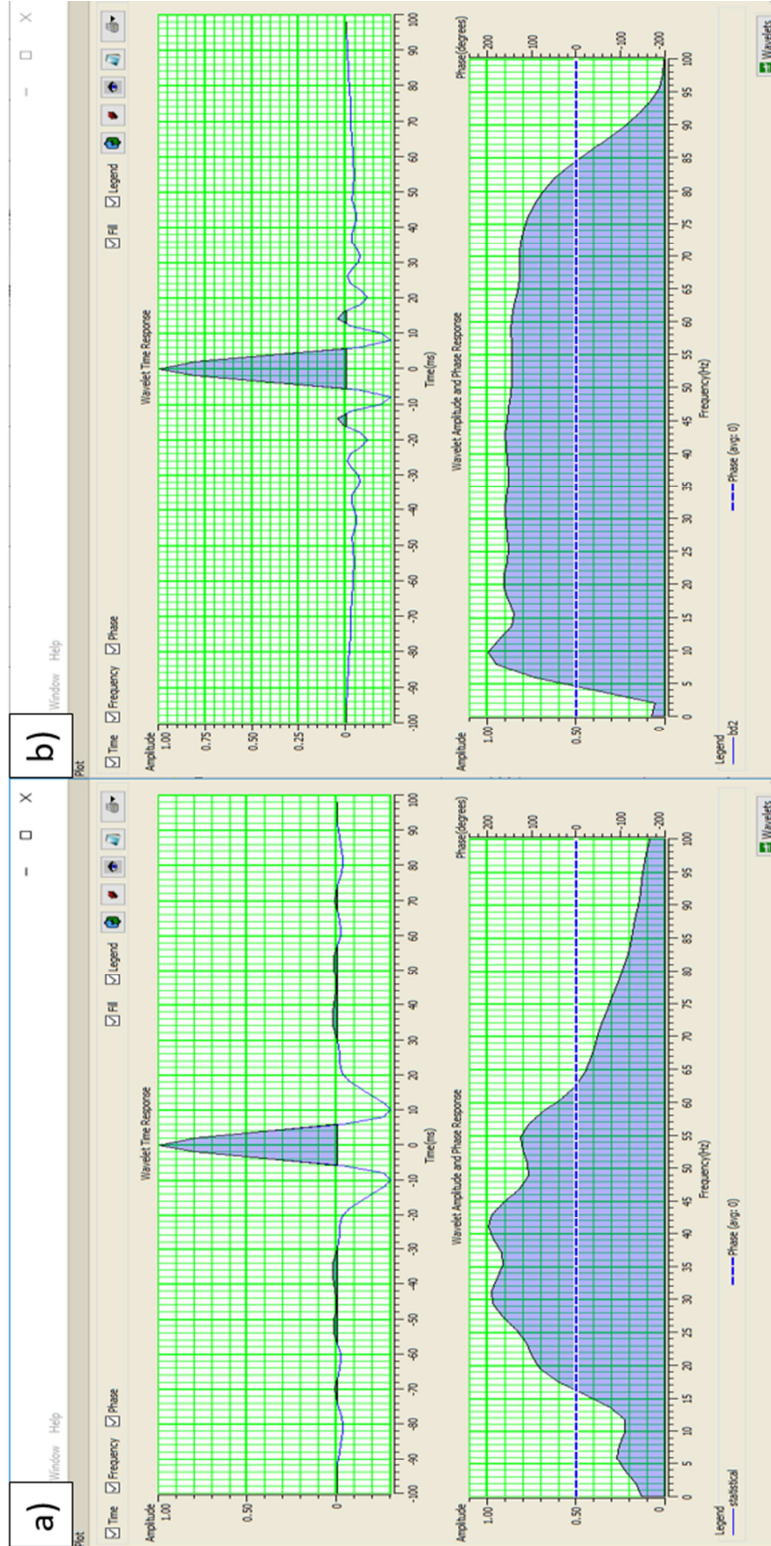


Figure 23. Extracted statistical wavelet from the input gathers used for inversion (a). Note the gathers provided did not include 5-dimensional interpolation nor any high frequency spectral recovery. After a pass of spectral whitening (b) the temporal resolution are more balanced and improved.

CHAPTER IV: INVERSION

Inversion affords the interpreter the ability to leverage the higher spatial resolution that 3-dimensional seismic data yields over the sparse nature of well logs. Inversion merges the well log data and pre or post stack seismic data to create a seismic volume consisting of rock property values. Acoustic impedance, Z_p , is the product of P-wave velocity, V_p and the density ρ of the medium (Russel 2006).

As Russel (2006) shows, a post-stack impedance inversion can be modeled as the earth's reflectivity series convolved with a band limited seismic wavelet

$$s_t = w_t * r_t, \quad (1)$$

where s_t is the seismic trace, w_t is the band limited seismic wavelet, and r_t is the reflectivity. The acoustic impedance of the earth is related to the reflectivity by

$$r_{Pi} = \frac{Z_{Pi+1} - Z_{Pi}}{Z_{Pi+1} + Z_{Pi}}, \quad (2)$$

r_{Pi} is the zero-offset P-wave reflection coefficient, $Z_{Pi} = \rho_i V_{Pi}$, ρ is density, V_p is P-wave velocity and $*$ denotes convolution where the i^{th} interface of a stack of N layers is the i^{th} p-impedance of the i^{th} layer (Russel 2006). Lindseth (1979) showed that by assuming the recorded seismic data as given in equation 2, one can invert to recover the P-impedance from the recursive equation

$$Z_{Pi+1} = Z_{Pi} \left[\frac{1+r_{Pi}}{1-r_{Pi}} \right]. \quad (3)$$

Equation 3 allows an inversion of the seismic reflection data to P-impedance. One problem with this method is that the seismic trace is not a reflectivity series but the convolutional model as shown in equation 1 (Russel, 2006). The approach to correct this is to use a low frequency model based from well log data and perturb the model

until we obtain a reasonable approximation to the measured seismic data and a synthetic trace (Russel 2006).

Goodway (2009) provides an excellent overview of obtaining Lamé parameters from our pre-stack inversion data. Specifically:

$$Vs = \sqrt{\frac{\mu}{\rho}}, \text{ and} \quad (4)$$

$$Vp = \sqrt{\frac{\lambda+2\mu}{\rho}}. \quad (5)$$

If one has values for λ and μ one can derive:

$$\text{Compressional P-wave Modulus} \quad M = \lambda + 2\mu, \quad (6)$$

$$\text{Young's Modulus} \quad E = \frac{\mu(3\lambda+2\mu)}{\lambda+\mu}, \quad (7)$$

$$\text{Bulk Modulus} \quad K = \lambda - \frac{2\mu}{3}, \quad (8)$$

$$\text{Poisson's ratio} \quad \nu = \frac{\lambda}{2\lambda+2\mu}, \quad (9)$$

$$\lambda\rho = (Vp * \rho)^2 - 2(Vs * \rho)^2, \text{ and} \quad (10)$$

$$\mu\rho = (Vs * \rho)^2. \quad (11)$$

Figure 19 shows the well log and synthetic used for the inversions within the Pink Lime and Inola Lime bounding the Red Fork interval. Utilizing this well log, I can check the ability to see different fluids in the matrix with a fluid substitution model.

Figure 24 is a petrophysical analysis provided by the company for the well with compressional and shear wave data over the Red Fork. This analysis will feed into the fluid substitution model seen in Figure 25. The reservoir is modeled as a clean sand with an average porosity of 16% and water saturation of 75% and a small amount of gas at 3%. Figure 26 highlights the expected p-wave and s-wave sonic velocities for

idealized brine, gas, or oil filled reservoirs. Brine has the fastest velocity with gas as the slowest and oil in between. These log responses are then modeled to generate synthetic seismic traces. It is evident that an amplitude anomaly is evident from brine, to oil, and to gas (Figure 27). Figure 28 shows the modeled traces side by side to visualize and chart the amplitude responses similar to a wedge model but as a fluid substitution model.

As noted by Trad (2009), an improved inversion result can be obtained by an amplitude preserving 5-dimensional trace interpolation. This inversion result has been provided by the company. To check the hypothesis this study was provided with the previously mentioned pre-stack migrated gathers that do not have 5-dimensional trace interpolation. Figure 29 highlights the cross plots between Z_p , Z_s and between Z_p and ρ in the well log. The breakouts from the trendline highlight the fluid anomalies present in the data (Russel, 2006). The well tie created for the inversion was obtained with very minimal stretching and has a 0.92 correlation (Figure 30). The data, being high frequency and relatively free from noise, affords a good tie to the well log synthetic.

Comparing results is relatively straightforward. Figure 31 shows the post stack p-wave inversion provided by the company. The data had 5-dimensional interpretation and a proprietary high frequency bandwidth recovery process applied. The image is unclear but could be worked with provided enough well control to constrain the interpretation. Figure 32 is the pre-stack p-wave inversion calculated in this study. Notice the better defined main channel cut and the more correct impedance result for the east-west narrower channel. Neither result is as accurate as the 5-dimensional, proprietary high frequency bandwidth p-wave inversion result (Figure 33).

Post stack inversion has shortcomings as seen previously. The main obstacle is the inversion is performed on a stacked dataset where the possible variations in amplitude vs. offset have been stacked into a single trace. Thus, a peak at near offsets turning into a trough at far offsets could sum to zero amplitude in the resultant stacked dataset. These variations are meaningful and handled properly with a pre-stack inversion. The driver behind the difference in the pre-stack inversions is twofold. First the extracted wavelets will be different because the data are different. This difference will impact the resultant outputs (Russel, 2006). The higher fold for the 5D dataset will also yield a better signal to noise ratio in the data for the algorithm to work with.

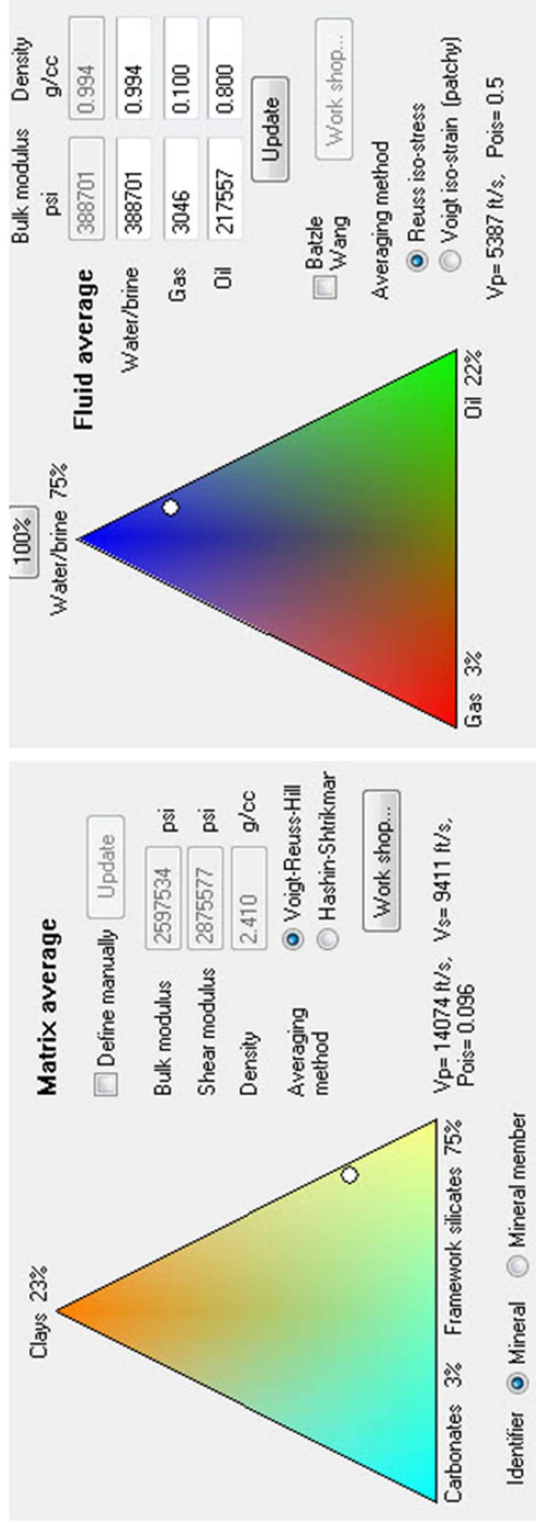


Figure 25. Initial fluid substitution parameters obtained from petrophysical analysis shown in Figure 24.

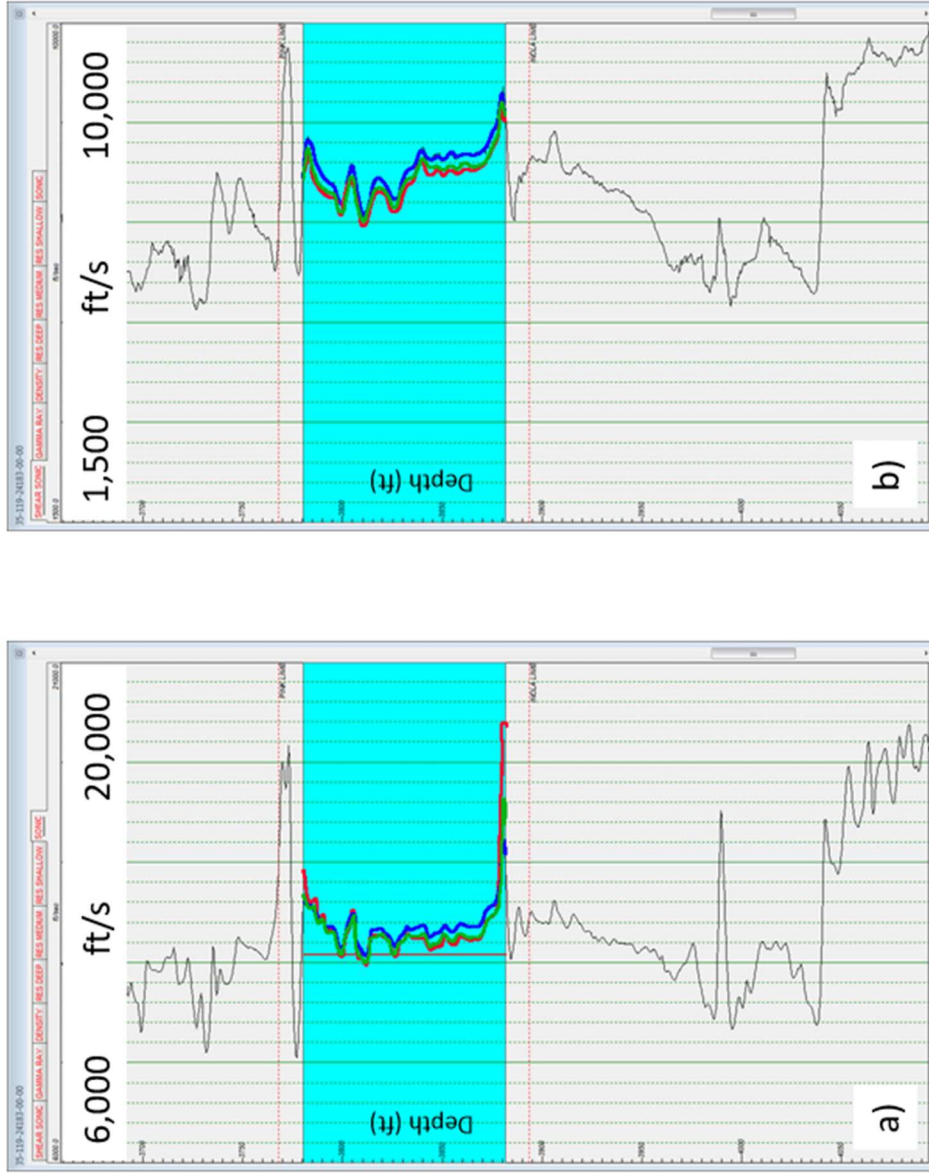


Figure 26. (a) compressional sonic data and (b) shear sonic data for (blue) 100% brine, (red) 100% gas, and (green) 100% oil. Red Fork interval highlighted in blue.

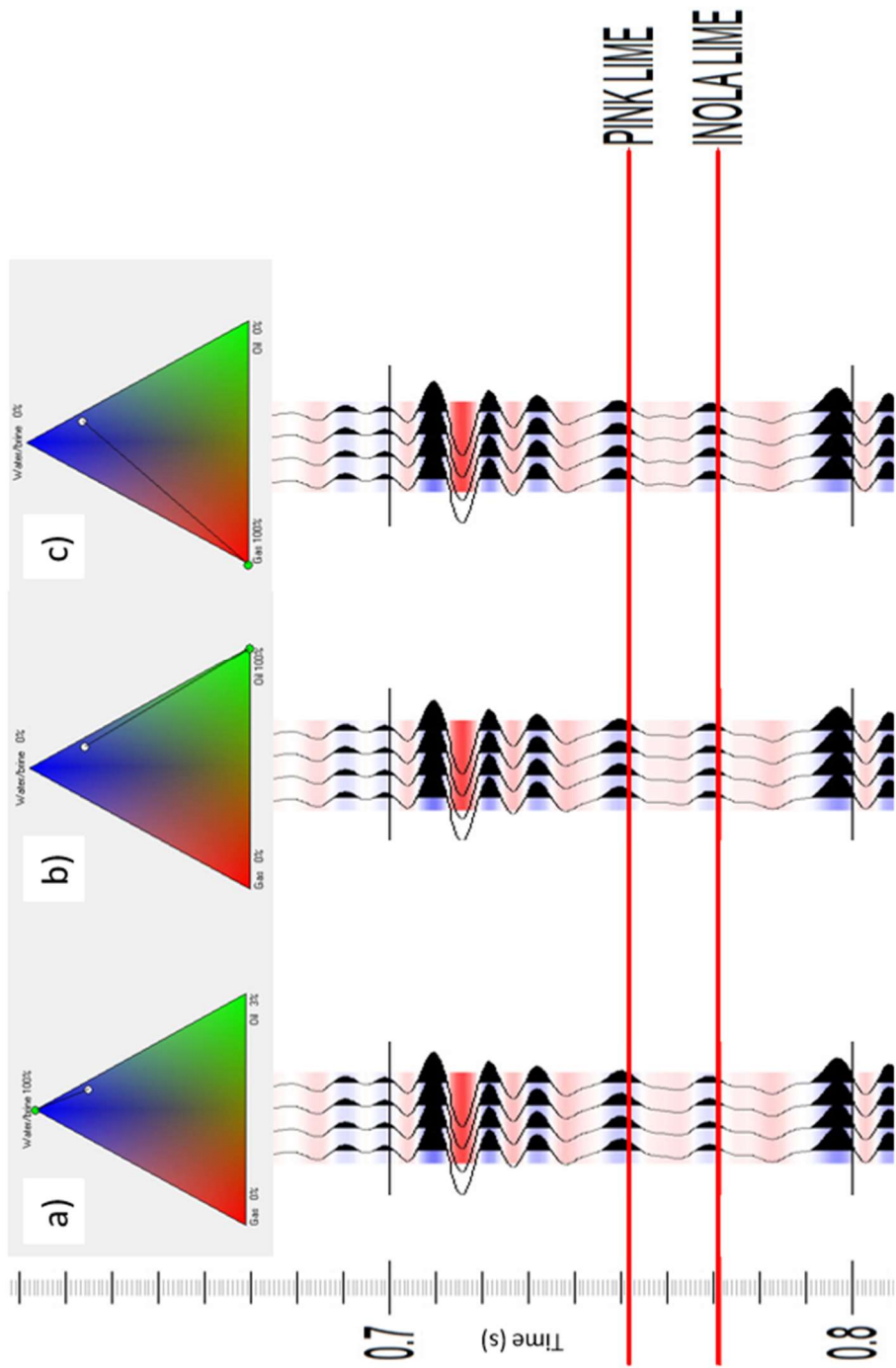


Figure 27. Synthetics modeled with (a) 100% water, (b) 100% oil, and (c) 100% gas in Red Fork interval bound by the Pink and Inola limestones.

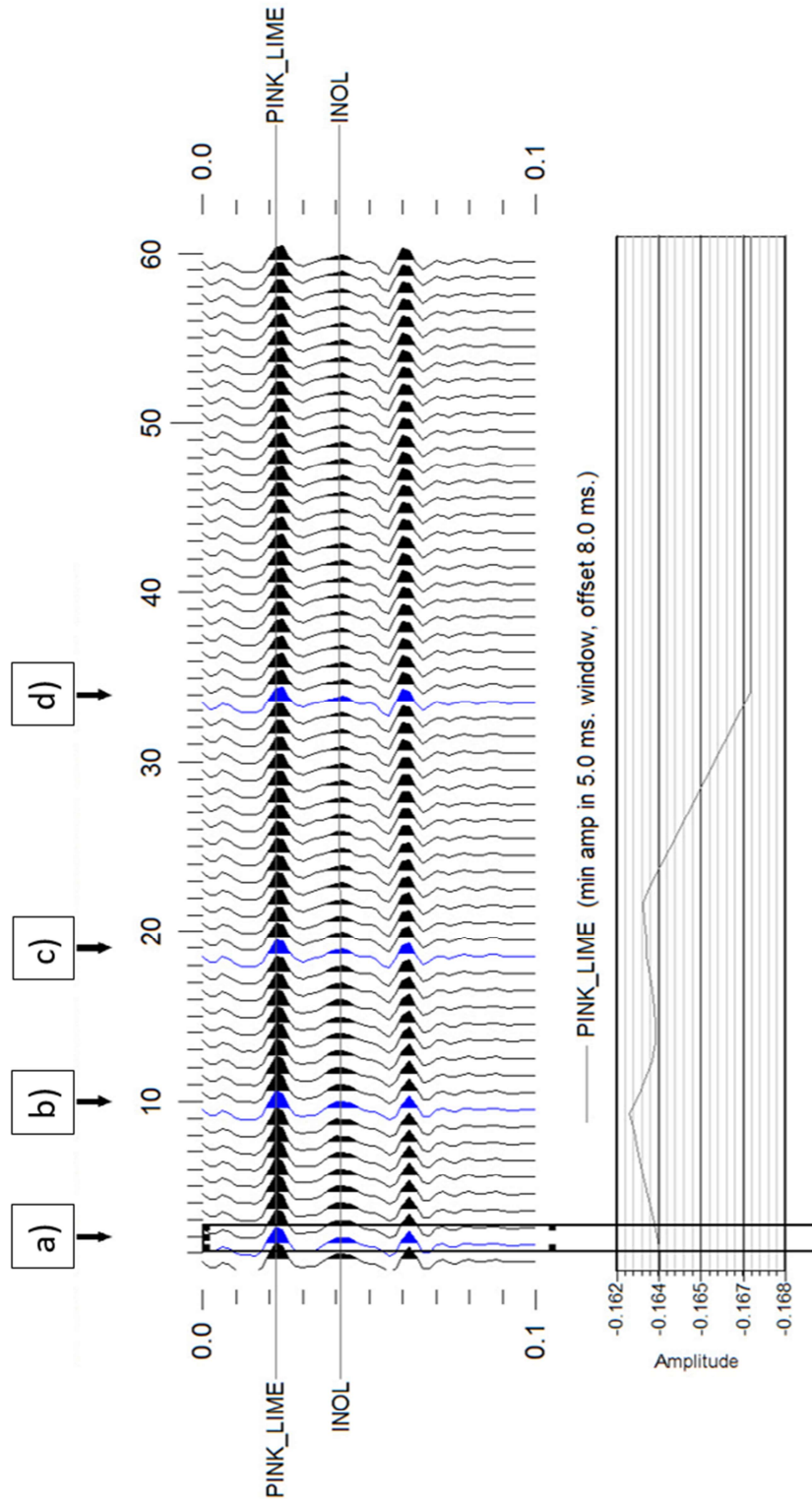


Figure 28. Amplitude data for Red Fork interval with fluid substitutions for well x with (a) original fluid content, (b) 100% brine, (c) 100% oil, (d) and 100% gas. Notice increase in amplitude for water, slight decrease for oil, and a large decrease for gas from initial reservoir fluids. Well locations indicated by arrows and blue traces.

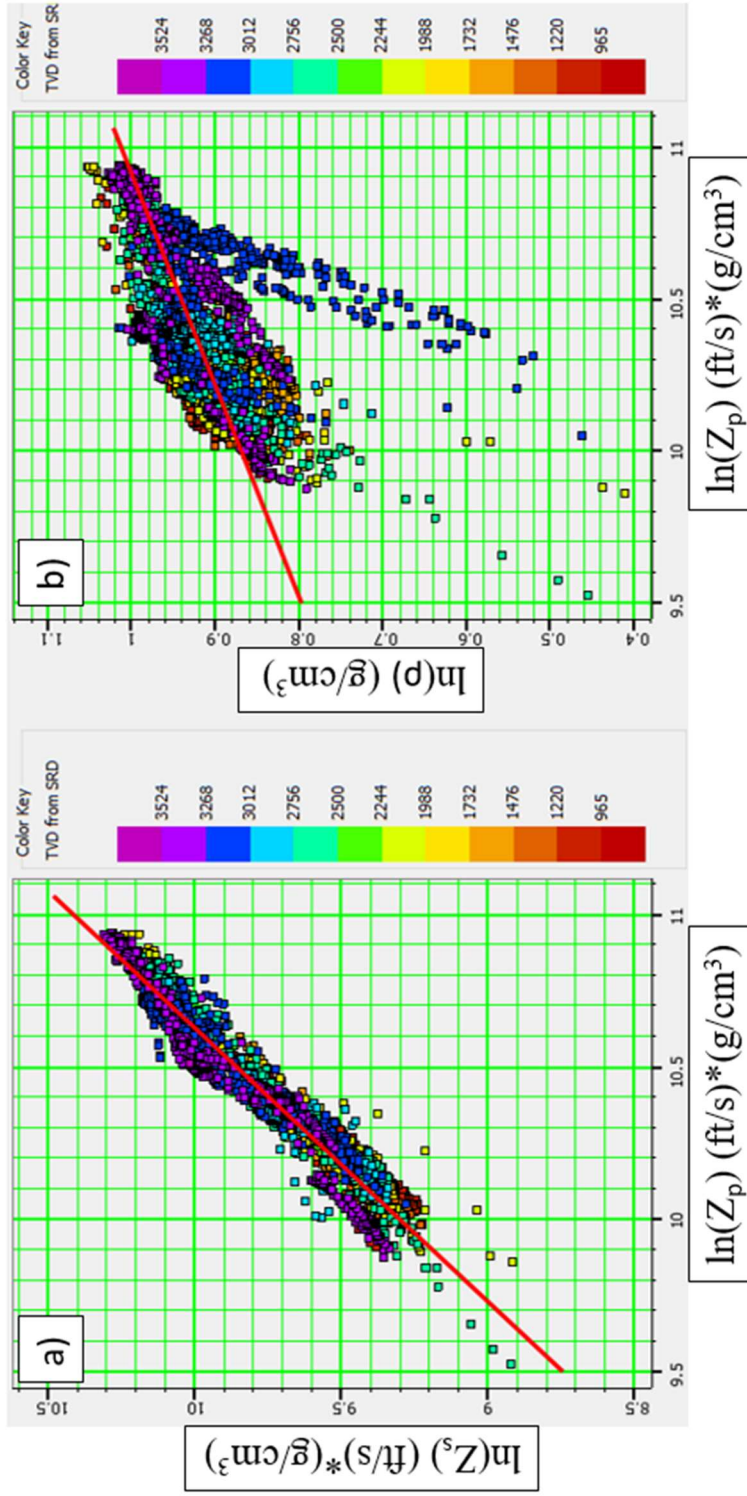


Figure 29. Cross plots of (a) $\ln(Z_s)$ vs. $\ln(Z_p)$ and (b) $\ln(\rho)$ vs. $\ln(Z_p)$. Best fit line added in red. Deviations from the line indicate desired fluid anomalies. (Modified from Russell, 2006).

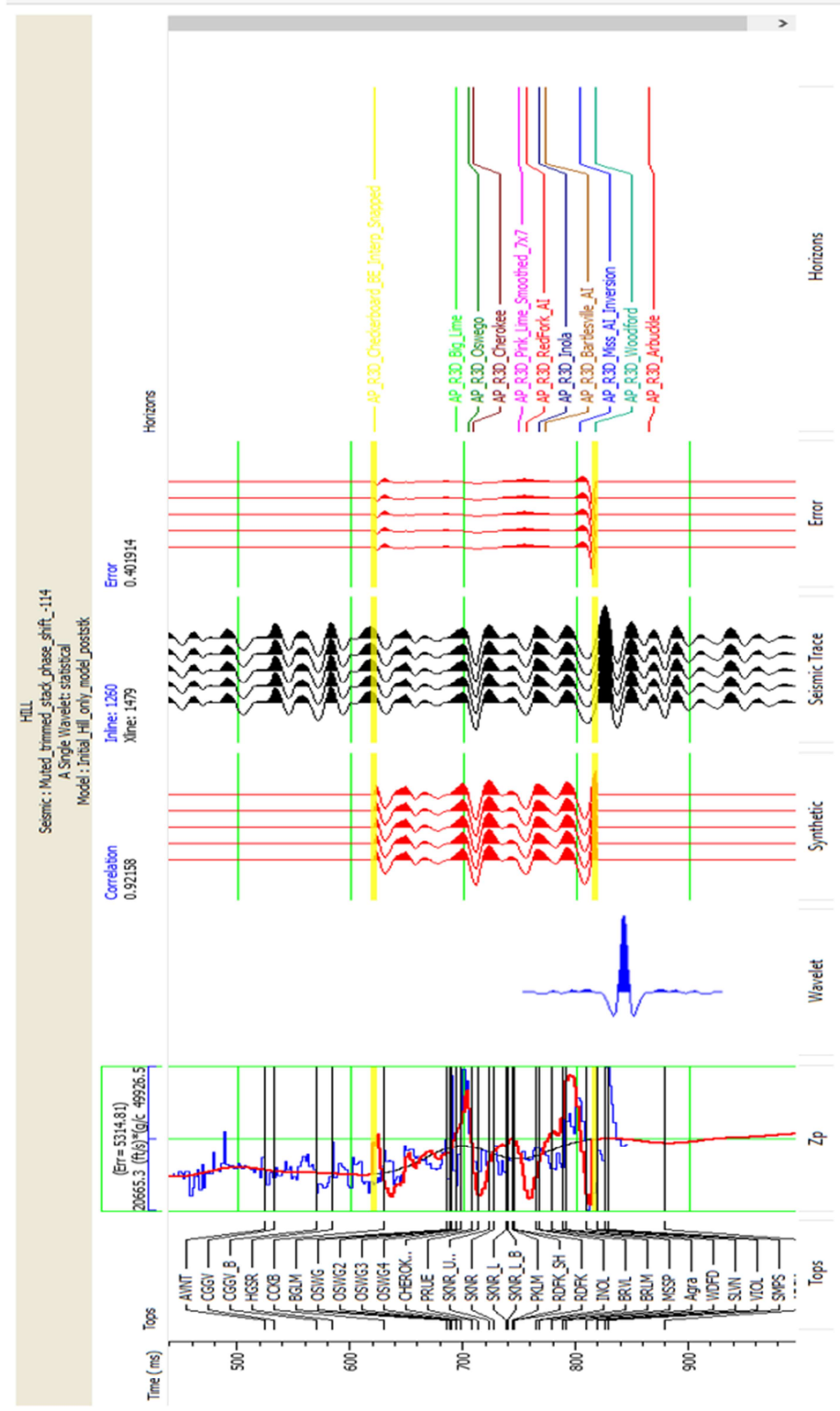


Figure 30. Well tie for the inversion with a .92 correlation with minimal stretching and squeezing. Error mainly contained to top and bottom of the window indicated by yellow lines.

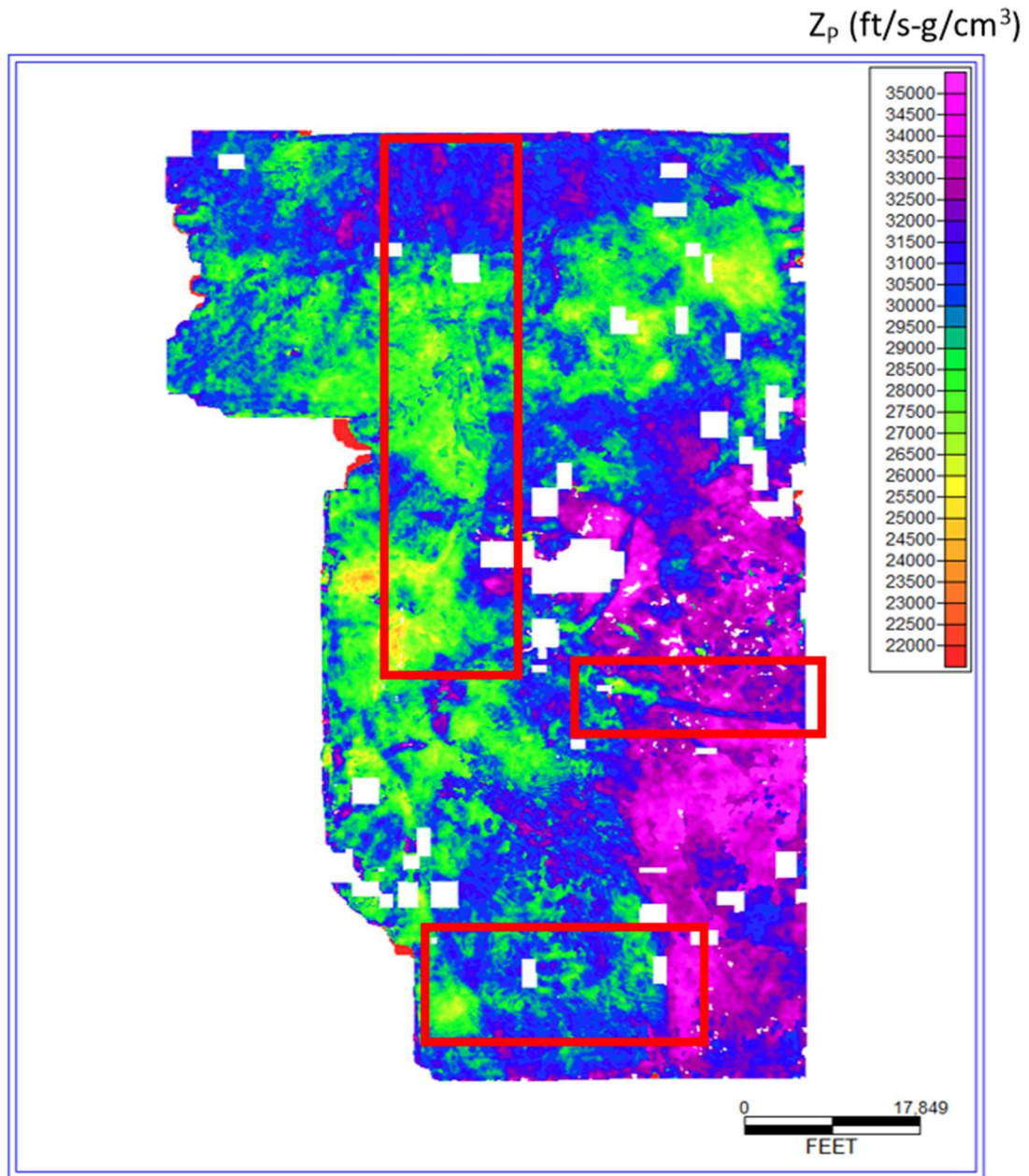


Figure 31. Horizon slice along the lowest impedance value in the Red Fork formation from a post-stack P-wave impedance volume. Input data have 5-dimensional interpolation and bandwidth recovery applied. Red boxes highlight sand filled channels that are not well delineated from the floodplain.

Z_p (ft/s-g/cm³)

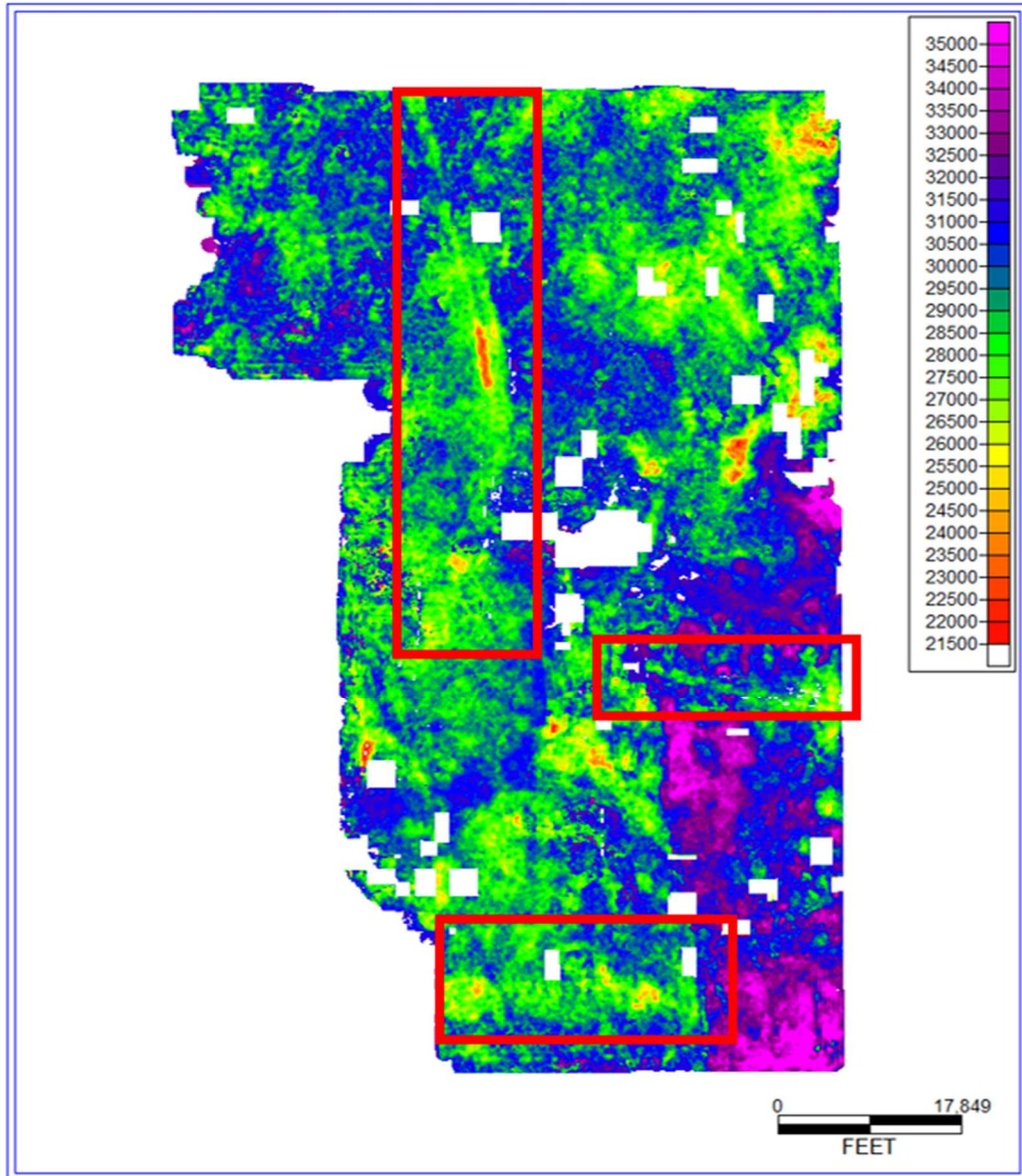


Figure 32. Horizon slice along the lowest impedance value in the Red Fork formation from a pre-stack P-wave impedance volume without 5-dimensional interpolation and bandwidth recovery. Note the better detail the pre-stack inversion yields in the northern main channel sand, the more appropriate lower impedance values for thinner east-west channel, and the southern sand bodies highlighted by red boxes.

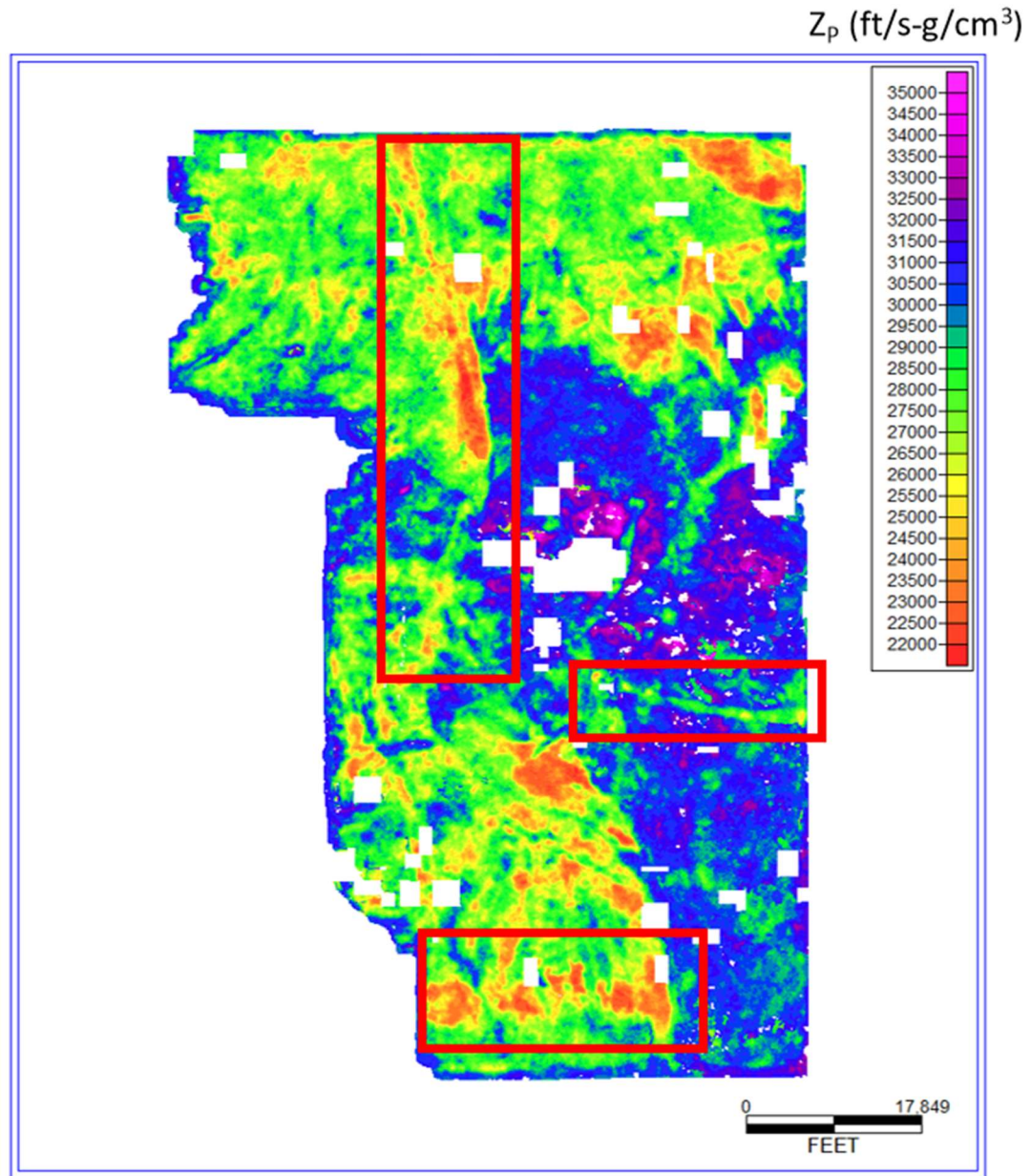


Figure 33. Horizon slice along the lowest impedance value in the Red Fork formation from a pre-stack P-wave impedance volume. Input data have 5-dimensional interpolation and bandwidth recovery applied. Note the improved delineation of low impedance sand bodies.

CHAPTER V: INTERPRETATION

Seismic data attributes are incredibly useful tools to quickly evaluate large amounts of data. Curvature and semblance can be used to delineate faults and highlight channels (Chopra and Marfurt, 2007; Chopra 2010). Figure 34 captures part of a workflow to pick faults in this data. Most negative curvature in combination with the seismic data and variance help to distinguish a subtle fault from a channel edge that is not readily apparent on the seismic data alone at first glance.

The compressional sonic data are used in tying seismic data to the wells and defining horizons in the seismic data. The shear sonic log is used in the pre-stack impedance inversion and the estimation of the mechanical rock properties. The remaining raster logs that cover the interval of interest will be used to aid in creating a velocity model to depth convert the seismic data for depth structure analysis and constrain the net sand thicknesses.

After picking horizons, faults, and well data, I am able to merge the data and create an average velocity field to the top of the Pink lime and an interval velocity field from the Pink lime to the Inola lime. This allows for a detailed depth structure map at the top of the Pink lime (Figure 35). Evident is the multitude of structural and stratigraphic trapping mechanisms within the survey. Several closed highs indicated by the Pink Lime structure and numerous stratigraphic pinch outs with shallowing dip with Red Fork sand present are exciting to a prospector. Rendering the Z_p data with known Red Fork producers validates the hypothesis that the Z_p data delineates sandstone targets (Figure 36).

The Kohonen Self-Organizing Maps (SOM) algorithm is applied with Z_p , Z_s , density, $\lambda\rho$, $\mu\rho$, and v_p/v_s to cluster the data and compare the clustered data to log data and evaluate the possibility of the clusters representing different rock types or facies. SOM provides effective visualization of multidimensional data via clustering then representing those cluster groups in 2 dimensions (Matos, 2007). Figure 37 shows the input data with Figure 38 showing the output. The SOM algorithm was able to separate sand from shale with ease but was also able to separate out a porous shale from a non-porous shale. The algorithm was also able to separate porous from non-porous sand facies but was unable to separate productive intervals from non-productive intervals.

With the difficulty of picking top and base of Red Fork sand intervals I needed a better way to use the seismic data with well control to map net sand and evaluate potential targets. I picked the Red Fork horizon as the minimum Z_p value between the Pink Limestone and the Inola Limestone. Figure 39 shows the similar visual appearance between the picked net sand in the wells and the Z_p data from the pre-stack inversion suggesting a statistical correlation. Extracting the Z_p grid at the wellbores I then cross plot Z_p vs. net sand thickness. A solid linear trend is evident with a negative correlation of -0.598 and an error of 20.8ft (Figure 40). I can be confident in the correlation below the previously described tuning frequency of 20 ft for a couple reasons. The main reason is that net sand under the 20 ft threshold does not imply there is no sand in the interval. I can also be confident in the detectability of $\lambda/25$ (Sheriff, 2006) yielding 3.7ft. of detectable resolution. Utilizing this linear regression, I can convert the Z_p rock property horizon to a net sand thickness horizon (Figure 41). This linear regression also highlights incomplete well data in in the northeast corner of the

3D survey (Figure 42). This field was drilled in the early 1950s producing out of the Red Fork and is either missing log data, does not cover the entire Red Fork interval, or it was never recorded. Similarly, the inversion has problems with acquisition gaps or survey obstacles (Figure 43). The high fold effort and 5-dimensional interpolation have limits. If there are enough acquisition gaps, doubly impacted by a survey edge, the algorithms and acquisition design cannot interpolate the missing data to obtain a correct rock property model even though the structure can be accurately imaged (Figure 44). Figure 45 shows that while the visual interpretation is similar between the Z_p data and the linear regression net sand thickness, I now have a sand thickness value to use instead of a rock property.

In theory, the 5-dimensional interpolation should provide a more accurate estimation of Z_p . To test this hypothesis, I cross plot the net sand of the Z_p with and without 5-dimensional interpolation (Figure 46). The results are similar with both exhibiting a negative correlation (lower impedance values correlate to higher net sand). However, the 5-dimensional interpolation has a better correlation with a smaller error. - 0.598 correlation and 20.8 ft of error for the 5-dimensional interpolated data vs. -0.313 correlation and 27 ft of error for the standard data. I can also show that the correlation of the 5D data is reasonable compared to the well control. I can use the well data, remove a single well, then interpolate with the remaining well data what the thickness would be at the well that was removed. Basically, creating a blind well test to show how well control can predict net sand thickness. Figure 47 shows that since this is a mature field, there is an abundance of well data, and the well data predicts the net sand

thickness with a correlation of .789 and an error of 15 ft. This is only 6 ft better than the Z_p correlation which further gives confidence to the Z_p correlation.

Production data affords the opportunity to make a quantitative estimation of prospective locations. The correlation between acoustic impedance and net sand allows an accurate thickness prediction of isolated, undrilled sand bodies. This correlation is key in being able to set a quantitative number to the prospective locations that is more meaningful than “good” or “bad”, thereby providing a better assessment for reservoir quality sand thickness and estimation of potential hydrocarbon pore volume. Utilizing known production from prior Red Fork wells, an estimation of likely outcomes can be obtained from the interpreted sand volume. These data can be used to evaluate a potential re-completion of an existing horizontal well bore or as a new vertical or horizontal targeted well in the Red Fork formation.

One potential candidate is presented in Figure 48. A horizontal well has become uneconomic to continue production from the deeper target. This well flanks a field that has produced over 8 BCF of gas with the original discovery well drilled in 1926. Figure 49 shows the well to well cross section through the field over to the shale east of the channel deposition. The company has provided a mud log from drilling the original horizontal well that indicates a good oil and gas show through the Red Fork sand interval with the best show from the lower interval (Figure 50). No resistivity, density, or porosity logs were acquired in the horizontal well so any evaluation will have to come from offsetting logs, core data, and the mud logger’s interpretation of the show.

The mud logger describes the upper section of sandstone as opaque, light grey to tan, fine grains that are sub rounded to sub angular, moderate sorting, fair to trace

visible intergranular porosity of 10-30% and a bright yellow fluorescing fair cut with small gas bubbles. The deeper sandstone is similarly described with the differences being, moderate to well sorted grains, visible intergranular porosity 40+% and a bright yellow fluorescing fair instant cut with small gas bubbles. Figure 51 highlights the separation of the upper and lower sands in the stacked seismic data and the inverted seismic. The presence of two sand bodies separated by a shale is confirmed with an offset log.

Core data were available outside of the 3D survey. Examining the core from the Hixson #1 provides some insight into the possibility of compartmentalization. Figures 52-55 show the core data. The erosional base of the core (Figure 52) is evident by large rip up clasts with a short fining up sequence and another high-energy episode with very large rip up clasts (Figure 53). Sand grain size is relatively consistent at medium with short lower energy episode with some clay beds present at 3300' to 3302' (Figure 54). The key separation happens at 3294' with relatively thick shale beds with some lenticular sand beds. Above the shale break there is another high-energy episode with very large clasts turning into intermittent episodes of smaller clasts and more fluvial cross bedded sands (Figure 55). The core ends before the top of the Red Fork interval.

With the better show occurring in the deeper sand body, two theories are in play. One is that the sands are compartmentalized and the older vintage wells produced from the upper portion leaving behind hydrocarbons in the lower sand. Another explanation is that the original wells drilled further up the structure produced most of the gas allowing the oil to migrate up filling the lower sand body. Ultimately the well was

recompleted and is successful in producing hydrocarbons. The well cut gas immediately and after producing most of the water used to treat the well it cut oil.

Other interesting targets nearby are shown in Figure 56. A similar sand body south-east of the major field has some nearby penetrations but none in the heart of the sand body. The wells in the cross section indicate that sand is present but there is conflicting information. A quick look Archie's water saturation (S_{wa}) is needed to further evaluate the risk associated with offsetting the dry holes into the thicker portion of the sand body.

$$S_{wa} = \sqrt{\frac{RW@FT}{PHIe^2 / RESD}} \quad (12)$$

where $RW@FT$ is the resistivity of the formation water at formation temperature, PHI is the fractional effective porosity, and $RESD$ is the resistivity of the formation (Crain 2015). Equation 12 assumes the tortuosity to be 1, cementation exponent to be 2 and the saturation exponent to be 2 from the full Archie Method. Figure 57 shows the special relationship and the raster logs of the wells to be evaluated. Based on the data obtained from Hubbard (1982) I set $RW@FT$ as 0.04 ohm for the Red Fork. These yield water saturation values for well 1 of 0.72, well 2 0.64, and well 3 0.45. Figure 58 provides evidence of a structural trap in the sand that is not expressed on the Pink Lime structure. With top of net sand in well 2 structurally higher than well 3 the risk of compartmentalization where well 2 in the higher structural position has a failed seal allowing well 3 to have hydrocarbons but with a more limited volume.

Sand body (b) from Figure 56 is also a risky location with some upside. It is an isolated sand body that has not been drilled (Figure 59). The offset to the east does not

have any cumulative production data but an initial production test showing 25 barrels of oil and 250 MCF of gas. The offset well also contains a log that shows 40 ft of net sand with the upper 2/3s at 15 ohms calculating 0.26 water saturation. Obvious risks are not knowing what is in the pore space of the sand or if the seal is intact. However, there is substantial upside to an isolated sand body with the offset producer calculating 74% hydrocarbon saturations out of 26 ft of sand.

The last location presented is an up dip location from a major field (Figure 60). It is the least risky location with proven down dip and equivalent structural position oil and gas production. The structure has known production of over 2 million barrels of oil from 7 unitized wells. There are approximately 46 total wells drilled into the main sand body with 32 producing wells giving 25 wells with un-accounted production. Pore pressure depletion could be a risk with so many producing wells in the sand body making this field an interesting opportunity for a water flood.

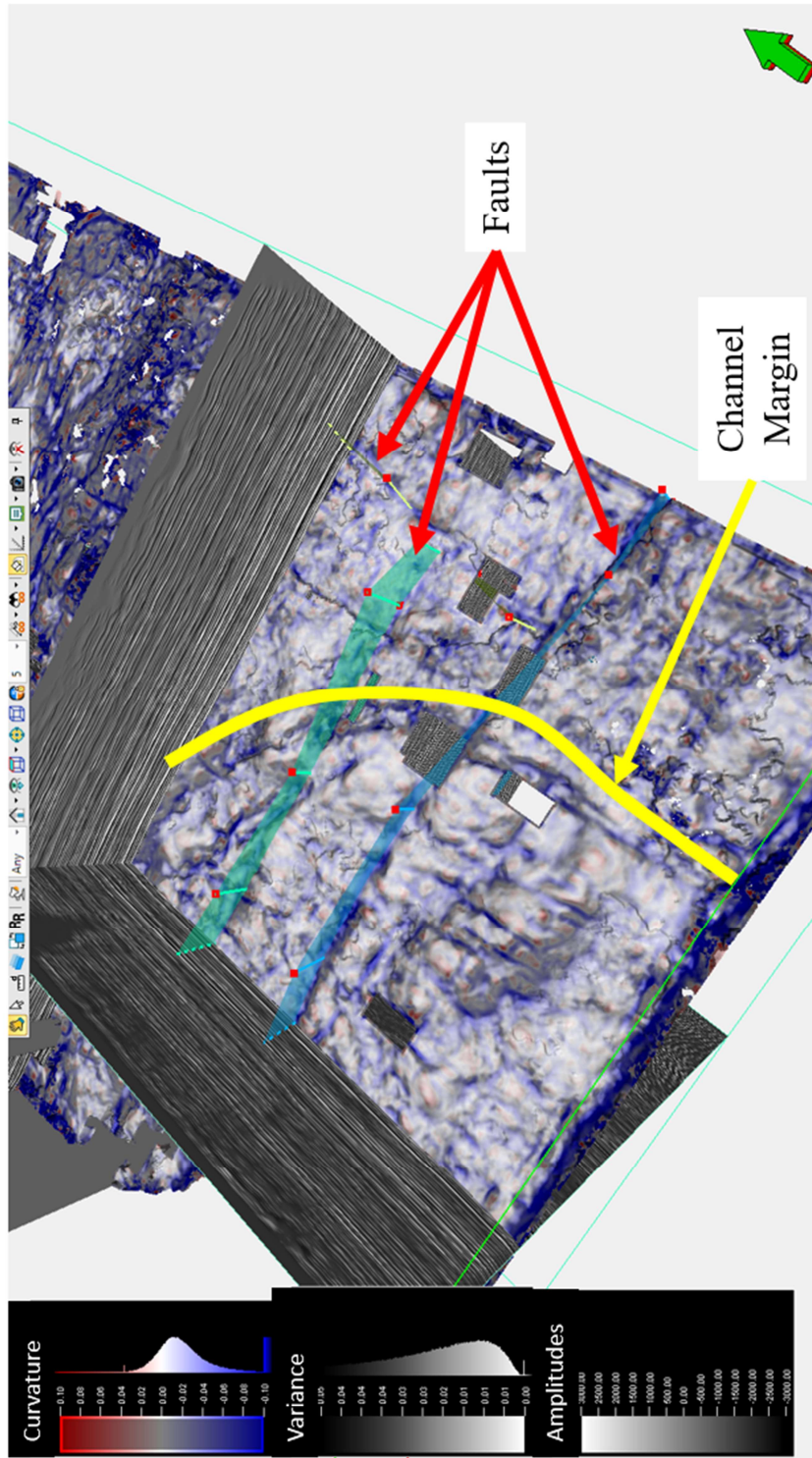


Figure 34. Most negative curvature co-rendered with variance to differentiate faults from channel edges.

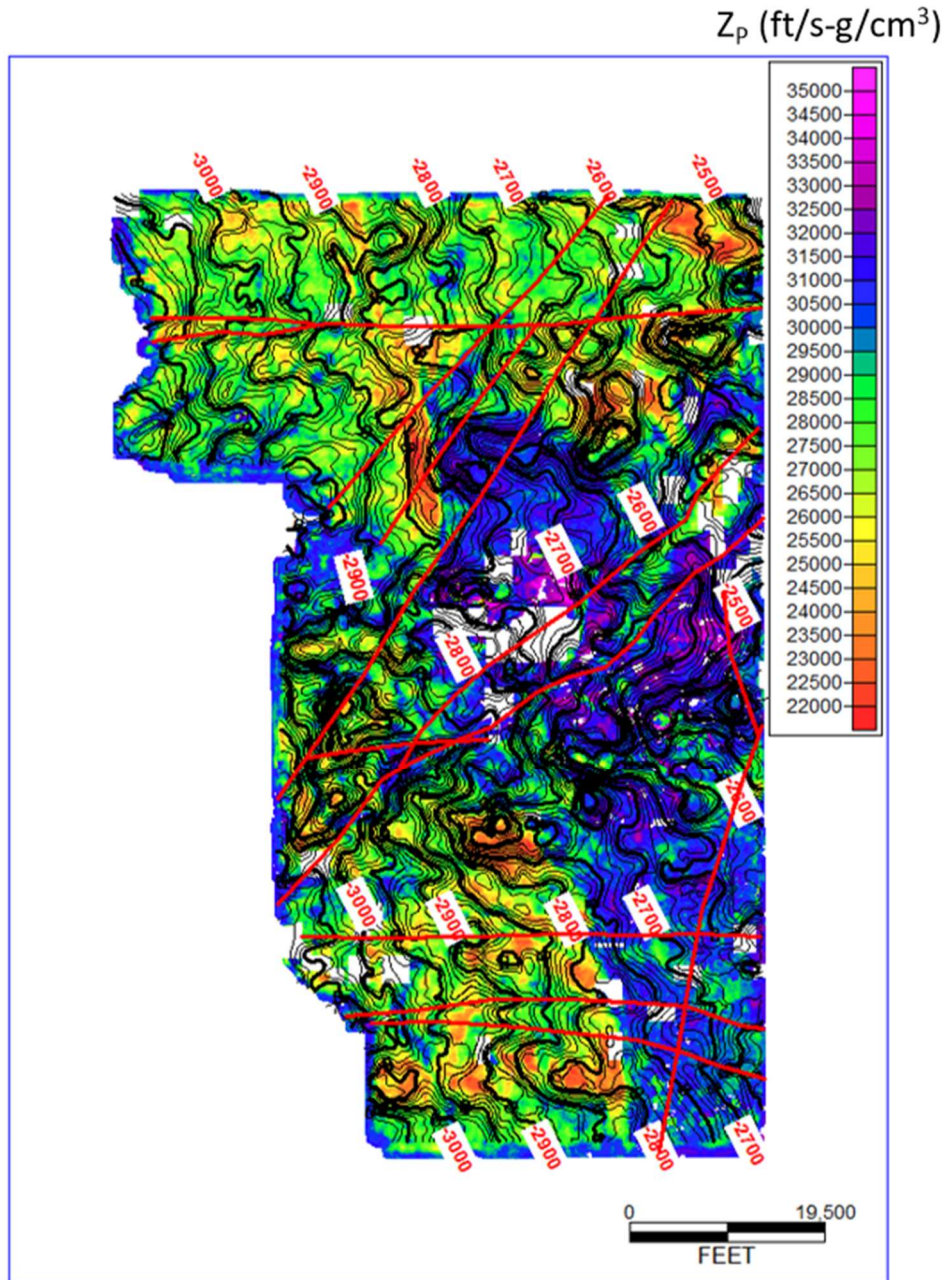


Figure 35. Horizon slice along lowest impedance value in the Red Fork formation through the pre-stack P-wave impedance volume with Pink Lime structure. Low impedance coupled with structural highs indicate potential targets (10 ft contours, bold contours at 50 ft and labeled at 100 ft).

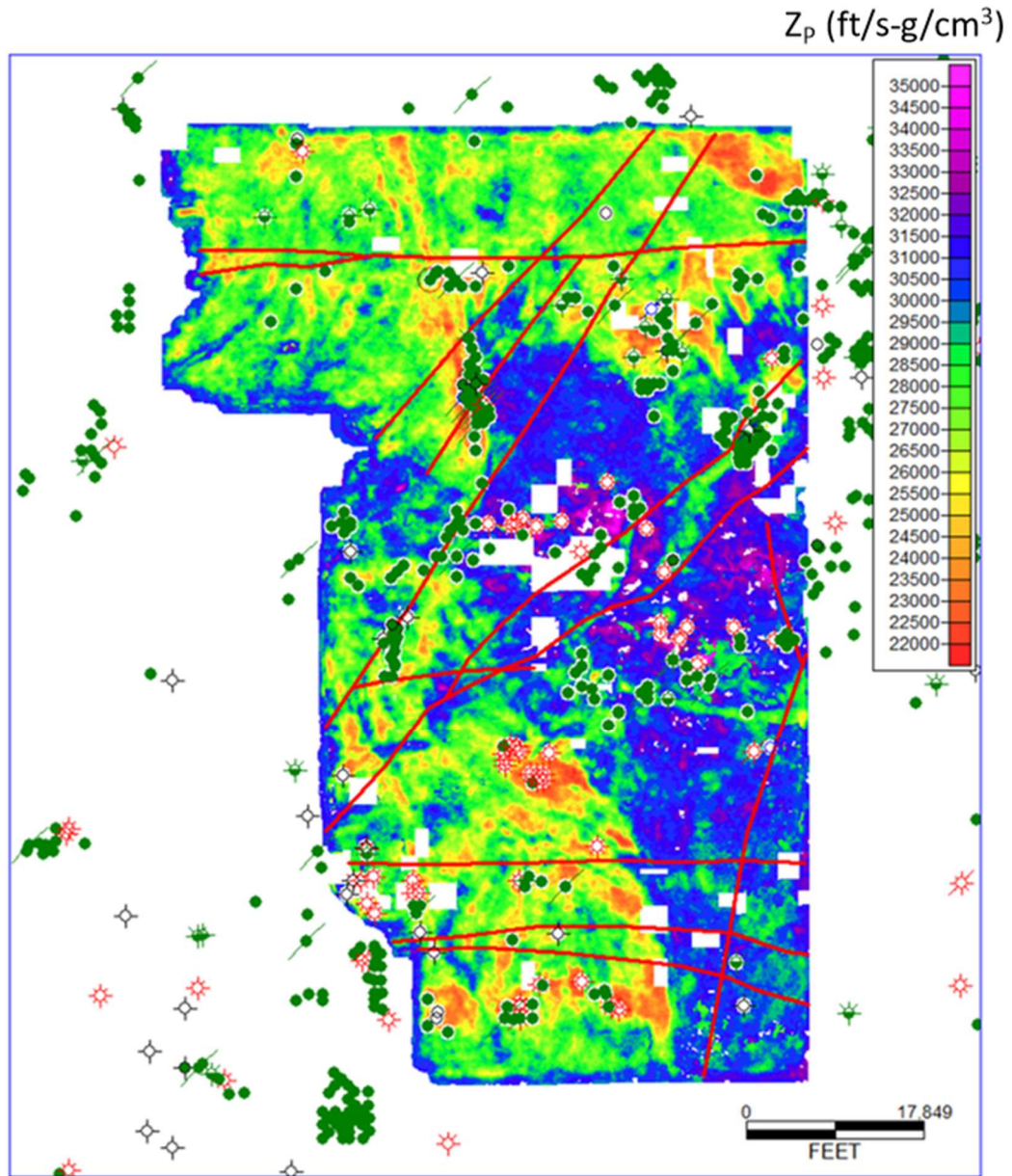


Figure 36. Horizon slice along lowest impedance value in the Red Fork formation through the pre-stack P-wave impedance volume with Red Fork producing wells. Structural and stratigraphic traps from Figure 35 are confirmed by producing wells.

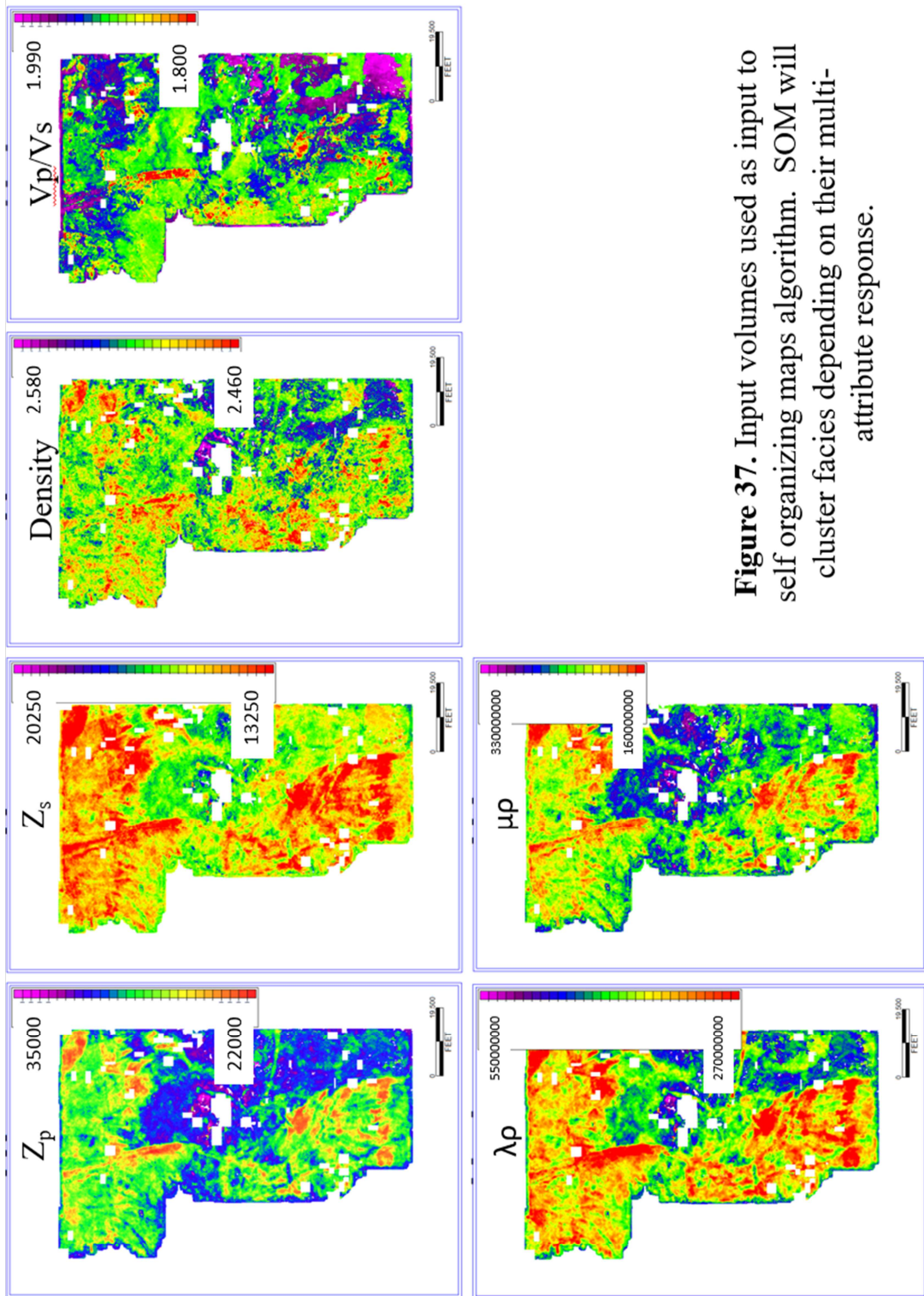


Figure 37. Input volumes used as input to self organizing maps algorithm. SOM will cluster facies depending on their multi-attribute response.

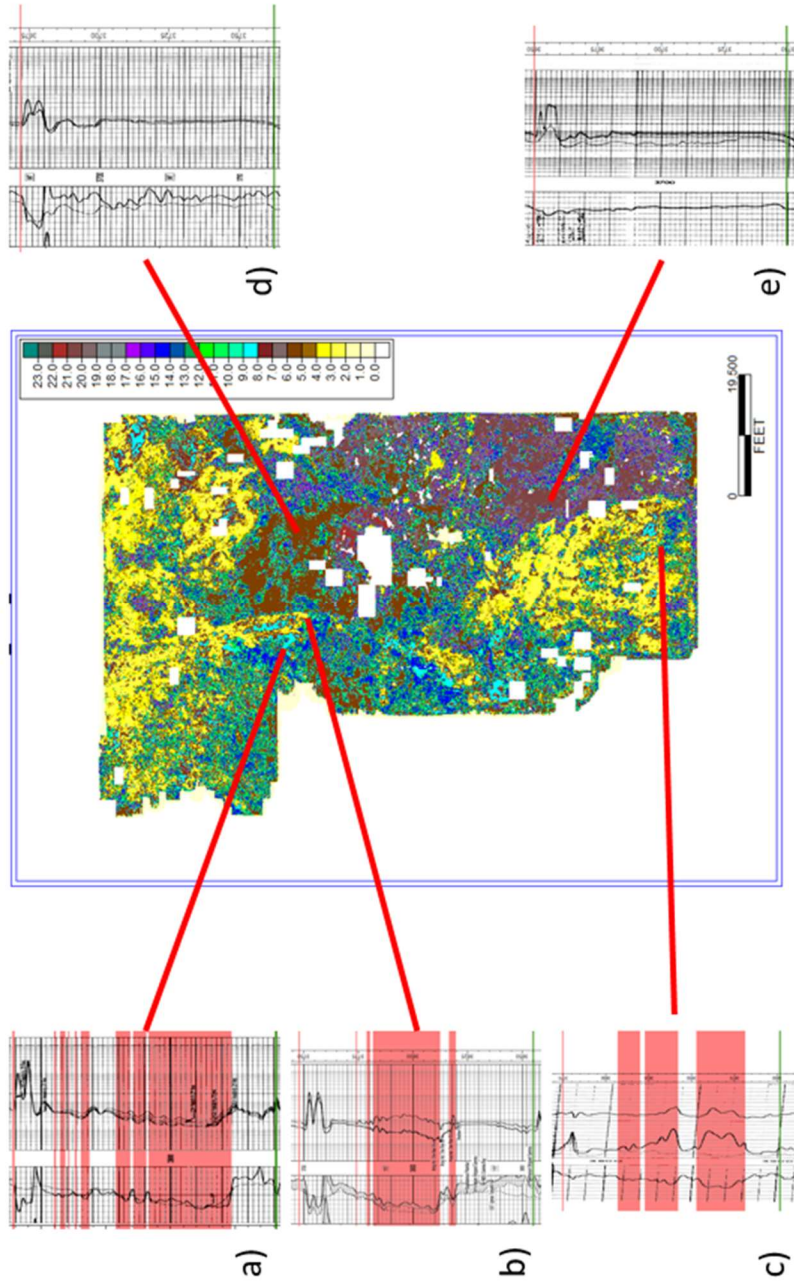


Figure 38. A posterior analysis of SOM clusters using well control separating (d, e) shales appearing brown and light tan (a, b, c) from sands appearing as yellow and light blue. SOM appears to resolve (e) a sandier shale from (d) a more conventional shale. The sands appear to separate based on (a) a tighter sand vs. (b, c) more porous sands but no clear evidence of gas or oil charged pore space is evident.

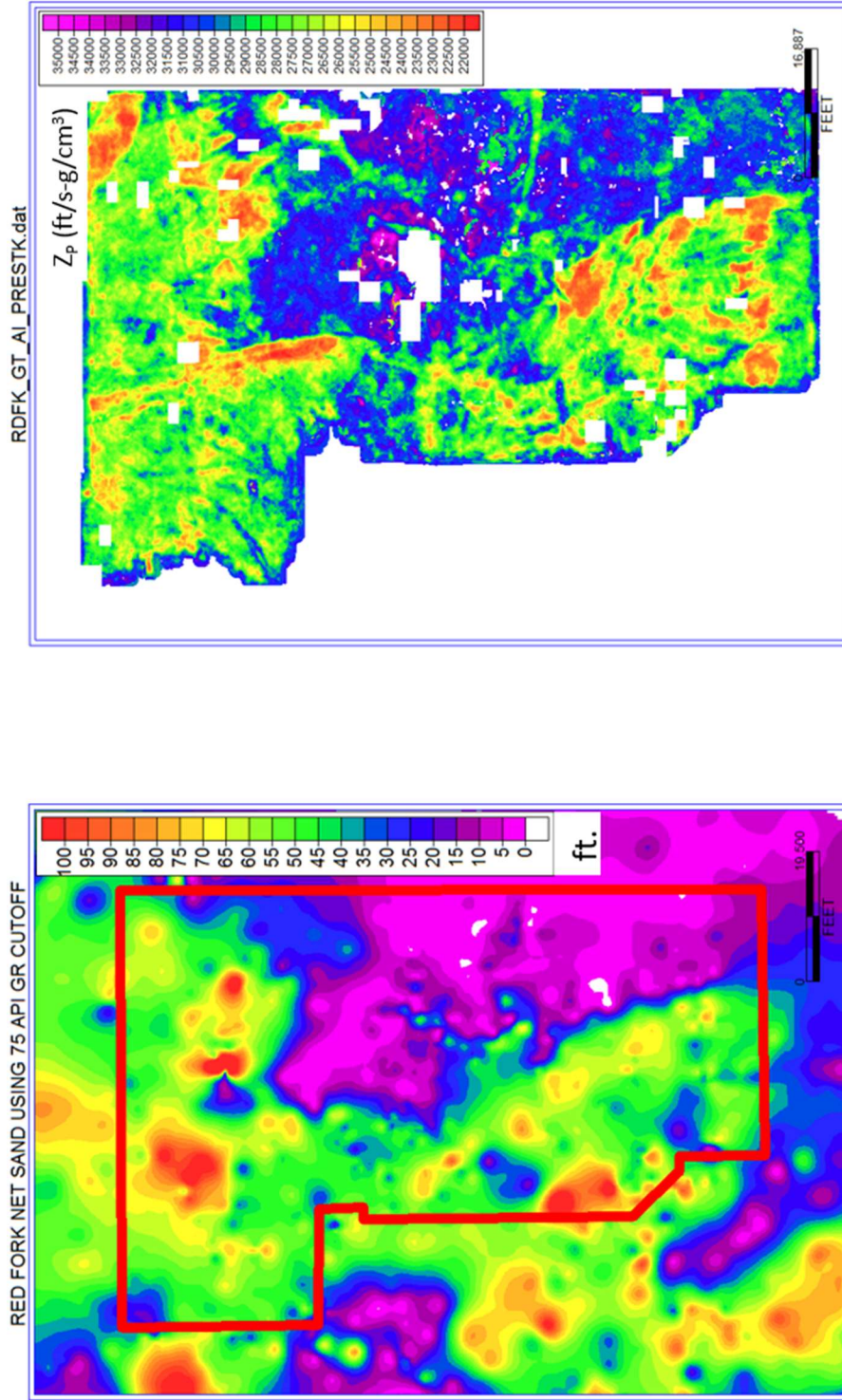


Figure 39. (a) Net sand (API<75) thickness map, computed from well control only, compared to (b) Z_p along the Red Fork formation. The roughly similar look between the two suggests a statistical correlation.

$$\text{NET SAND} = (-0.00910094) * Z_p + 294.937 \quad \text{Correlation} = -0.598 \quad \text{StdErr} = 20.7931$$

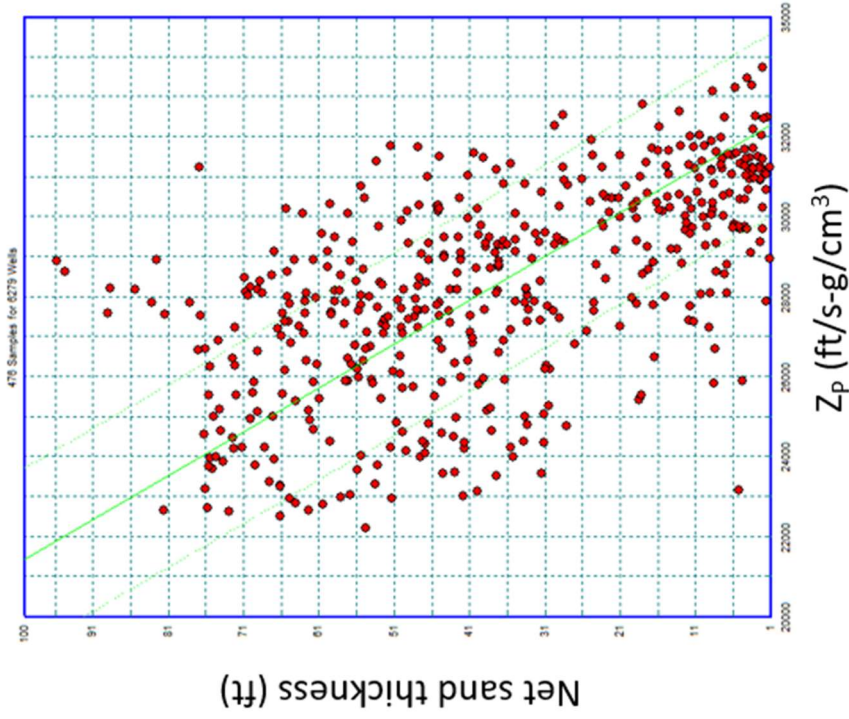


Figure 40. Acoustic impedance response cross plotted with net sand from raster logs. A clear trend is evident with a lower Z_p trending towards higher clean net sand (API<75).

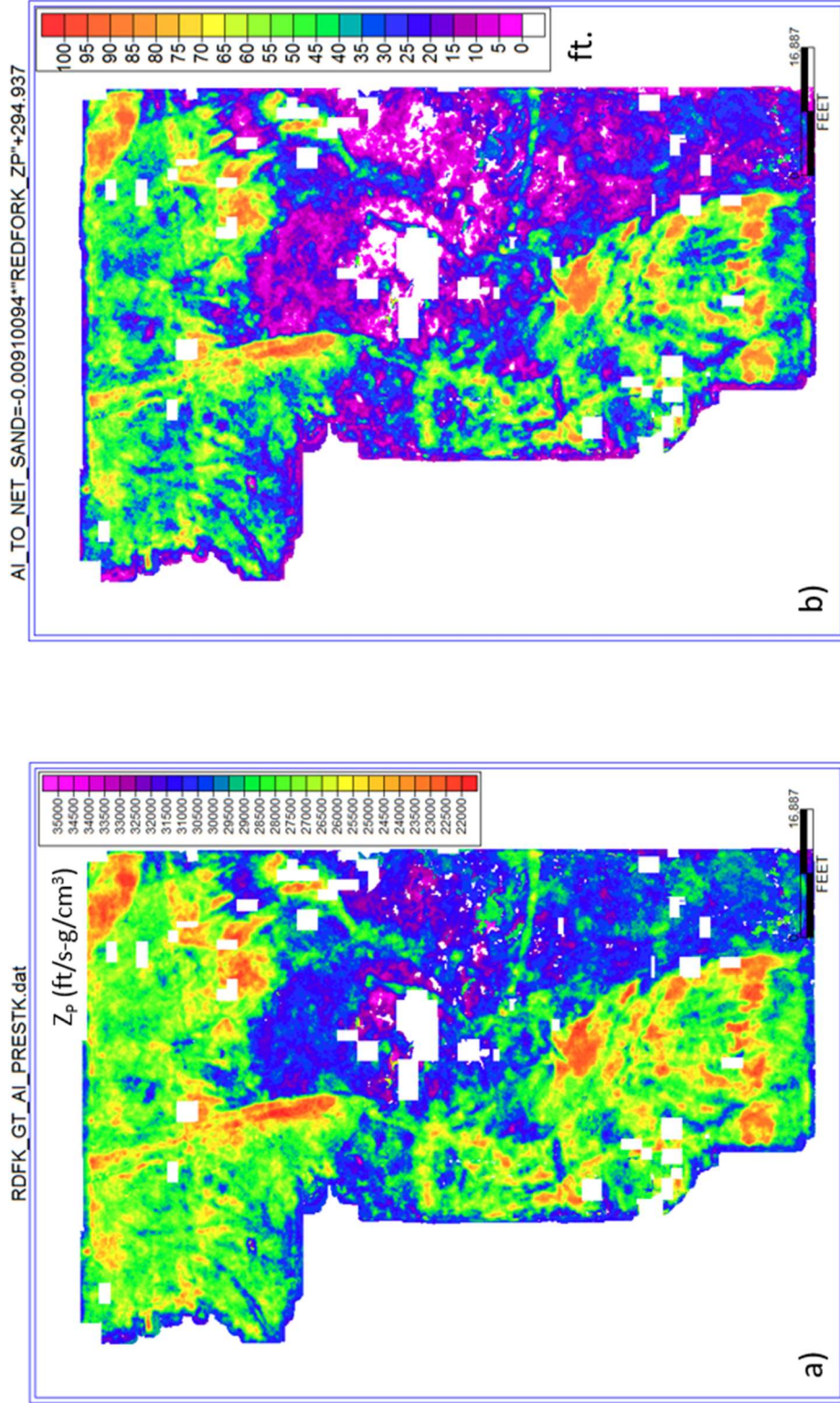


Figure 41. (a) Z_p and (b) the converted net sand data computed from the previously derived linear regression (NET SAND = (-0.0091) * Z_p + 290)

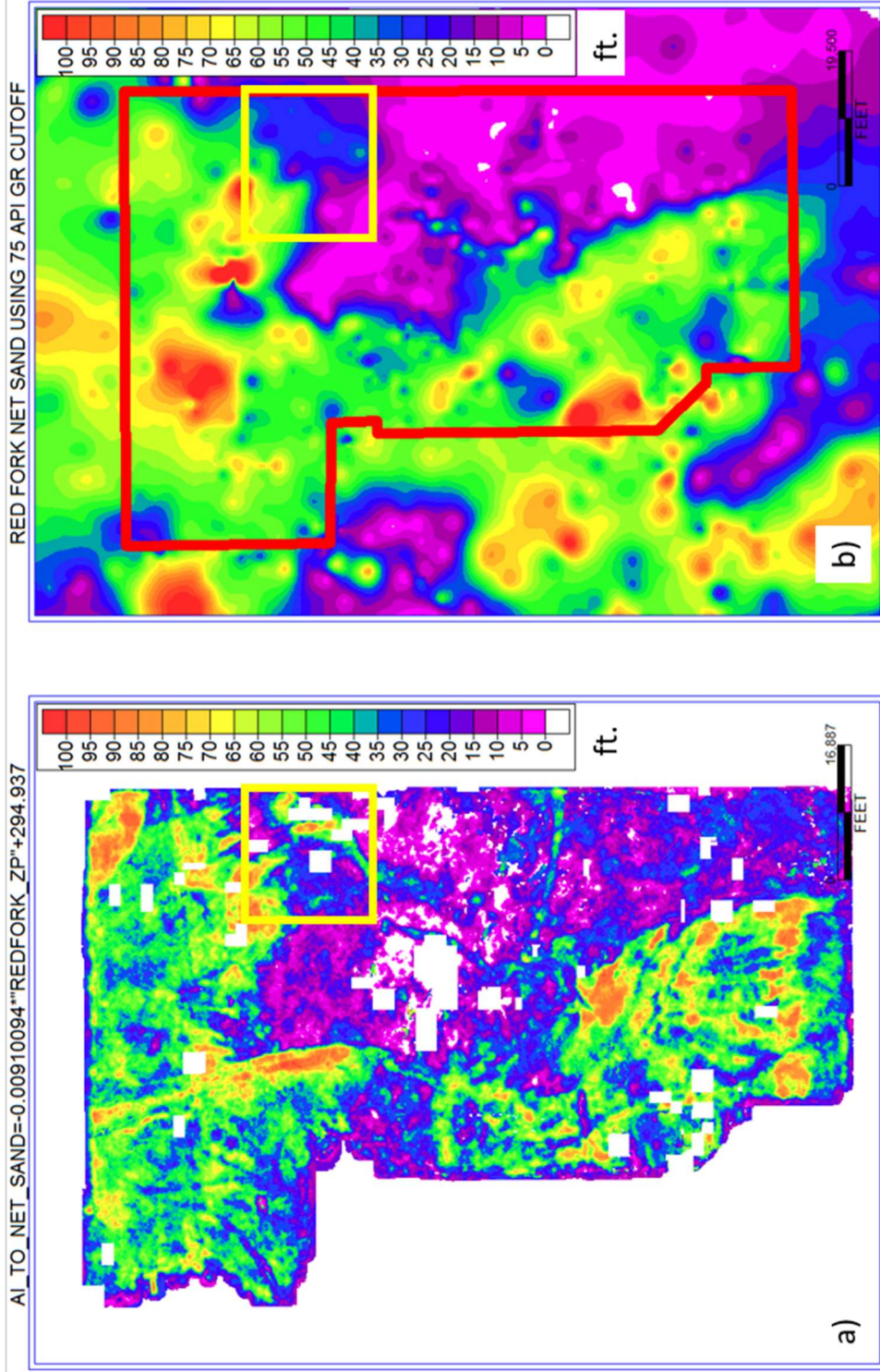


Figure 42. Net sand from (a) Z_p linear regression compared to (b) the well log data. Note the higher detail in the area of the isolated sand in the northeast (yellow box) where limited well data are available due to pre 1950's wells with no logs.

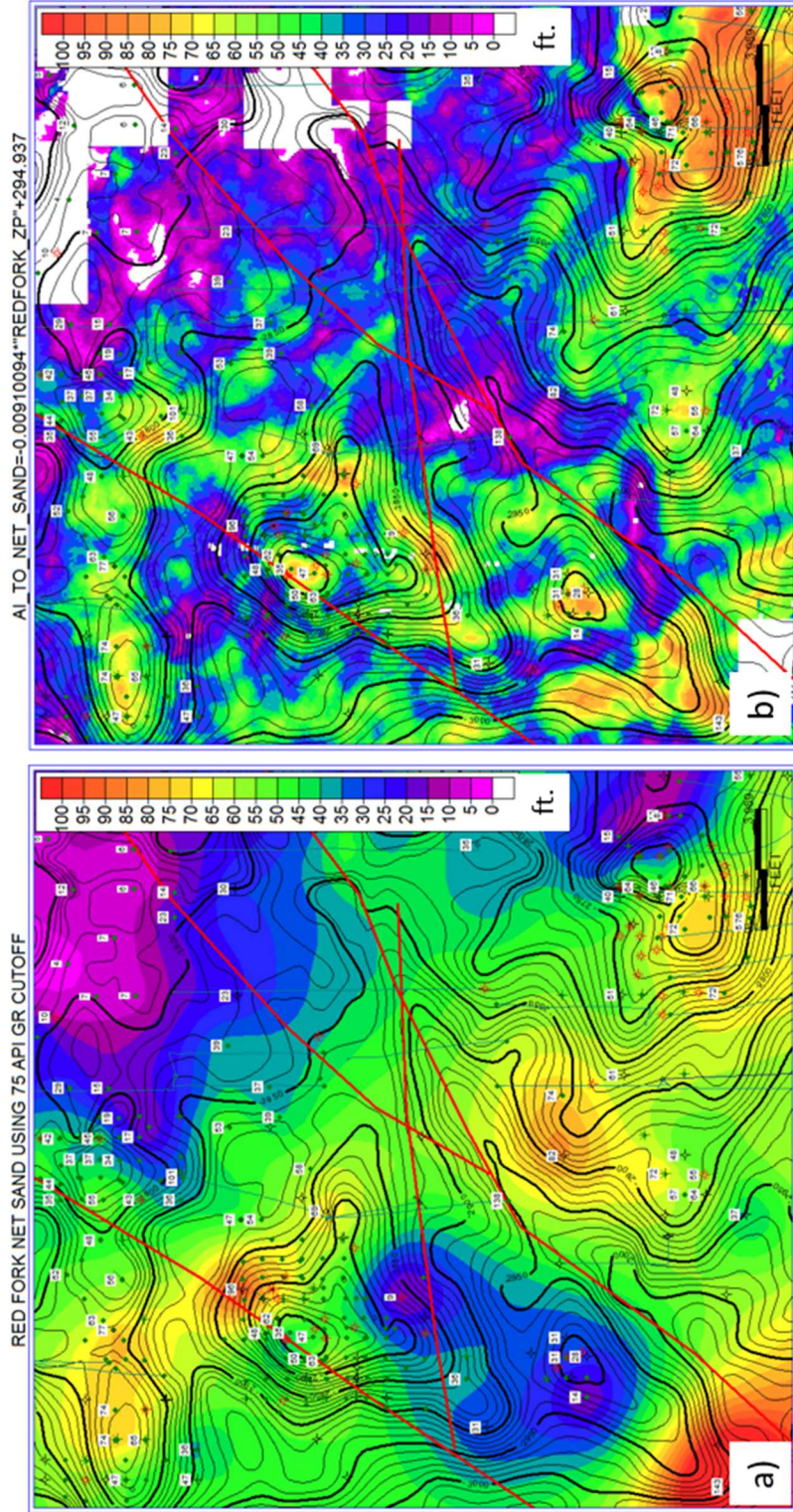


Figure 43. Net sand from (a) interpolated well data and (b) linear regression using the well data and seismic impedance data. The anomalous area in the northwest of the image comes from a large amount of source and receiver gaps due to survey obstacles (Figure 44).

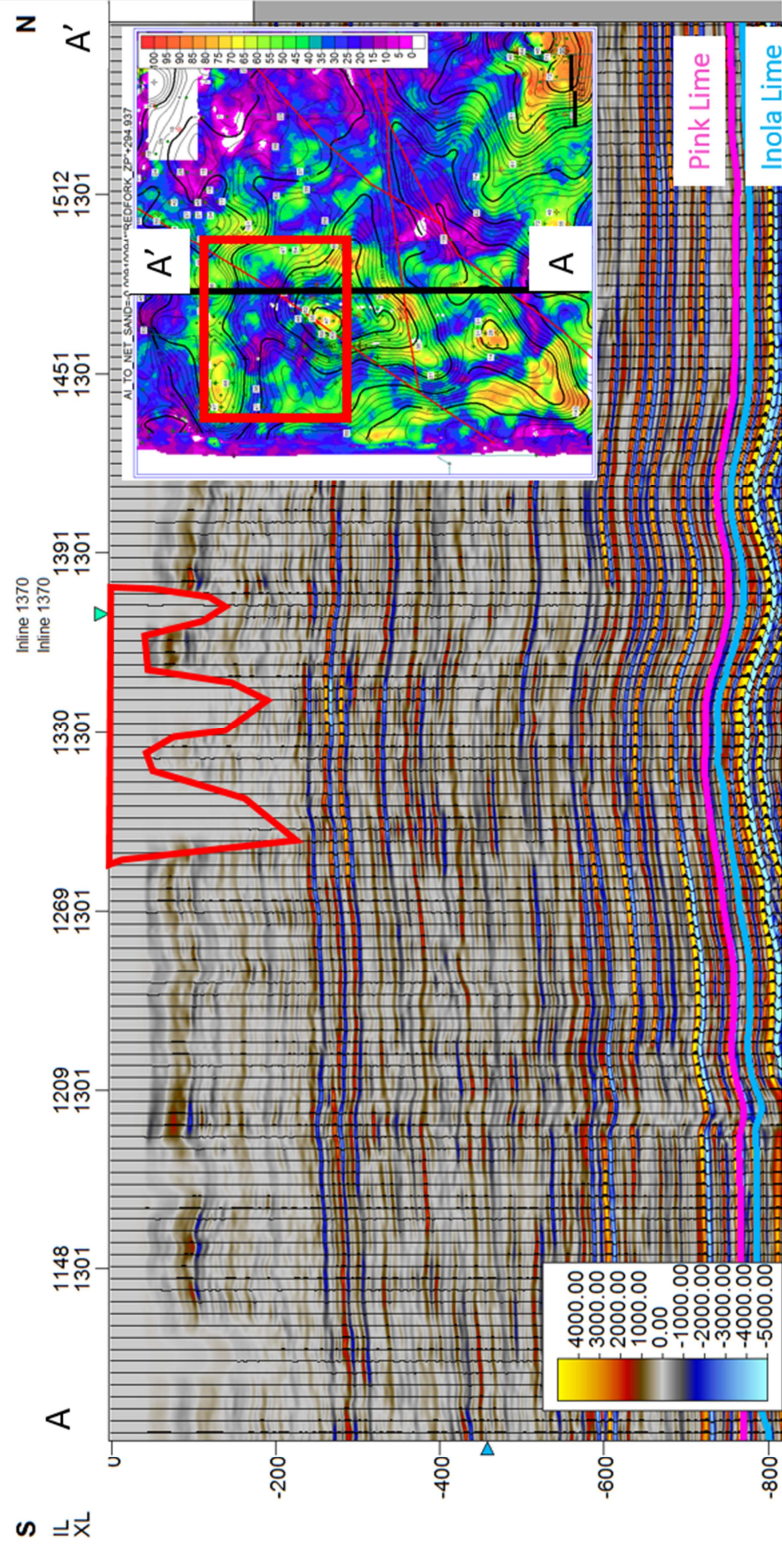


Figure 44. South to North crossline highlighting the near surface cultural moves (red polygon) from the existing producing field. Map view with red box outlining impacted area. 5-dimensional interpolation is able to predict the structural nature of the image but without enough real data due to the survey obstacles and the proximity to survey boundary it is unable to accurately predict the amplitudes.

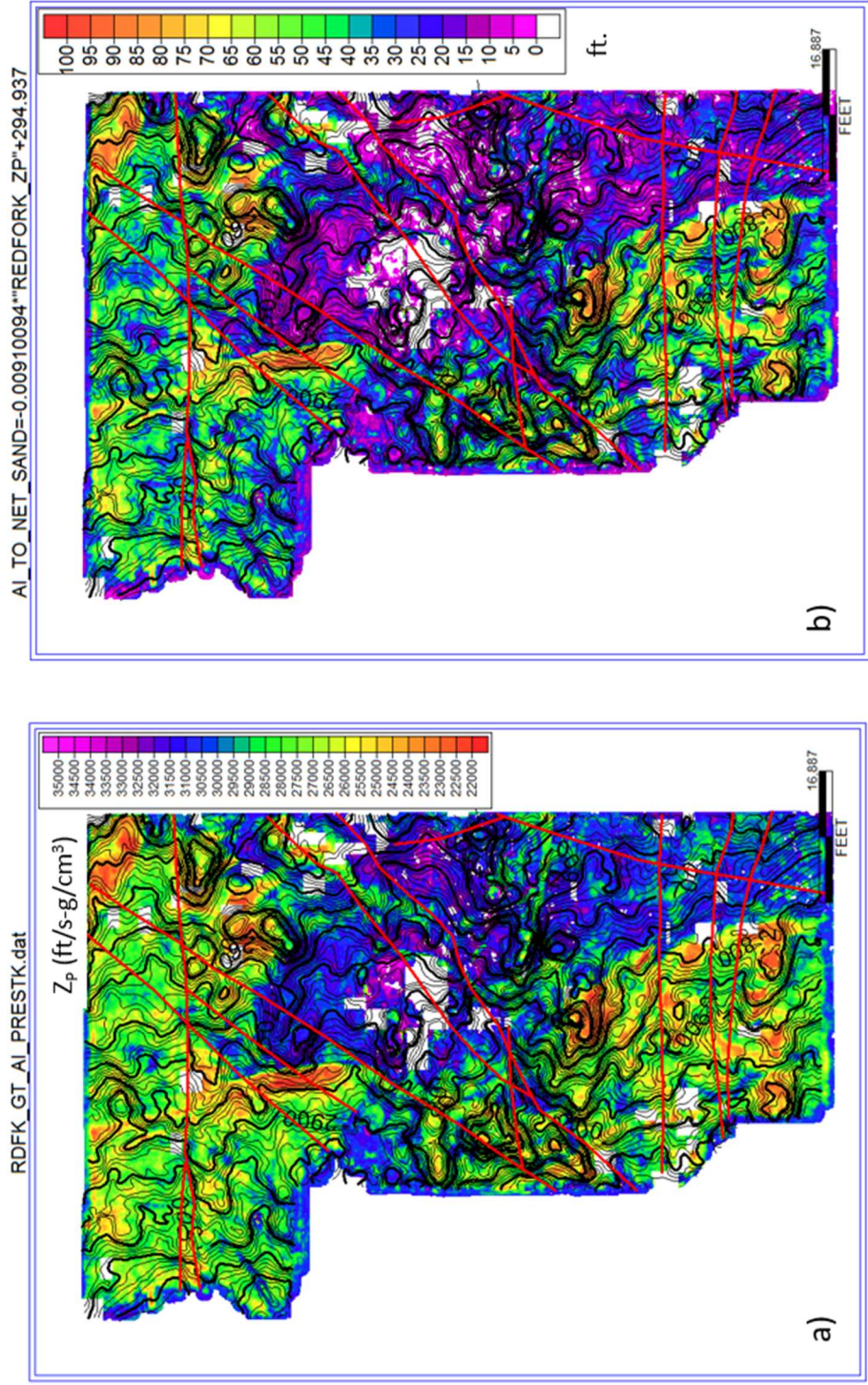


Figure 45. (a) Minimum Z_p value along the Red Fork interval with Pink Lime structural contours compared to (b) net sand derived from the linear regression with Pink Lime structure.

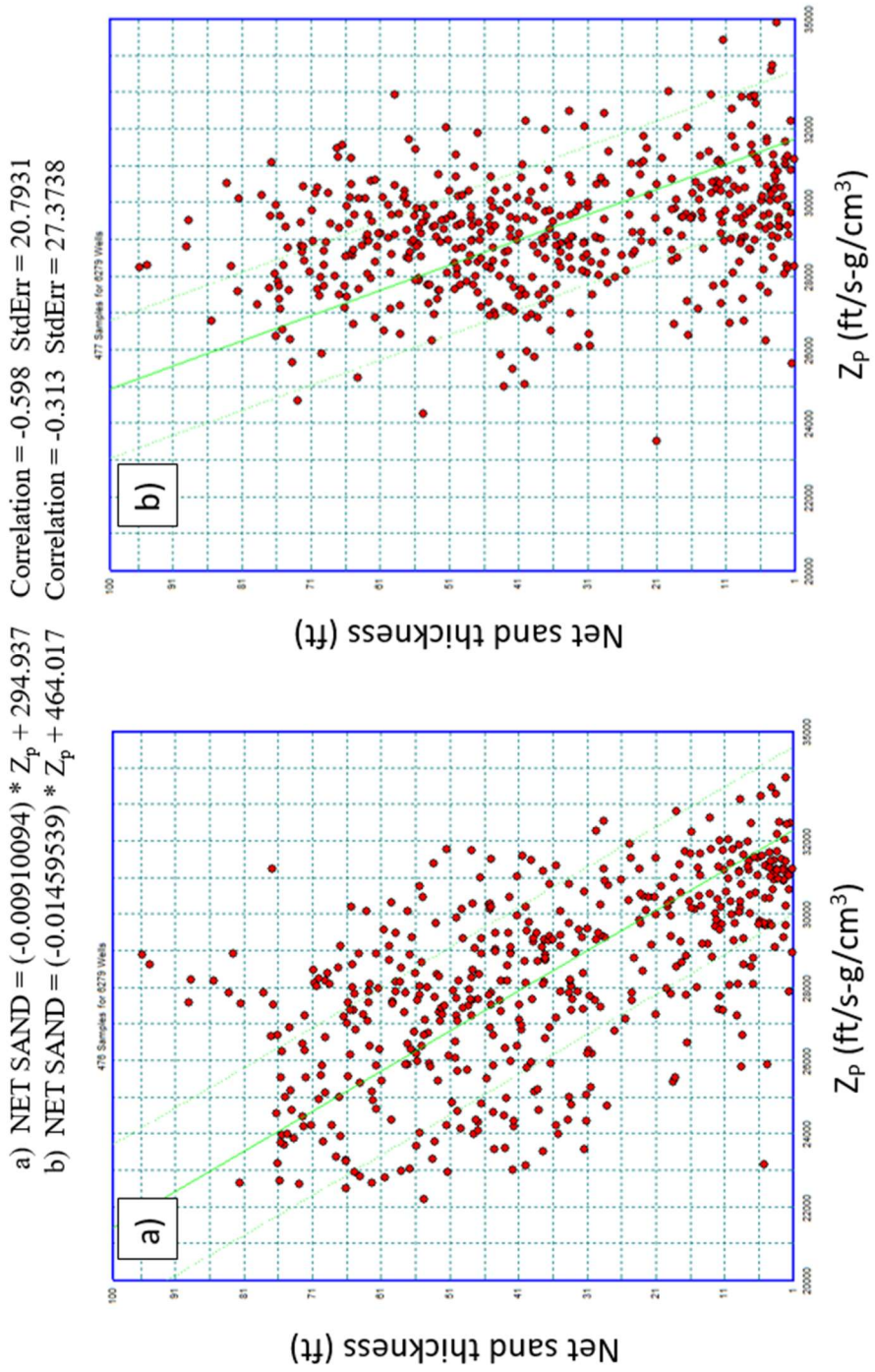
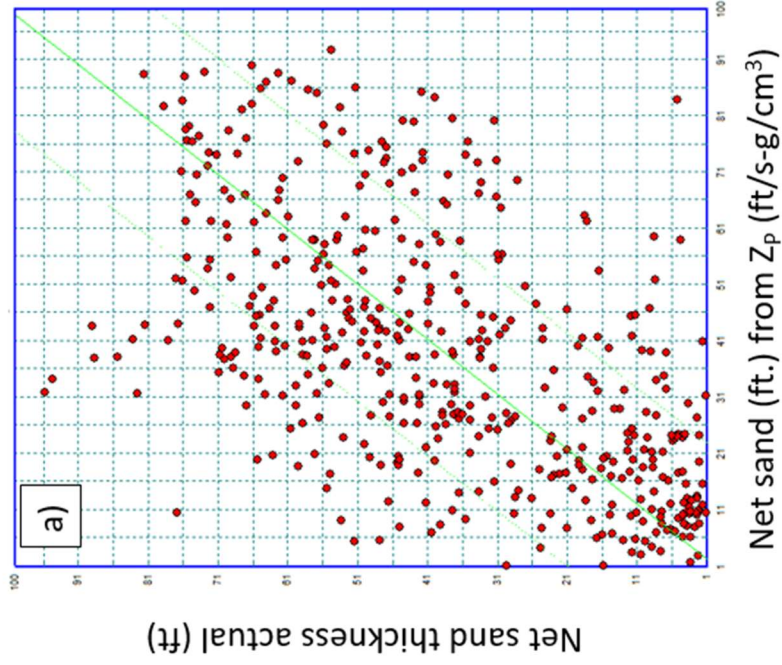


Figure 46. Acoustic impedance response cross plotted with net sand from raster logs. Confirmation that the 5-dimensional interpolation and spectral enhancement (a) provides a more correct result than without (b).

a) Correlation = -0.598 StdErr = 20.7931



b) Correlation = .789 StdErr = 14.9931

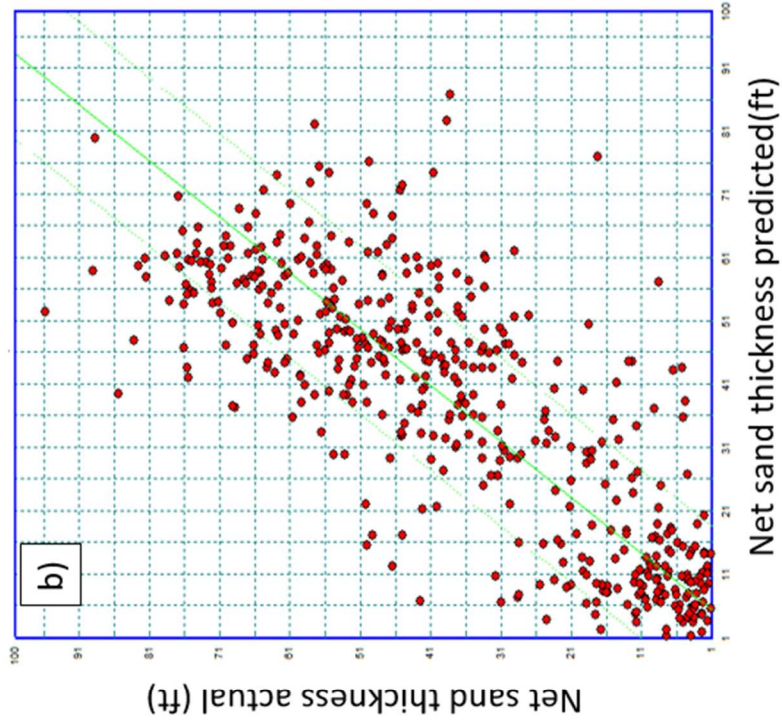


Figure 47. (a) Acoustic impedance response cross plotted with net sand from raster logs compared to (b) net sand calculated by removing and predicting each well from surrounding well data. 6 ft difference in error between each method lends confidence to net sand from Z_p .

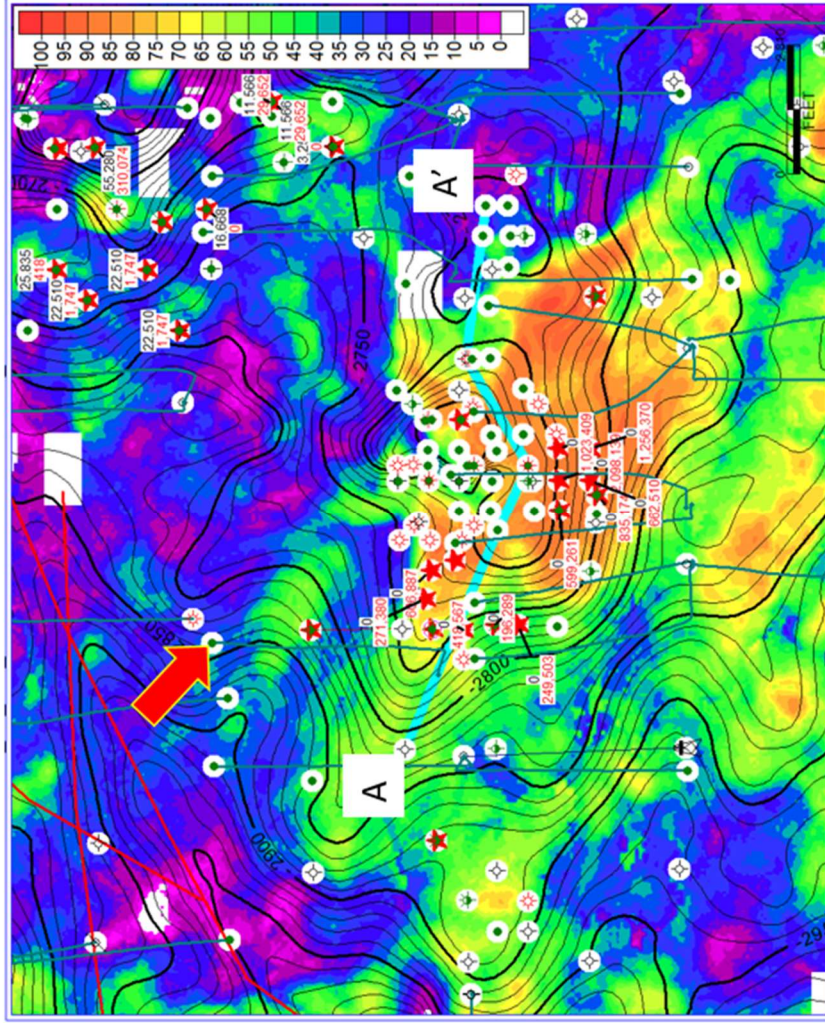


Figure 48. Map view of Red Fork sand body with drilled wells. Figure 49 shows well to well cross section highlighted in turquoise. Horizontal well highlighted in red arrow is a recompletion candidate. Red stars indicate Red Fork producers. Green text reports cumulative oil production, red text cumulative gas production.

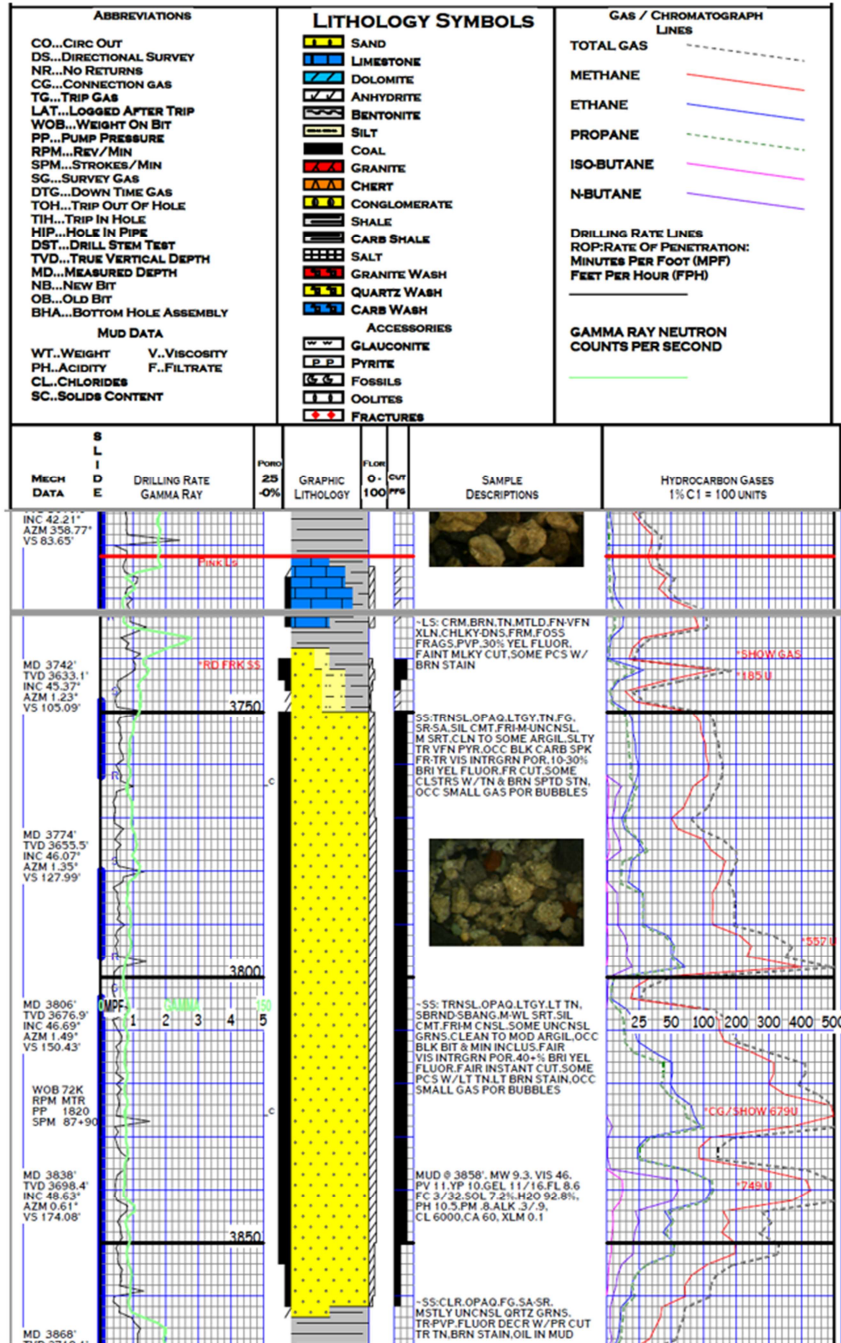


Figure 50. Red Fork interval from the horizontal recompletion candidate. Notice the significant gas show, oil cut, and visible porosity. The better show also appears deeper in the sand body.

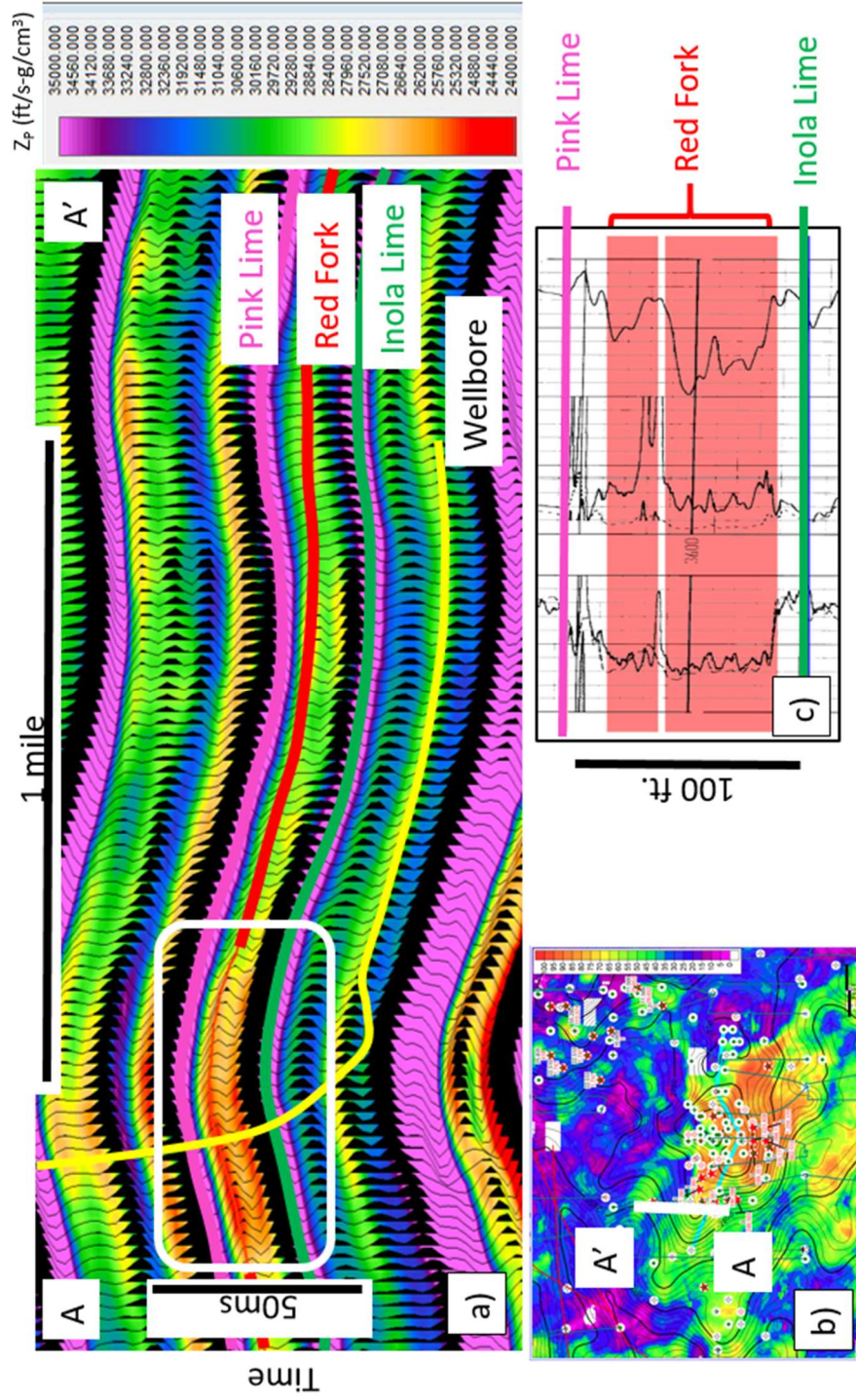


Figure 51. (a) White box highlights intersection of horizontal wellbore and the Red Fork formation and (b) the special location highlighted by white line. Note that (a) shows an upper and lower Red Fork sand corresponding to (c) an offset well log showing an upper and lower sand separated by a shale break. The sands appear to be compartmentalized as indicated by the better oil cut and gas show in the lower sand indicated by the mud log (Figure 50).

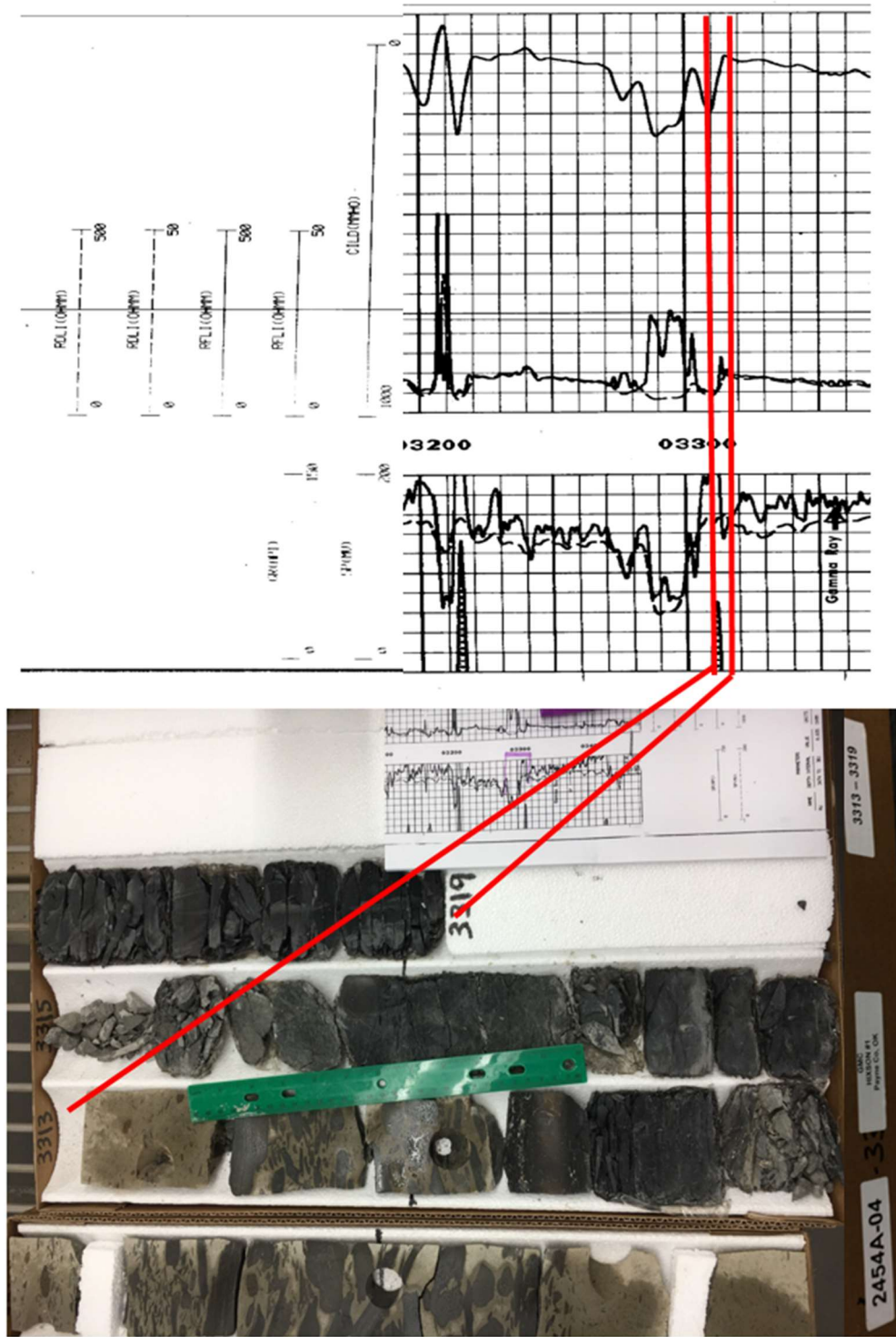


Figure 52. Hixson #1 (3313'-3319') showing basal shale with erosional contact with large rip up clasts. 12" ruler for scale.

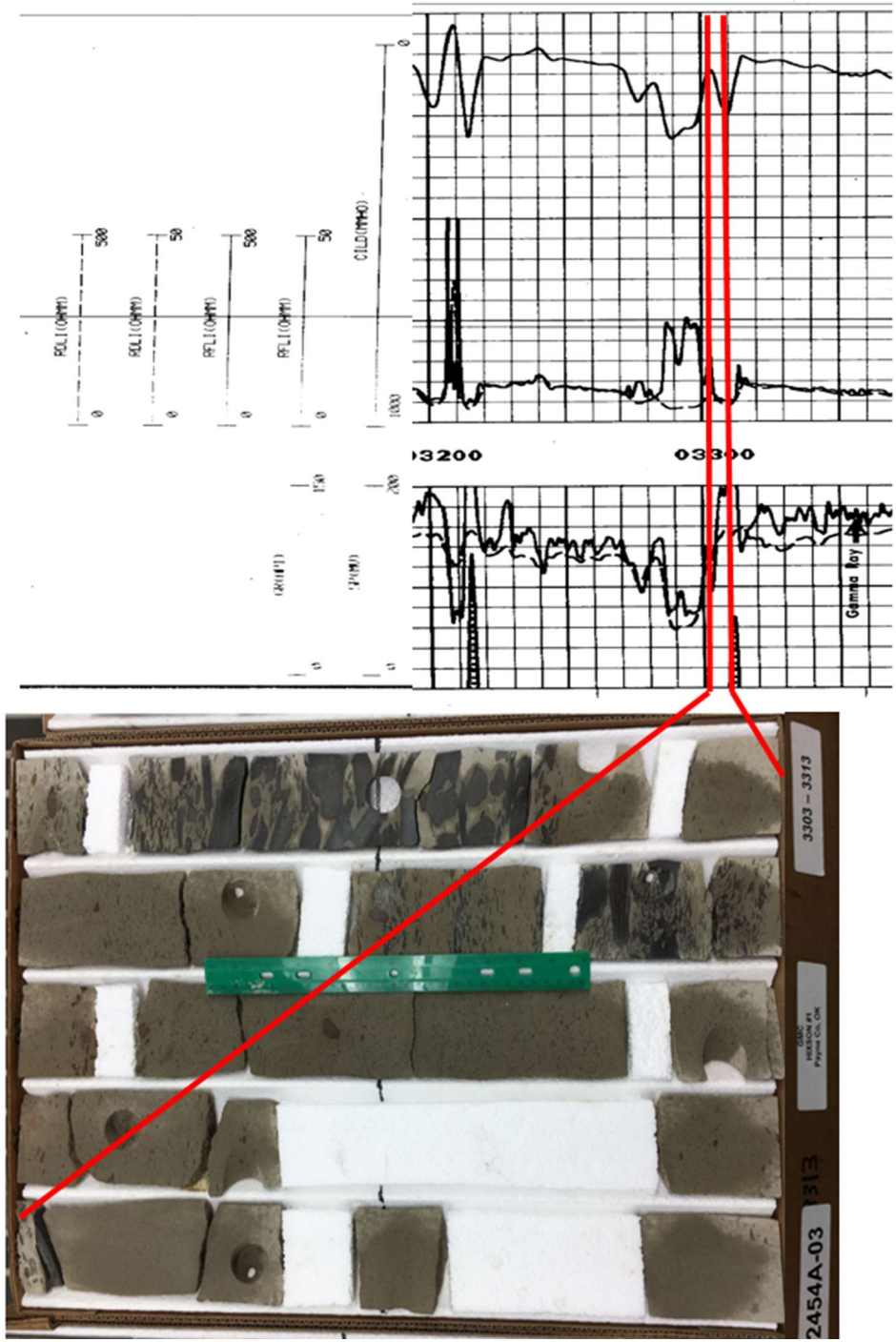


Figure 53. Hixson #1 (3303'-3313') showing a general coarsening up trend. Grain sizes are generally consistent, sub rounded, sub angular. Coarsening up log signature appears from fewer clasts in the matrix. 12" ruler for scale.

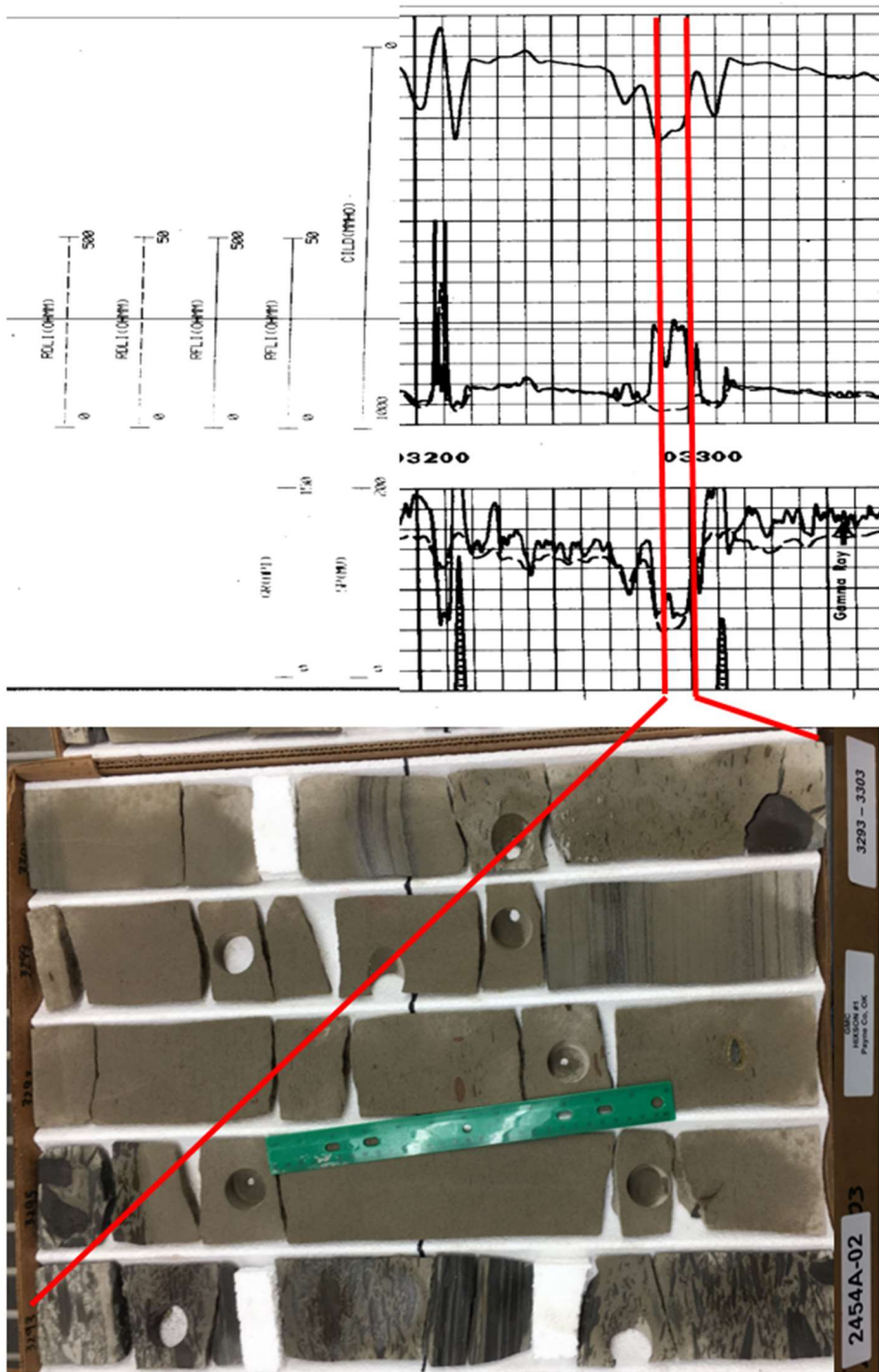


Figure 54. Hixson #1 (3293'-3303') showing coarsening up sequence with an erosional storm deposit at roughly 3295.3' below which corresponds to the cleanest gamma response and highest inferred porosity/permeability. Erosional surface evident at 3295.2' with abundant clasts again. 3294' is a relative thick shale package that could serve as a flow barrier. 12" ruler for scale.

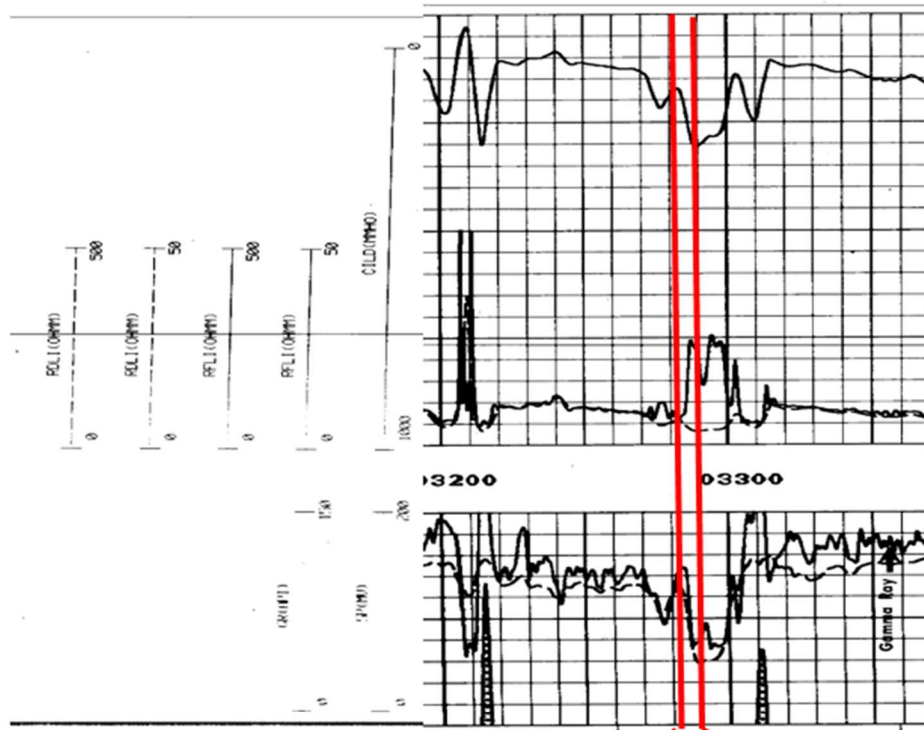


Figure 55. Hixson #1 (3283'-3293') Abundant clasts with a smaller fluvial interval that is low in mud content. Water sprayed on core highlights mud content in the abundant ripple sets from 3284'-3286.5'. 12" ruler for scale.

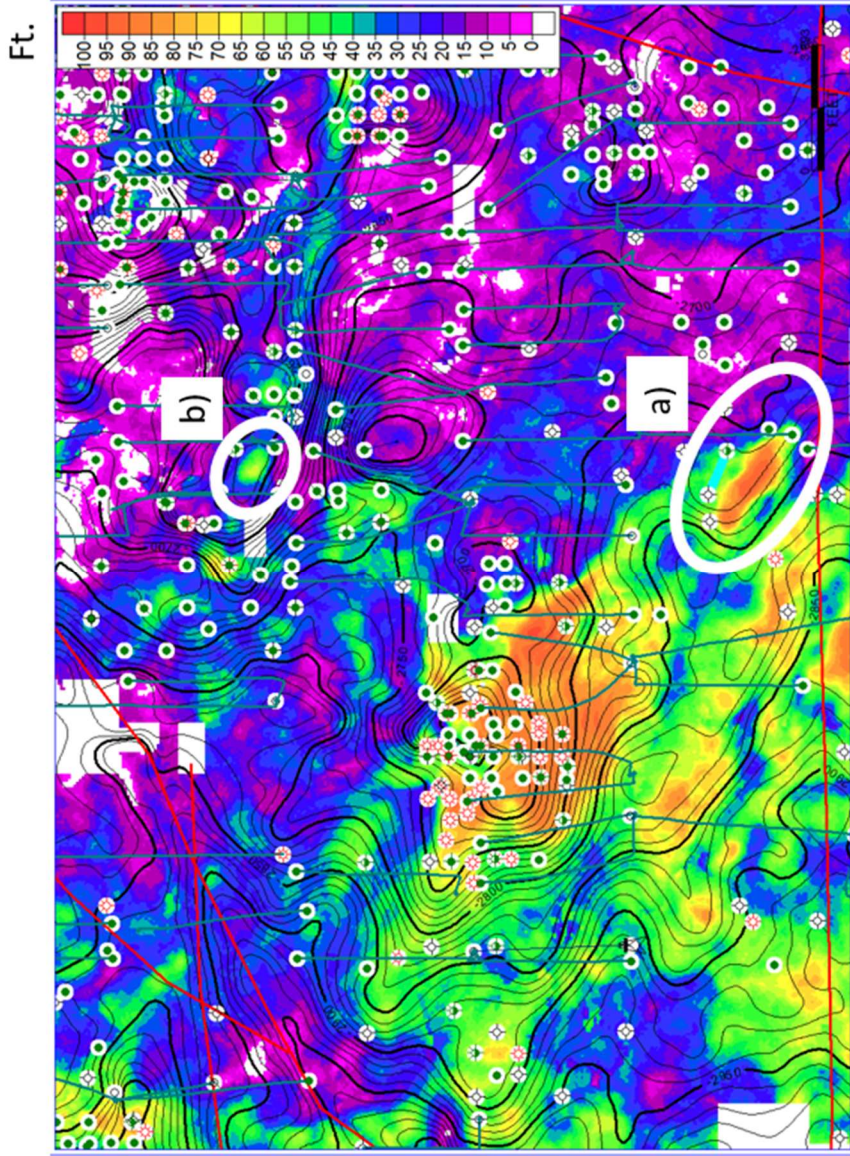


Figure 56. Two appealing targets for new drilling are (a) an isolated sand body similar to the main larger sand body and (b) a completely isolated sand body. Note that the setup is similar to the proven sand with equivalent net sand values, a similar structural position, and a stratigraphic pinch out for body (a). Body (b) is a riskier option but with upside potential for production.

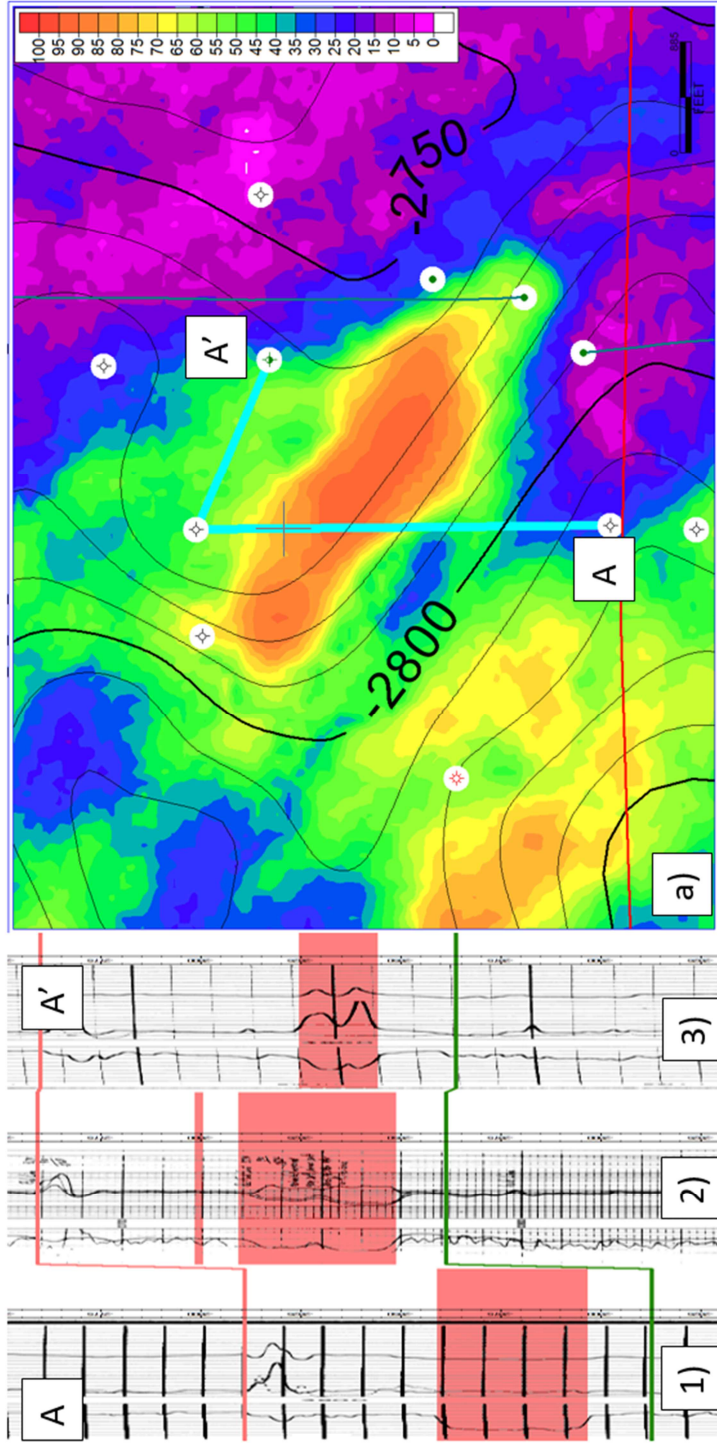


Figure 57. Prospective sand body flanked by dry holes. Deep resistivity values are (1) 2 ohm, (2) 2.5 ohm, and (3) 5 ohm. (a) Map view shows the relative position of the wells. Assuming 16% porosity from the well used in the inversion workflow and a formation water resistivity of 0.04 ohm the water saturation for well (1) is .72, (2) .64, and (3) .45.

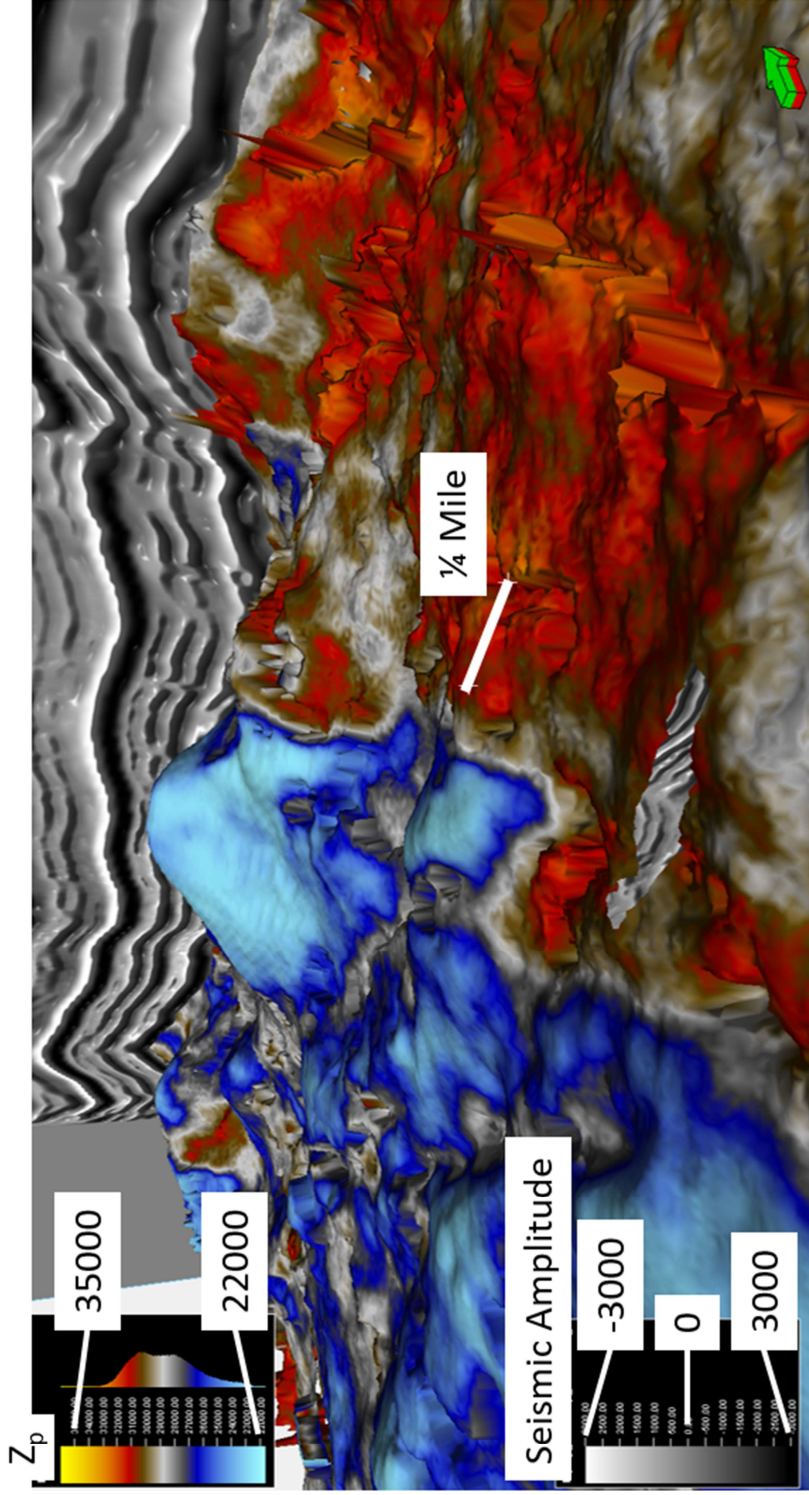


Figure 58. Red Fork time horizon with Z_p values in color. Seismic vertically exaggerated 25x. Evidence that the sand body does dip to the south-southwest.

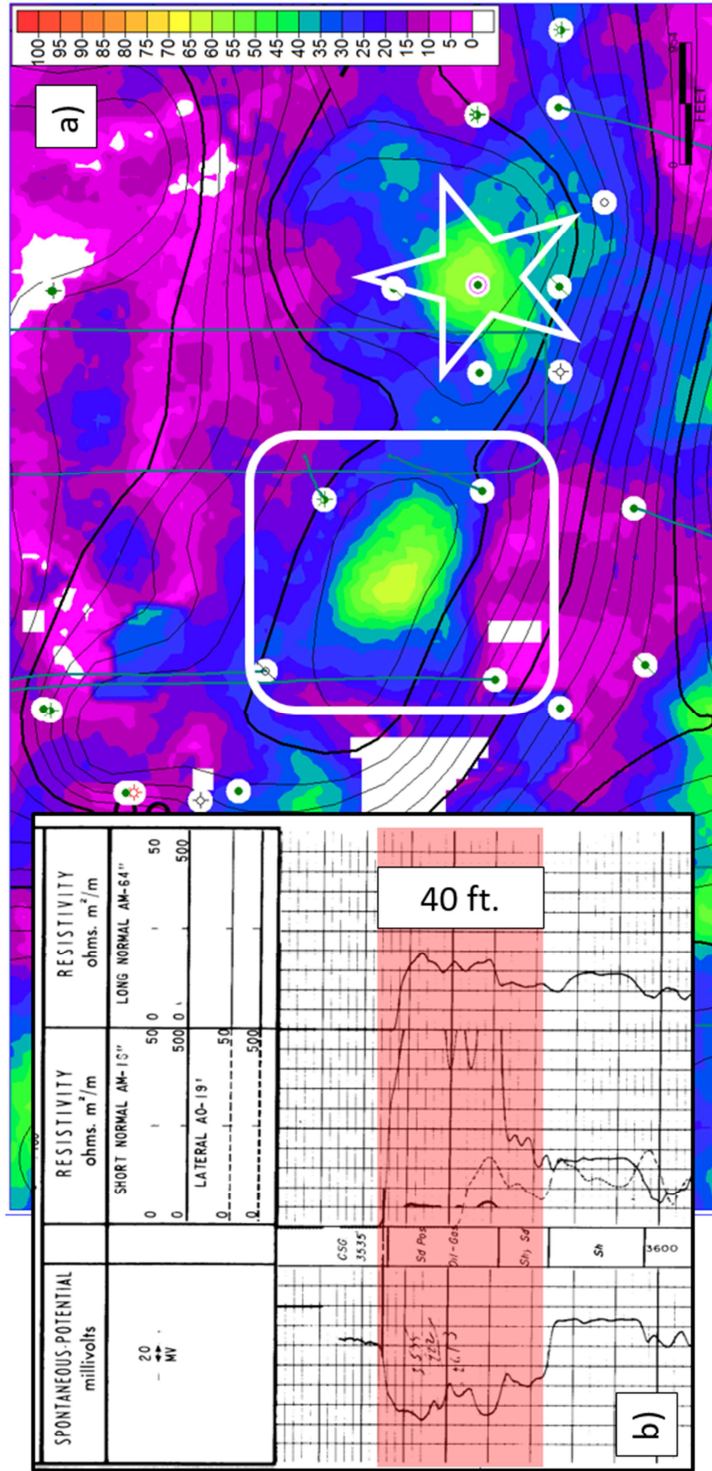


Figure 59. (a) White box highlights undrilled sand body similar to offsetting drilled body highlighted by star. (b) Well log from offsetting body shows 40 ft. of net sand with the upper 2/3s showing 15 ohm yielding 0.26 water saturation. No cumulative production is available but the wells initial production was 25 barrels of oil and 250 MCF of gas.

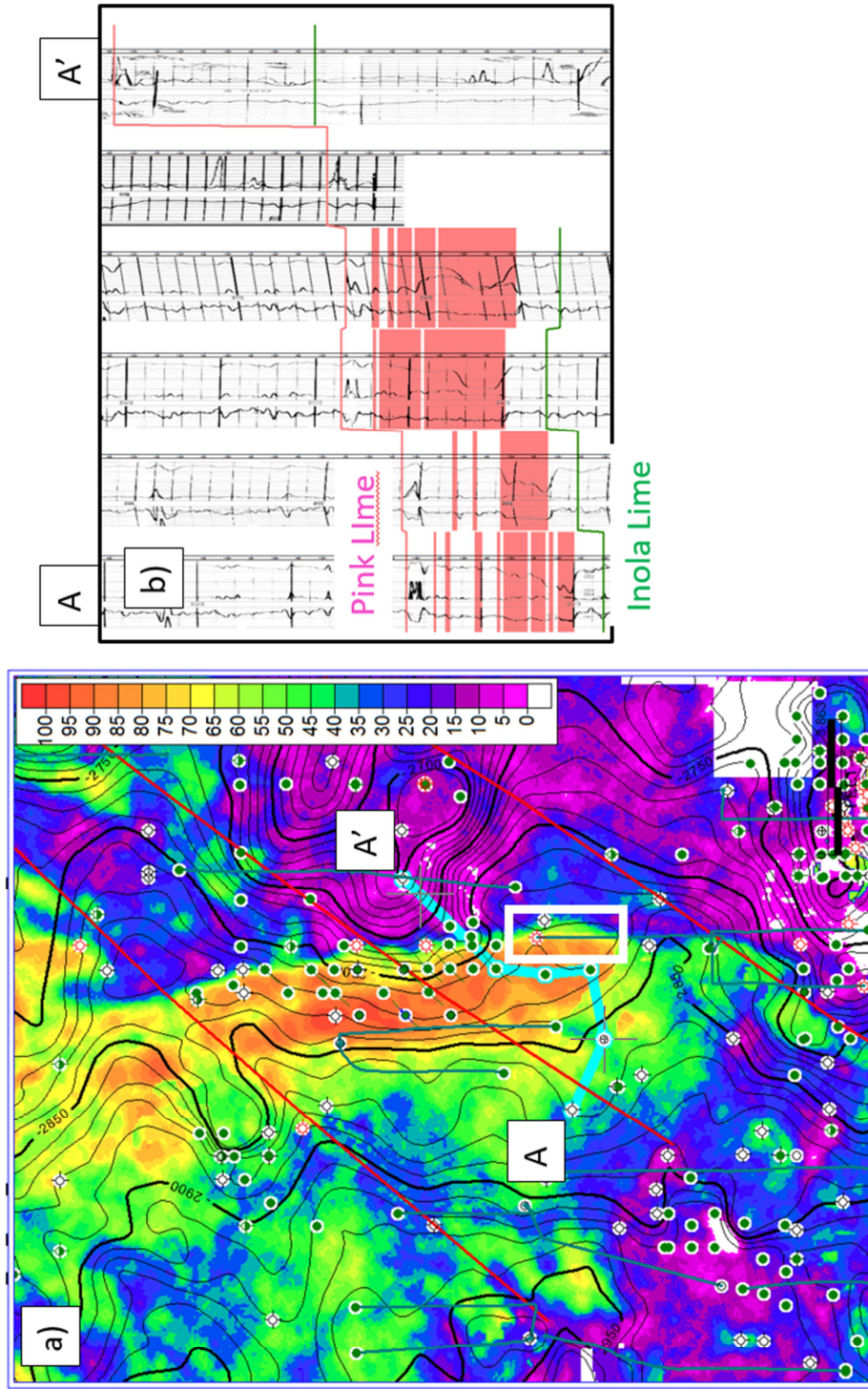


Figure 60. (a) White box highlights up dip portion of productive field. (b) Cross section A-A' (highlighted in light blue on map). Down dip portions of sand body non productive with the last well out of the sand body showing no sand in Red Fork interval (Pink Lime to Inola Lime). Field has produced over 2 million barrels of oil from known production.

CHAPTER VI: CONCLUSIONS

Modern 3D seismic data clearly illuminates conventional sandstone reservoirs. Using a modern processing workflow, I show that with careful processing pre-stack impedance inversion highlights previously untapped reserves in the Red Fork formation that can be commercially viable. I further show the value of 5-dimensional trace interpolation in refining the impedance estimation and image quality. This allows for a better statistical correlation to be used interpreting the data for hydrocarbon exploration.

Self-organizing maps can be a useful tool to make sense of multiple attribute volumes. In my example, it distinguishes porous and tight shales and sands but struggles to differentiate any hydrocarbons in the pore space.

I show that the relationship of Z_p to porosity can be extended to clean net sands. Given enough well control, I was able to statistically correlate Z_p and net sand to provide a more detailed net sandstone thickness map to aid in hydrocarbon exploration. This lead to multiple locations of bypassed pay that would be potential future drilling locations.

References

- AAPG Wiki. 2014. Lithofacies and environmental analysis of clastic depositional systems (17 June 2016 revision), http://wiki.aapg.org/images/5/50/Lithofacies-and-environmental-analysis-of-clastic-depositional-systems_fig3.png (accessed 5 February 2017)
- Aisenberg, M., 2013, The value of reprocessing legacy data: A case study of Bios D'arc, a Mississippi play in northeastern Oklahoma: Masters Thesis, The University of Oklahoma.
- Andrews, R. D., J. A. Campbell, and R. A. Northcutt, 1997, Fluvial-Dominated Deltaic (FDD) oil reservoirs in Oklahoma: The Red Fork Play: Oklahoma Geological Survey Special Publication 97-1, 1-115.
- Barber, R., 2010, Challenges in mapping seismically invisible Red Fork channels, Anadarko Basin, OK: Masters Thesis, The University of Oklahoma
- Crain R., 2015. Water saturation from Archie method (1 January 2015 revision), <https://www.spec2000.net/14-swa.htm> (accessed 3 April 2017)
- Chopra, S., and K. J. Marfurt, 2007, Seismic attributes for prospect identification and reservoir characterization: Society of Exploration Geophysicists.
- Chopra, S., 2010, Seismic curvature attributes for mapping faults/fractures, and other stratigraphic features: CSEG Recorder, **39**, 37-41.
- Chopra, S., 2010, Integration of coherence and volumetric curvatures images: The Leading Edge, **29**, 1092-1107.

- Del Moro, Y., 2012, An integrated seismic, geologic and petrophysical approach to characterize the Red Fork incised valley fill system in the Anadarko Basin, Oklahoma: Masters Thesis, The University of Oklahoma.
- Goodway, B., 2009, The magic of Lamé, Honorary lecturer 2009 - North America: <http://seg.org/Education/Lectures/Honorary-Lectures/2009-HL-Goodway>, accessed February 18, 2017.
- Hubbard R., 1982, Resistivities of water in selected formations, north-central Oklahoma: Masters Thesis, Oklahoma State University.
- Johnson, K. S., 2008, Geologic history of Oklahoma; Oklahoma Geological Survey Educational Publication 9:2008.
- Keller, G. R., 2008, Stratigraphic Guide to Oklahoma Oil and Gas Reservoirs: <http://www.ogs.ou.edu/fossilfuels/pdf/StratChartfr.pdf>, accessed January 18, 2017.
- Lindseth, R. O., 1979, Synthetic sonic logs - A process for stratigraphic interpretation: *Geophysics*, 44, no. 1, 3-26.
- Matos, M. C., P. L. Osorlo, P. L., and P. R. Johann, 2007, Unsupervised seismic facies analysis using wavelet transform and self-organizing maps: *Geophysics*, **72**, P9-P21.
- Mills-Bullard, B., 1928, Digest of Oklahoma oil and gas fields: Oklahoma Geological Survey Bulletin No. 40-Q.
- Northcutt, R.A., and J.A. Campbell, 1988, Geologic provinces of Oklahoma: Oklahoma Geological Survey, http://www.faqs.org/sec-filings/111201/North-Texas-Energy-Inc_S-1/ex99-1.htm#b, accessed January 18, 2017.

- Petro Wiki. 2012. Spectral gamma ray logs (24 June 2015 revision),
http://petrowiki.org/Spectral_gamma_ray_logs (accessed 1 April 2017)
- Russell, B., and D. Hampson, 2006, The old and the new in seismic inversion: CSEG Recorder, v31, 5-11.
- Sheriff, R. E. (2006). Encyclopedic dictionary of applied geophysics: Society of Exploration Geophysics. Geophysics References Series, 13, 4th edition.
- Trad, D., 2009, Five-dimensional interpolation: Recovering from acquisition constraints: Geophysics, Vol. 74, NO. 6, V123-V132.
- Way, H. S. K., 1968, Structural study of the Hunton Lime of the Wilzetta Field, T12-13N, R5E, Lincoln County, Oklahoma, Pertaining to the Exploration for Hydrocarbons: Masters Thesis, Oklahoma State University
- Zhou, H., (2014) Practical Seismic Data Analysis. New York, New York: Cambridge University Press.

Appendix A: 5D INTERPOLATION

5-dimensional interpolation is a means to regularize and interpolate missing data within a seismic dataset. Survey obstacles are generally the main challenge in regular sample intervals for onshore 3D data. In contrast, marine data are usually well sampled in the inline direction but poorly sampled in the crossline direction due to the design of the streamers (Trad, 2009). The underlying challenge, as Trad (2009) notes as a general principle, is that “missing data are assumed to have a similar nature to data recorded in their neighborhood.” I show that the inversion results for 5D interpolation statistically correlate better than the data without 5D interpolation (Figure 46) but the faulted portions of the data can be smeared (Figure 61). The interpreter needs to keep in mind the pitfalls that can accompany the underlying processing techniques.

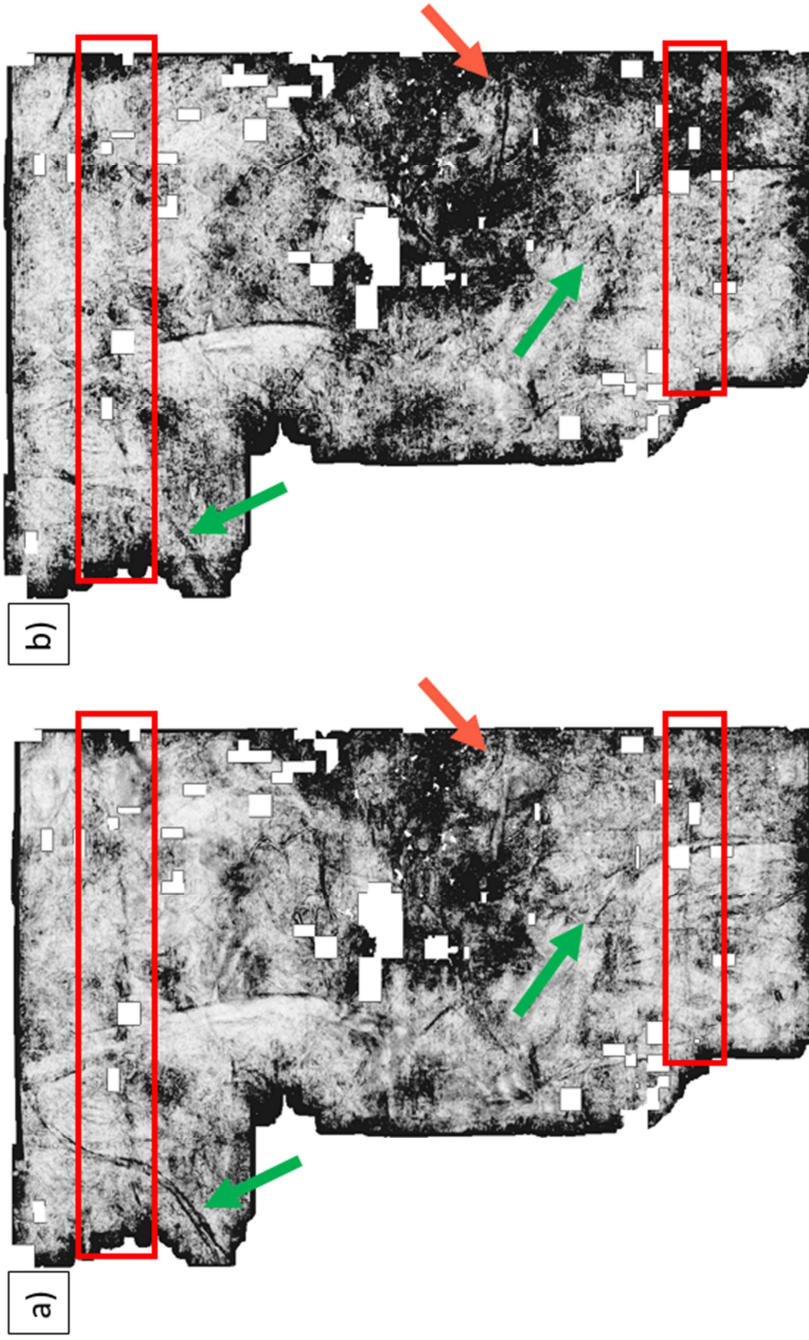


Figure 61. Horizon slices through a coherence volume in (a) a dataset without 5D interpolation and (b) a dataset with 5D interpolation. Notice the (Red boxes) missing faults in the 5D interpolated volume that is noticeable in the data without 5D interpolation. Also evident are the missing and difficult to see (Green arrows) narrow channels. The 5D dataset does help the (Orange arrows) edge of the data.